CANCER CELLS THAT SURVIVE CHECKPOINT ADAPTATION (MITOSIS WITH DAMAGED DNA) ACQUIRE MAJOR CHROMOSOMAL REARRANGEMENTS

DANI KALSBEEK
Bachelor of Science, University of Groningen, 2016

A Thesis
Submitted to the School of Graduate Studies
of the University of Lethbridge
in Partial Fulfillment of the
Requirements for the Degree

MASTER OF SCIENCE

Department of Biological Sciences
University of Lethbridge
LETHBRIDGE, ALBERTA, CANADA

CANCER CELLS THAT SURVIVE CHECKPOINT ADAPTATION (MITOSIS WITH DAMAGED DNA) ACQUIRE MAJOR CHROMOSOMAL REARRANGEMENTS

DANI KALSBEEK

Date of Defense: December 10, 2018

Dr. R.M. Golsteyn Thesis Supervisor	Associate Professor	Ph.D.
Dr. S.D. Wetmore Thesis Examination Committee Member	Professor	Ph.D.
Dr. A.G. Russell Thesis Examination Committee Member	Associate Professor	Ph.D.
Dr. M. Weinfeld External Examiner University of Alberta	Professor	Ph.D.
Dr. S. Wiseman Chair, Thesis Examination Committee	Associate Professor	Ph.D.

ABSTRACT

We investigated the relationship between checkpoint adaptation and chromosomal change in human cancer cells. HT-29 and M059K cells treated with pharmacological concentrations of camptothecin acquired damaged DNA, overcame the DNA damage checkpoint and entered mitosis with damaged DNA, a phenomenon named checkpoint adaptation. We observed that cells that survived checkpoint adaptation acquired major chromosomal rearrangements. Surviving cells had fewer chromosomes and increased numbers of interchromosomal rearrangements per cell, compared to cells that did not undergo checkpoint adaptation. We investigated whether the DNA repair enzyme polynucleotide kinase 3'-phosphatase (PNKP) participates in checkpoint adaptation by using the PNKP inhibitor A12B4C50. We showed that A12B4C50 reduced the interaction between the DNA repair complex PNKP-XRCC1 in cells; however, no effect on checkpoint adaptation was observed. Future studies would need to focus on DNA repair pathways that may reduce the chromosomal change caused by checkpoint adaptation. This can provide insight into the biology of genotoxic treatments used in cancer patients.

ACKNOWLEDGEMENTS

I would like to thank my supervisor Dr. Roy Golsteyn for his patience, guidance and continuous support throughout my M. Sc. program. I am grateful for the encouragement that I have received and the opportunities that I have been given. His knowledge and approachable, optimistic, and passionate character were an invaluable guidance that motivated me and taught me essential research skills and values. Special thanks to my committee members Dr. Tony Russell and Dr. Stacey Wetmore, for their feedback and time dedication to help advance my project. A special thanks goes to Dr. Michael Weinfeld for being my external thesis examiner and for collaborating. I also like to thank Dr. Steve Wisemen for contributing to my thesis defence as the thesis examination chair.

I am also grateful to members of the Biological Sciences Department for their intellectual and technical support throughout my M. Sc. program, and to Dr. Olu Awosaga for sharing his knowledge on statistical analysis. My research has benefitted greatly from the support, advice and friendship of laboratory members: Alessandra Bosco, Jan Tuescher, Layla Molina, and the undergraduate students that joined the lab over the past years. I am thankful for their knowledge and valuable discussions shared.

This achievement would not have been accomplished without the moral support, patience, encouragement and kindness of friends and family. I am profoundly thankful to Rob van Koert, my parents Martin and Marjon Kalsbeek, and my sister Shanna Kalsbeek for their unconditional love and support over the last two years. Also, I would like to thank the Woordman family, their welcoming home and kind friendship helped me feel home in Canada.

TABLE OF CONTENTS

LIST OF FIGURES

LIST OF ABBREVIATIONS

53BP1	Tumour suppressor p53-binding protein 1
AMCD	Anti-microtubule cancer drug
ANOVA	Analysis of variance
APC	Anaphase promoting complex
APC/C	Anaphase promoting complex/cyclosome
ATCC	American Type Culture Collection
ATM	Ataxia telangiectasia mutated
ATP	Adenosine triphosphate
ATR	ATM and RAD30-related
BSA	Bovine serum albumin
CAS 10	Checkpoint Adaptation Survival for ten days
CAS 2	Checkpoint Adaptation Survival for two days
CAS 4	Checkpoint Adaptation Survival for four days
CAS	Checkpoint Adaptation Survival
Cdc20	Cell division cycle 20
Cdc25	Cell division cycle 25
Cdh1	Cadherin-1
Cdk1	Cyclin-dependent kinase 1
Cdk4	Cyclin-dependent kinase 4
CETSA	Cellular Thermal Shift Assay
Chk1	Checkpoint kinase 1
Chk2	Checkpoint kinase 2
CIN	Chromosome instability
CPT	Camptothecin
CtIP	CtBP-interacting protein
DAPI	4',6-diamidino-2-phenylindole
DDR	DNA damage response
DM	Double minute
DMEM	Dulbecco's Modified Eagle's medium
DMSO	Dimethyl sulfoxide
DNA	Deoxyribonucleic acid
DNA-PKcs	DNA-dependent protein kinase catalytic subunit
DNase	Deoxy ribonuclease
DSB	Double-strand DNA break
DTT	Dithiothreitol
EDTA	Ethylenediaminetetraacetic acid
EGTA	Ethylene glycol tetra-acetic acid
FBS	Fetal bovine serum
FEN-1	Flap endonuclease 1
G1 phase	Gap 1 phase
G2 phase	Gap 2 phase
HEPES	4-(2-hydroxyethyl)-1-piperazineethanesulfonic acid
Histone γH2AX	Phosphorylated histone H2A family member X
HR	Homologous recombination
HT1080	Human fibrosarcoma
HT-29	Human colorectal adenocarcinoma cell line
ICC	Intermediate chromosome configuration
IDC	Interphase and DNA-damaged cells

IgG	Immunoglobulin G
IP	Immunoprecipitation
IR	Ionizing radiation
kDa	Kilo Dalton
M phase	Mitotic phase
M059K	Human glioblastoma cell line
MDC	Mitotic and DNA-damaged cells
MRE11	Meiotic recombination 11
NBS1	Nibrin
NHEJ	Non-homologous end joining
P21	Tumour suppressor p21
P53	Tumour suppressor p53
PARP1	Poly [ADP-ribose] polymerase 1
PBS	Phosphate buffered saline
PCNA	Proliferating cell nuclear antigen
pH3	Phospho-Ser^{10} histone H3
PNA	Peptide nucleic acid
PNKP	Polynucleotide kinase 3'-phosphatase
Rcf	Relative centrifugal force
RNase	Ribonuclease
RPA	Replication protein A
RPMI	Roswell Park Memorial Institute medium
S phase	DNA synthesis phase
SAC	Spindle Assembly Checkpoint
SCC	Shattered chromosome configuration
SDS	Sodium dodecyl sulphate
SEM	Standard error of the mean
SSB	Single-strand DNA break
SSC	Saline-sodium citrate
TAME	Tosyl-L-arginine methyl ester
TBS	Tris-buffered saline
TDC	Total and DNA-damaged cells
Tdp1	Tyrosyl-DNA phosphodiesterase
Topo1	Topoisomerase 1
UV	Ultraviolet
WCC	Whole chromosome configuration
Wee1	Nuclear kinase Wee1
XRCC1	X-ray repair cross-complementing protein 1
XRCC4	X-ray repair cross-complementing protein 4

GENERAL INTRODUCTION

This thesis is about how checkpoint adaptation can change chromosome number and structure in human cells. There are increasing amounts of evidence that checkpoint adaptation occurs in human cancer cells when they are treated by genotoxic agents. The most commonly used cancer therapies are genotoxic agents, however, they are not as effective as hoped (Helleday et al., 2008). Therefore, a better understanding of how cancer cells respond to them is needed to improve treatment outcomes (Swift & Golsteyn, 2014). One example of a genotoxic agent is the chemical camptothecin (CPT). CPT and its derivatives are frequently used to treat colon cancer (Giovanella et al., 1989). This genotoxic agent inhibits topoisomerase I (Topo1), which is an essential enzyme that nicks DNA strands to relieve topological constraints that arise during replication. Inhibition of Topo1 by CPT leads to DNA breaks and cell death in some types of cancer cells, such as those from the colon (Chen & Liu, 1994).

As their name indicates, genotoxic agents damage DNA and lead to the activation of the DNA damage response (DDR). One of the proteins involved in this response is the protein histone H2AX, which becomes phosphorylated (ɣH2AX) upon recognition of double-strand DNA breaks (DSBs) by ataxia telangiectasia mutated (ATM) or ATM and RAD30-related (ATR) kinases. Protein complexes involved in DNA repair are recruited by histone ɣH2AX to the sites of DSBs, promoting cell cycle arrest and DNA repair (Jackson & Bartek, 2009). An important protein involved in DNA repair is polynucleotide kinase 3’-phosphatase (PNKP). It modifies the phosphorylation status of DNA termini at breaks to make these sites accessible for DNA polymerases and ligases. PNKP forms a complex with other proteins, such as X-ray repair cross-complementing protein 1 (XRCC1) and X-ray repair cross-complementing protein 4 (XRCC4), to initiate single-strand DNA break (SSB) repair and DSB repair, respectively. The inhibition of PNKP has shown to increase the sensitivity of cancer cells to genotoxic agents (Rasouli-Nia et al., 2004; Freschauf et al., 2010).

When cells are unable to repair DNA, they arrest their progress in cell cycle phases and either die, enter senescence or undergo G2/M-checkpoint adaptation (from here on named checkpoint adaptation) (Helleday et al., 2008). Checkpoint adaptation is a recently discovered process and little is known about it. It is characterized by three steps: the first step is cell cycle arrest in the G2/M-checkpoint upon activation by damaged DNA; the second step is the overriding of this cell cycle arrest, and the last step is the entrance into mitosis with damaged DNA (Syljuasen, 2007; Kubara et al., 2012; Swift & Golsteyn, 2014, 2016a). The majority of cells that undergo checkpoint adaptation will die in mitosis and it is therefore suggested that checkpoint adaptation is a primary cell death pathway in cancer cells that are treated with pharmacological concentrations of genotoxic agents (Brown & Attardi, 2005; Swift & Golsteyn, 2016a). However, it has been previously shown that a small number of cells that enter mitosis with damaged DNA can survive and are able to proliferate (Kubara et al., 2012).

During mitosis, DNA repair is inhibited to maintain genome fidelity (Orthwein et al., 2014). This suggests that cells that are able to exit mitosis after checkpoint adaptation transfer their damage to daughter cells. In these cells, damage could be repaired in G1 phase, however, it is possible that genomic change has occurred due to mitosis with damaged DNA and micronuclei formation (Tkacz-Stachowska et al., 2011). Additionally, many cancer cells have defective p53, resulting in a defective G1/S checkpoint. This could cause cells to go through a second cell cycle with damaged DNA after checkpoint adaptation, which might contribute to genomic change (Swift & Golsteyn, 2016b). For these reasons, checkpoint adaptation survival cells are predicted to have altered genomes due to processes of DNA damage repair and adaptation to the checkpoint (Kubara et al., 2012; Orthwein et al., 2014; Swift & Golsteyn, 2016a).

It has been proposed that checkpoint adaptation creates an opportunity for genomic change, which is suggested to be one of the factors that may contribute to treatment inefficiency seen in cancer patients (Kandoth et al., 2013). This led to our hypothesis that cancer cells that survive checkpoint adaptation after treatment with genotoxic agents have genomic changes, which is

supported by the finding of micronuclei acquisition upon checkpoint adaptation (Palmitelli et al., 2015; Lewis & Golsteyn, 2016). In collaboration with Dr. Michael Weinfeld at the University of Alberta, we tested the role of PNKP inhibitors in checkpoint adaptation. To investigate our hypothesis we had two objectives:

Objective 1: To determine if chromosome structure and number in cancer cells that survive checkpoint adaptation are different from those of not-treated cells.

Objective 2: To investigate whether inhibitors of the DNA repair enzyme PNKP affect the number of cells undergoing or surviving checkpoint adaptation.

Our laboratory has developed an experimental model using colon cancer cells (HT-29) treated with CPT to study checkpoint adaptation. In this model, about 90% of the cancer cells treated with clinically relevant genotoxic agents will enter mitosis with damaged DNA and approximately 2% of these cells are able to exit mitosis and survive (Kubara et al., 2012). A key question about this process is whether cells that survive checkpoint adaptation acquire chromosomal changes relative to the not-treated parental cells, which may be significant in the understanding of treatment inefficiency seen in cancer patients. It is known that patients that are treated with anti-cancer agents can develop a secondary tumour that is genetically different from the primary tumour and therefore more difficult to treat (Bartek & Lukas, 2007). This research project is built on published and unpublished data prior to joining the laboratory, in which it was observed that checkpoint adaptation survival cells had fewer chromosomes, a reduction of telomeres, and acquired micronuclei. These promising data provided the building blocks for this research project.

In this thesis, we first discuss checkpoint adaptation and micronuclei formation as mechanisms contributing to genomic instability in human cells in our published review paper (chapter I). In chapter II, we investigated changes in chromosome structure and number in cancer cells that survived checkpoint adaptation compared to not-treated cells. Lastly, in chapter III we test PNKP inhibitors and their effect on checkpoint adaptation entrance and survival.

CHAPTER I – REVIEW PAPER

G2/M-Phase Checkpoint Adaptation and Micronuclei Formation as Mechanisms That Contribute to Genomic Instability in Human Cells

Danî Kalsbeek and Roy M. Golsteyn

This chapter has been published by the "International Journal of Molecular Sciences"

November 2017

Abstract

One of the most common characteristics of cancer cells is genomic instability. Recent research has revealed that G2/M phase checkpoint adaptation—entering mitosis with damaged DNA—contributes to genomic changes in experimental models. When cancer cells are treated with pharmacological concentrations of genotoxic agents, they undergo checkpoint adaptation; however, a small number of cells are able to survive and accumulate micronuclei. These micronuclei harbor damaged DNA, and are able to replicate and reincorporate their DNA into the main nucleus. Micronuclei are susceptible to chromothripsis, which is a phenomenon characterised by extensively rearranged chromosomes that reassemble from pulverised chromosomes in one cellular event. These processes contribute to genomic instability in cancer cells that survive a genotoxic anti-cancer treatment. This review provides insight into checkpoint adaptation and its connection to micronuclei and possibly chromothripsis. Knowledge about these mechanisms is needed to improve the poor cancer treatment outcomes that result from genomic instability.

1. Introduction

Most cancer cells have genomes that are extensively altered relative to normal, non-transformed human cells. The Cancer Genome Sequencing Atlas project has sequenced the genomes of solid tumours from thousands of patients, and all showed different chromosomal organisation and DNA sequences. This genomic complexity likely contributes to treatment inefficiency (Network, 2008, 2012; Kandoth et al., 2013).

One way to target cancer cells in treatments is to induce irreparable amounts of DNA damage by the application of genotoxic agents. These agents activate the cell cycle checkpoints, leading to cell cycle arrest and/or cell death (Helleday et al., 2008). However, research has shown that some cancer cells treated with genotoxic anti-cancer drugs can overcome a G2 phase cell cycle arrest and enter mitosis with damaged DNA, a mechanism called G2/M phase checkpoint adaptation (Syljuasen, 2007; Kubara et al., 2012; Swift & Golsteyn, 2014, 2016a). Most cells that undergo G2/M phase checkpoint adaptation (hereafter called checkpoint adaptation) after treatment with a genotoxic agent die in mitosis. However, a small number of those cells survive, and are likely to have extensively altered genomes due to the processes of repair and adaptation (Kubara et al., 2012; Swift & Golsteyn, 2016a). Recent research on checkpoint adaptation led to the idea that this process contributes to genomic instability, hence genomic complexity (Swift & Golsteyn, 2016b).

Investigation of checkpoint adaptation led to the finding that it causes the formation of micronuclei in cells (Tkacz-Stachowska et al., 2011; Lewis & Golsteyn, 2016). Micronuclei are distinct from the main nucleus and encapsulate full lagging chromosomes or fragments of chromosomes that are not incorporated in the main nucleus after anaphase (Terradas et al., 2010; Fenech et al., 2011; Crasta et al., 2012). Micronuclei contribute to genomic instability, and are a characteristic of cancer cells. Cells that undergo checkpoint adaptation show a 50% increase in the number of micronuclei compared with non-treated cancer cells (Tkacz-Stachowska et al., 2011; Lewis & Golsteyn, 2016). The cells containing micronuclei are able to survive for several cycles, and chromosomes enclosed in these micronuclei could be reunited in the main nucleus of the

daughter cells. Furthermore, more than 7.5% of micronuclei in cancer cells were found to contain shattered chromosomes, which is part of a phenomenon called chromothripsis (Stephens et al., 2011; Crasta et al., 2012; Holland & Cleveland, 2012; Zhang et al., 2015; Terradas et al., 2016). Micronuclei are proposed to play a role in the initiation of this phenomenon (Fenech, 2006; Crasta et al., 2012; Storchova & Kloosterman, 2016).

This review provides insight into checkpoint adaptation and its connection to micronuclei and chromothripsis. In reviewing these topics, we hope to provide knowledge for a better understanding of mechanisms that might be involved in poor cancer treatment outcomes as a result of genomic instability. Altered genomes can result in cells that do not respond to death signals, and hence become treatment resistant (Rode et al., 2015). We suggest that cells treated with DNA damaging anti-cancer agents and survive checkpoint adaptation become candidates for cells that sustain further genomic change through the formation of micronuclei and chromothripsis.

2. Checkpoint Adaptation

To maintain the integrity of the genome, cells have cell cycle checkpoints that detect damaged DNA and aneuploidy, and prevent them from transmitting changed genomes to daughter cells (Kastan & Bartek, 2004; Bartek & Lukas, 2007). The majority of cancer cells are mutated in genes encoding tumour suppressors such as p21, p53, or retinoblastoma (Rausch et al., 2012; Kandoth et al., 2013). In normal cells, the activation of p53 leads to a G1/S-checkpoint arrest that prevents cells from proliferating. Mutation in p53 results in a defective G1/S-checkpoint, which means that cells can only rely on a G2/M-checkpoint to detect damaged DNA (Kastan & Bartek, 2004). It is noteworthy that the absence of p53 may be an obligatory event for cells to tolerate a changed genome (Soto et al., 2017).

In addition to the p53-dependent checkpoint, cells respond to damaged DNA by the DNA damage ataxia telangiectasia mutated (ATM)/ataxia telangiectasia and Rad3-related protein (ATR) signaling in which histone H2AX is phosphorylated (histone γH2AX) (Paull et al., 2000). This pathway also phosphorylates checkpoint kinase 1 (Chk1), which in turn prevents the activation of cyclin-dependent kinase 1 (Cdk1) by the induction of Wee1 kinase activity and the inactivation of cell division cycle 25 (Cdc25) phosphatases (Dalal et al., 1999; Rothblum-Oviatt et al., 2001; Jazayeri et al., 2006). Cdk1 is a protein kinase that phosphorylates a large number of substrates whose activities are required for mitosis. Activation of Chk1 thus arrests cells in the G2/M-checkpoint (Lewis & Golsteyn, 2016), and its inactivation by either dephosphorylation (Syljuasen et al., 2006; Kubara et al., 2012) or degradation (Zhang et al., 2005) is required before cells enter mitosis under conditions of damaged DNA signaling. Whereas p53 is mutated in the majority of human tumours, Chk1 mutations in tumours are extremely rare (Solyom et al., 2010). Chk1 can be activated by nearly all genotoxic treatments (Swift & Golsteyn, 2014), including neo-synthetic compounds (Cahuzac et al., 2010). The activation of the DNA damage checkpoints by UV irradiation appears to be more dependent upon the p53 pathway than the Chk1 pathway (Warmerdam et al., 2013).

It has been observed that after treatment with genotoxic agents such as irradiation, topoisomerase I inhibitors, topoisomerase II inhibitors, or cross-linking agents such as cisplatin, cancer cells are able to enter mitosis with damaged DNA. This process is called checkpoint adaptation, and is characterised by three steps: initiation of cell cycle arrest at the G2/M-checkpoint by damaged DNA, overcoming the arrest, and entering mitosis with unrepaired DNA damage (Demarcq et al., 1994; Toczyski et al., 1997; Clifford et al., 2003; Hall & Giaccia, 2006; Syljuasen et al., 2006; Cahuzac et al., 2010). To undergo checkpoint adaptation, Chk1 is either degraded (Zhang et al., 2005) or dephosphorylated (Syljuasen et al., 2006), which enables Cdk1 to be activated despite the presence of damaged DNA (Lewis & Golsteyn, 2016). Checkpoint adaptation is likely to be a primary pathway that leads to cell death after treatment with pharmacological amounts of genotoxic agents in cancer cells (Brown & Attardi, 2005; Kubara et al., 2012).

2.1 Identification of Checkpoint Adaptation

Checkpoint adaptation was first described by Sandell et al. in 1993 as a process in the yeast *Saccharomyces cerevisiae* that allows cells to enter mitosis with unrepaired DNA (Sandell & Zakian, 1993). They demonstrated that specifically mutated haploid yeast cells, which were unable to repair double-stranded DNA breaks (DSB), arrested at the G2/M-checkpoint after the induction of DNA damage. However, instead of undergoing cell death, these cells overcame the checkpoint and entered mitosis with damaged DNA (Sandell & Zakian, 1993). Further studies in yeast revealed that cells identified a relationship between single-stranded DNA and the capacity to exit the G2/M phase checkpoint (Lee et al., 1998). Later, pharmacological approaches enabled the detection of human cancer cells that entered mitosis with damaged DNA (Dewey et al., 1995). Furthermore, human cancer cells treated by ionising radiation (IR) underwent several cell cycles. The DNA in these cells contained damage in the form of gaps, acentric DNA fragments, and chromatid breaks (Hall & Giaccia, 2006). It was suggested that human cancer cells with damaged DNA induced by IR can overcome the G2/M-checkpoint and enter mitosis despite the genomic alterations (Syljuasen,

2007). Syljuåsen investigated this hypothesis in 2006, and found that human osteosarcoma cells treated with 6 Gy IR arrested at the G2/M-transition, where after they entered mitosis without repairing the DNA. This complies with the characteristics of checkpoint adaptation (Syljuasen et al., 2006). In cases where the damage to DNA can be repaired, cells undergo a process known as checkpoint recovery, and continue to proliferate (Bartek & Lukas, 2007).

More recent work investigating checkpoint adaptation in human cancer cells suggests that mitosis plays an important role in the response to treatment with genotoxic agents (Kubara et al., 2012). Cell-based assays were used to observe the events that follow the arrest at the G2/M-transition after cells were treated with genotoxic agents that induced DNA damage. Treatment with cytotoxic and pharmacological amounts of camptothecin (25 nM CPT) induced cells to acquire a rounded morphology after 40 or more hours of treatment, and tested positive for mitotic markers (Figure 1). Human colorectal adenocarcinoma (HT-29) cells treated with a pharmacological concentration of CPT showed histone γH2AX foci in all of the cells arrested at the G2/M-transition with activated Chk1 (Kubara et al., 2012). In addition to CPT, cisplatin-treated or etoposide-treated cells also showed the ability to undergo checkpoint adaptation (Swift & Golsteyn, 2014, 2016a). In cells treated with 30 μM of cisplatin, a pharmacological concentration, 80% of treated cells entered mitosis before dying. On the other hand, at a supra-pharmacological cytotoxic concentration of 100 μM, only 7% of treated cells entered mitosis, whereas the remaining cells died by apoptosis. These outcomes led to the prediction that checkpoint adaptation is a key pathway in cell death induced by genotoxic agents (Swift & Golsteyn, 2016a); however, checkpoint adaptation in human cells treated by ultraviolet light energy has not yet been reported. Notably, approximately 2% of cells that underwent checkpoint adaptation survived and showed increased numbers of micronuclei (Kubara et al., 2012; Lewis & Golsteyn, 2016). For an additional discussion on the importance of concentrations of cytotoxic compounds and cell death, see Swift & Golsteyn and Brown & Attardi (Brown & Attardi, 2005; Swift & Golsteyn, 2014).

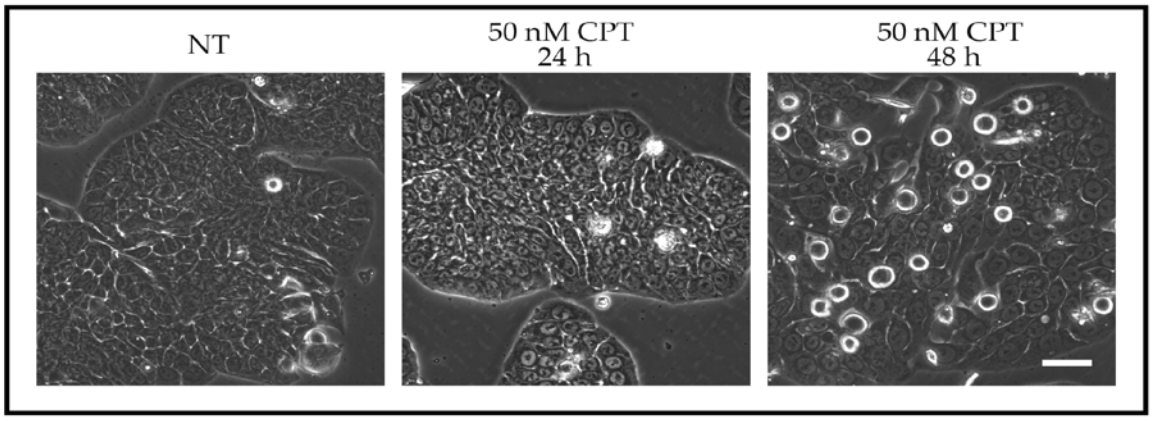

Figure 1. Checkpoint adaptation in human cancer cells. Human HT-29 cells were either not-treated (NT), or treated with a cytotoxic amount of camptothecin (50 nM CPT) and observed by phase-contrast microscopy at 24 or 48 h. The rounded cells in the 48 h image are in mitosis as they undergo the G2/M phase checkpoint adaptation. Refer to Kubara et al. (Kubara et al., 2012) or Swift and Golsteyn (Swift & Golsteyn, 2016a) for addition experimental data of damaged DNA in rounded, mitotic cells. Bar represents 50 µm.

3. Micronuclei

Micronuclei are small DNA containing structures surrounded by one lipid bilayer, which are independent from the main nucleus in a cell. Whole chromosomes, as well as chromosome fragments, can be in micronuclei, depending on how it was formed. The DNA in micronuclei can be replicated, transcribed, and repaired in a manner that is similar to the main nucleus (Kisurina-Evgenieva et al., 2016). However, research on micronuclei *in vitro* has shown that they may have defects in the localisation of structural proteins, such as pores, when compared with the main nucleus (Hoffelder et al., 2004; Terradas et al., 2009; Xu et al., 2011; Crasta et al., 2012; Terradas et al., 2012). Although micronuclei are considered as a marker for genomic change, there are biological processes in which micronuclei appear normally, such as during the embryonic development of species such as *Xenopus* (Lemaitre et al., 1998). The number and size of micronuclei can vary in the cell depending on the origin of the micronucleus (Geraud et al., 1989; Fenech, 1993; Fenech et al., 2011). Micronuclei are tightly associated with mitotic errors, and therefore they are considered indicators of aneuploidy and genomic instability (Fenech, 2007).

3.1 Factors Leading to the Formation of Micronuclei

The formation of micronuclei can be initiated by errors in chromosome segregation or damaged DNA, which can be induced by chemical and physical factors. The factors are divided into two groups: aneugens and clastogens. Aneugens induce the formation of micronuclei that contain complete chromosomes by targeting the segregation of chromosomes into a nucleus. By contrast, clastogens result in micronuclei that contain acentric chromosome fragments, which are caused by the induction of DNA breaks (Hermine et al., 1997; Fenech, 2006; Kisurina-Evgenieva et al., 2016).

3.1.1 Aneugens

Aneugens are chemical antimitotic agents that affect mitotic spindle formation, and thus the segregation of chromosomes. Cells treated with such agents can form micronuclei that contain intact chromosomes. These chemicals can arrest cells in the cell cycle and cause death, including

by apoptosis activated by a p53-dependent pathway (Kisurina-Evgenieva et al., 2016). Human breast carcinoma cells treated with Taxol, vincristine, or nocodazole showed a 20% increase in micronuclei number and cell death rate (Kisurina-Evgenieva et al., 2006). Other types of aneugens can suppress DNA and histone methylation, and disrupt the condensation of chromosomes in the centromere (Fenech, 2006; Heit et al., 2009). These agents can also show a clastogenic effect by the induction of DSBs. Furthermore, metals that bind to DNA and proteins show both aneugenic and clastogenic effects. They can influence gene expression, the condensation of DNA, and mitotic spindle assembly (Luzhna et al., 2013; Kisurina-Evgenieva et al., 2016).

3.1.2 Clastogens

Agents that display a clastogenic effect are anthracycline agents that perturb DNA replication and repair (Luzhna et al., 2013; Kisurina-Evgenieva et al., 2016). In addition, hypoxia and oxidative stress have also been shown to contribute to the formation of micronuclei in cells (Shibata et al., 1996; Snyder & Diehl, 2005). Platinum-based drugs, such as cisplatin, which are used in testicular and ovarian cancers (Kelland, 2007; Helleday et al., 2008), form mono-functional DNA adducts that block replication, which leads to DNA strand breaks and thus causes a clastogenic effect (Swift & Golsteyn, 2014). Treatment with cisplatin was shown to increase the number of micronuclei by 24% to 48% in cultured human glioblastoma cells that underwent checkpoint adaptation (Lewis & Golsteyn, 2016). Most of the physical factors are clastogenic. Physical factors that can lead to micronuclei formation in cells include, for example, changes in pressure and temperature, radiation, UV, and ultrasound (Kisurina-Evgenieva et al., 2016). Radiation exposure causes various DSBs that can lead to chromosomal rearrangements when the fragments are fused in a random order (Krishnaja & Sharma, 2004; Holland & Cleveland, 2012). Exposure to 2 Gy of radiation resulted in DSBs in 80% of human fibroblast cells, and 48 h after treatment, 80% of the cells contained micronuclei, which correlates with the fraction of cells with DSBs (Terradas et al., 2009).

3.2 Micronuclei Formation Pathways

The structure of a micronucleus is dependent on how it was formed. Chemical and physical factors are attributable to the different mechanisms through which micronuclei can be formed. These mechanisms involve changes in protein quantity or defects caused by mutation that affect the nuclear envelope, the structure of the chromosome centromeric region, attachment to spindle microtubules, DSBs, chromoanagenesis, oncogene amplification, and double minute (DM) chromosomes (Kisurina-Evgenieva et al., 2016). In the case of the induction of micronuclei by checkpoint adaptation, disruptions in the structure of centromeric region, defects of attaching to spindle microtubules, and DSBs are believed to be involved.

3.2.1 Defective Microtubule–Kinetochore Attachments

Most micronuclei are formed at the end of mitosis. Defects in the separation of chromosomes in the daughter nucleus leads to the occurrence of aneuploid cells. These cells are used as markers for tumours, and may play a predominant role in tumour initiation and development. Defects in chromosome segregation during mitosis can change how the genome is organised in a cell (Fenech et al., 2011; Luzhna et al., 2013). For example, it may lead to daughter cells that contain micronuclei that enclose either whole intact chromosomes, or chromosomes with structural aberrations (Janssen et al., 2011).

Irregularities in the centromeric region structure of chromosomes and kinetochores can be caused by centromeric DNA replication defects, DNA and histone methylation defects in the centromeric region, and mutations in genes that encode for kinetochore proteins (Kisurina-Evgen'eva et al., 2006; Gieni et al., 2008; Fenech et al., 2011; Bakhoum & Compton, 2012b; Gelot et al., 2015). These defects can lead to the formation of micronuclei, as these chromosomes cannot properly align at the metaphase plate (Crasta et al., 2012). Delayed chromosomes are randomly distributed to one of the daughter cells at the end of mitosis, where they form a micronucleus. These micronuclei may have different fates, depending upon the nuclear envelope that forms around them.

If the lagging chromosome is enclosed by a normal organised nuclear envelope, it might escape subsequent DNA damage. Under these conditions, if a chromosome was unable to bind to microtubules because of damage in the kinetochore, the damage can be repaired, and the chromosome might attach to the mitotic spindle in the subsequent mitosis and no longer form a micronucleus. By contrast, if the chromosome is enclosed by a nuclear envelope that contains irregularities in its organisation, it might be not be correctly replicated, transcribed, or repaired, leading to additional changes in the genome (Crasta et al., 2012; Kisurina-Evgenieva et al., 2016).

Normal kinetochores and microtubules can form incorrect interactions during mitosis, which can be detected and resolved by checkpoint mechanisms. When these incorrect interactions are not resolved, such as when both kinetochores attach to the same division pole, then both chromosomes will be directed to the same daughter cell. When microtubules from both division poles bind to the same kinetochore, a merotelic chromosome interaction is formed, which can also lead to micronuclei harbouring intact chromosomes (Cimini et al., 2001; Cimini et al., 2002; Gregan et al., 2011). Combinations of microtubule dynamics that are guided by motor proteins (Bakhoum & Compton, 2012b) and protein kinases such as Aurora B ensure correct kinetochore–microtubule interactions (Cimini et al., 2006). Aurora B regulates these events by phosphorylating substrates that are proximal to it, depending upon mechanical tension. The overexpression of proteins in the Aurora B mediated correction mechanism can lead to the hyperstabilisation of kinetochore–microtubule attachments, which increases the number of incorrectly attached kinetochores (Bakhoum et al., 2009). Furthermore, new substrates for Aurora B have been identified, such as 53BP1, which participates in kinetochore and microtubule interactions, and if mutated, may lead to micronuclei (Wang et al., 2017).

3.2.2. DSBs and DM-Chromosomes

Acentric fragments are formed during mitosis as a result of DSBs and DM chromosomes, which is a clastogenic effect. These fragments are unable to interact with microtubules, and are randomly

divided between daughter cells. During telophase, these fragments are encapsulated by a generated nuclear envelope that contains lamina and nuclear pores. These micronuclei can be functionally active, and are not excluded from the cell (Shimizu, 2011; Okamoto et al., 2012). One characteristic of these micronuclei is breaks in their DNA. These lesions are caused by the incomplete replication of the DNA in the preceding interphase. Micronuclei that are formed during this process are likely to be degraded. However, when there are no DNA breaks in micronuclei, and the nuclear envelope develops normally, micronuclei are able to function normally in the following interphase (Kisurina-Evgenieva et al., 2016).

3.2.3. Micronuclei Formation in Interphase

Micronuclei can also be formed during interphase by a mechanism called nuclear blebbing. Extrachromosomal pieces of the main nucleus are transported to the nuclear envelope, where a bud is formed. Separation from the main nucleus forms a micronucleus. These micronuclei are typically small, and are located in proximity of the main nucleus. There are two different disturbances that are described as leading to this type of micronuclei: amplified oncogenes, and the appearance of multiple DSBs (Kisurina-Evgenieva et al., 2016).

One of these disturbances leads to the formation of the double minute (DM) micronuclei. DM chromosomes are small, circular fragments of DNA that occur extrachromosomally, and play an important role in tumour genetics. These DM chromosomes mostly contain genes that are amplified. These DM chromosomes are formed in response to the structural rearrangements of chromosomes, such as chromothripsis, after which the pieces are joined together in a circular matter (Stephens et al., 2011; Holland & Cleveland, 2012). Most DM chromosomes have increased copies of oncogenes, which contributes to the proliferative activity of tumour cells (Stephens et al., 2011). The DM micronucleus emerges as a result of the occurrence of these DM chromosomes. It is suggested that the occurrence of DM micronuclei can be a mechanism to exclude DM chromosomes from the cell (Shimizu et al., 2000; Shimizu et al., 2007). DM chromosomes occur at the periphery

of the nucleus during interphase, where they can pass through a lamina break, and get included into a nuclear bud. This bud is a precursor for micronucleus formation, including the DM chromosomes. This suggests that these DM micronuclei that are formed during interphase have irregular nuclear envelopes that restrict them in their functional activity (Utani et al., 2011). These micronuclei can be degraded in the cell (Terradas et al., 2010) or extruded out of the cell (Shimizu et al., 2000).

Nuclear blebbing also produces another type of micronuclei in interphase cells. These micronuclei enclose DNA fragments that are damaged. Treatment with radiation results in many DSBs. The damaged DNA is positive for histone γH2AX, and 24 h after treatment, many micronuclei test positive for γH2AX (Medvedeva et al., 2007). This can be seen as indirect proof that these micronuclei are formed as a result of nuclear blebbing (Kisurina-Evgenieva et al., 2016). It is suggested that enclosing damaged DNA fragments in micronuclei is associated with failing DNA repair mechanisms and cell cycle checkpoints. When this fails, the damaged DNA is included into a micronucleus, and subsequently degraded by autophagy (Terradas et al., 2010).

3.3 Nuclear Envelope

The nuclear envelope is formed from an association of endoplasmic reticulum membranes with chromatin followed by fusion of the endoplasmic reticulum sheets in late anaphase and telophase (Anderson & Hetzer, 2008; Lu et al., 2011). This formation requires the recruitment of proteins, which eventually form the major structures of the envelope such as nuclear pore complexes, nuclear lamina for envelope stabilisation, and the proteins for the inner nuclear membrane (Burke & Ellenberg, 2002). The inner nuclear membrane proteins bring the endoplasmic reticulum to the chromatin, and connect the lamina to the membrane (Gant & Wilson, 1997). The nuclear envelope is crucial to chromatin organisation in the main nucleus, as it determines the compactness, functional activity and structural organisation of chromatin. These factors are influenced by proteins that are involved in the structure maintenance, and the transport between the nucleus and the cytoplasm (Kisurina-Evgenieva et al., 2016).

Terradas et al. reported that the capacity to replicate DNA differed among micronuclei in cells. Almost half of the micronuclei that were formed in response to irradiation in human lymphocyte cells were able to replicate their DNA. However, only 9% of the micronuclei in human fibroblast cells had this capacity after exposure to radiation (Obe et al., 1975; Terradas et al., 2009). DNA replication in micronuclei can occur asynchronously relative to the replication of the main nuclear DNA. Delayed replication is thought to be caused by a reduction in the number of nuclear pores and deficiencies in the transport of proteins between the micronucleus and the cytoplasm. The integrity of the nuclear envelope is necessary to ensure the access of macromolecules to the genome inside the envelope.

Undamaged micronuclei may also show dysfunctions in the recruitment of proteins involved in DNA replication and repair (Crasta et al., 2012; Terradas et al., 2012). Micronuclei show similarities with the main nucleus; however, the nuclear lamina is not properly organised (Hatch et al., 2013). As a consequence, the nuclear envelope collapses, and functioning of the undamaged micronuclei are affected, because the changes in lamin B1 organisation impair transcription and replication in the main nucleus (Spann et al., 1997; Spann et al., 2002; Tang et al., 2008). Hatch et al. identified that the disruption of the micronucleus causes an accumulation of damaged DNA (Hatch et al., 2013). It was suggested that damaged DNA in the micronucleus is an outcome of a deficient replication event (Xu et al., 2011; Crasta et al., 2012). DNA replication sensitises an intact micronucleus to DNA damage that is triggered by micronuclear disruption. The deficiencies in transcription and genomic replication, as well as damaged DNA, can all contribute to aneuploidy in different ways. Defective transcription can lead to a short-term aneuploidy in interphase cells. If segregated chromatin encodes crucial regulators for mechanisms involved in genomic stability, it could lead to permanent genome alterations. Furthermore, deficiencies in replication can lead to the entry into mitosis, with irregular amounts of DNA causing the daughter cells to be aneuploid (Terradas et al., 2009; Crasta et al., 2012; Hatch et al., 2013). Damaged DNA in micronuclei might lead to DNA shattering in interphase and mitosis. DNA fragments are believed

to be reassembled randomly, leading to massive genomic rearrangements, through a process called chromothripsis (Stephens et al., 2011; Crasta et al., 2012). It is shown that there is a clear association between the collapse of the nuclear envelope in the micronucleus, and an increase in the amount of DNA damage (Hatch et al., 2013). This will lead to the pulverisation of the immature condensed chromosomes when cells enter mitosis. This pulverisation is accompanied by several DSBs and chromothripsis (Crasta et al., 2012).

The formation of one type of micronuclei can lead to the production of other types of micronuclei in the subsequent cell cycle. In this case, the newly formed micronucleus is likely to contain a nuclear envelope with fewer than normal nuclear pores, which leads to the deregulation of the nuclear-cytoplasmic transport. These micronuclei will undergo delayed genomic replication compared with the main nucleus, and will continue through the G2 phase (Crasta et al., 2012). However, these micronuclei are likely to constitute the basis for the formation of premature condensed chromosomes. Mitotic entrance with DNA that is not completely replicated results in the development of various micronuclear DSBs or chromothripsis, which can lead to amplification of the genome and formation of DM micronuclei (Meyerson & Pellman, 2011; Crasta et al., 2012).

The asynchronous replication observed in micronuclei is likely due to a disrupted nuclear envelope that affects the intake of proteins required for DNA replication (Hatch et al., 2013; Terradas et al., 2016). Another factor that may delay DNA replication is damaged DNA, which could potentially be amplified if a cell enters mitosis. In experiments using cultured M059K cells, almost 50% of the micronuclei contained histone γH2AX, which suggests that these micronuclei had damaged DNA (Figure 2) (Lewis & Golsteyn, 2016). The damage signal was linked to DNA replication, because the frequency of histone γH2AX positive micronuclei was reduced when DNA replication was blocked. An increase in histone γH2AX positive micronuclei could be induced by treating cells with cisplatin. This suggests that the asynchronously DNA replication of the main nucleus and the micronucleus may be the cause of continuous DNA damage.

Micronuclei in normal cells, and in some cancer cells, can result in a p53-mediated cell cycle arrest followed by apoptotic cell death (Kisurina-Evgenieva et al., 2006; Apraiz et al., 2011). However, there is evidence that cancer cells have the ability to exclude micronuclei (Fenech et al., 2011; Luzhna et al., 2013), which can promote survival when cells are treated with chemotherapy (Kisurina-Evgenieva et al., 2016). In p53 wildtype cancer cells, the exclusion of the micronucleus can result in the stimulation of the cell cycle and tumour development. Genetic alterations drive aneuploidy and genomic instability, which in turn promote the cancer configuration. Micronuclei are found to be major contributors to genomic instability and genomic rearrangements (Kisurina-Evgenieva et al., 2016).

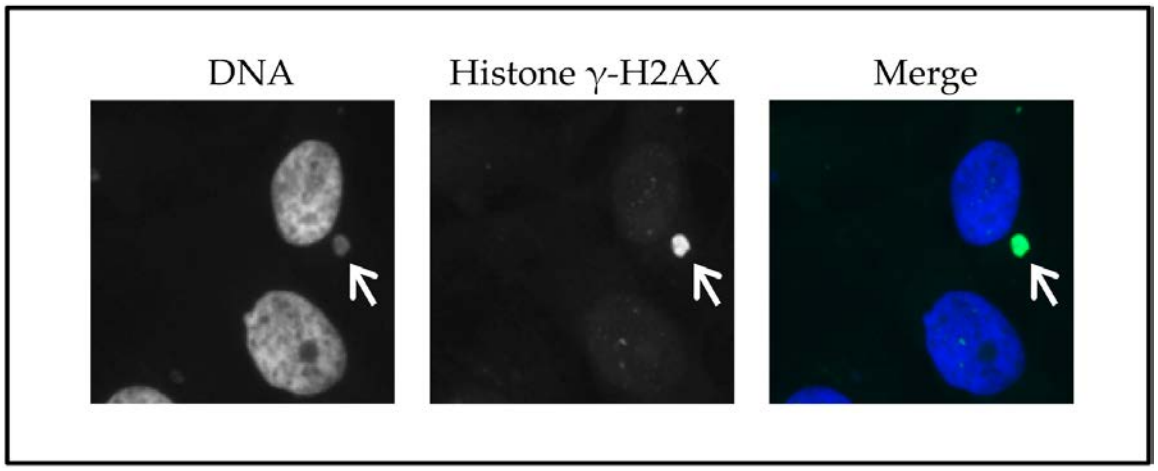

Figure 2. Micronuclei can signal damaged DNA independently of a main nucleus. HT-29 cells that survived checkpoint adaptation were cultivated. Cells were then fixed, stained with DAPI to identify nuclei and micronuclei, and treated with antibodies to histone γ-H2AX to detect damaged DNA. The arrow points to a micronucleus that is positive for damaged DNA, whereas the main nuclei do not signal damaged DNA. For further information, see Lewis and Golsteyn (Lewis & Golsteyn, 2016).

4. Checkpoint Adaptation and Micronuclei

Chang et al. identified that cells that underwent checkpoint adaptation after treatment with genotoxic agents contained increased levels of micronuclei (Chang et al., 1999). This relationship was found in fibrosarcoma cells (HT1080). The genotoxic agents, doxorubicin, aphidicolin, cisplatin, etoposide, vincristine, cytarabine and γ-irradiation, were tested at concentrations that induced 85% growth inhibition after 4 days of continuous exposure. Notably, the treated cells showed a 45–66% increase in the number of micronuclei (Chang et al., 1999). Lewis and Golsteyn (2016) demonstrated that glioblastoma cells treated with 30 μM cisplatin underwent checkpoint adaptation and had an increased number of micronuclei per cell, more cells that contained micronuclei, and an increased number of nucleoplasmic bridges. These micronuclei persisted for at least 8 days after treatment (Lewis & Golsteyn, 2016). Inhibition of Chk1 allowed more cells to enter mitosis with damaged DNA (Mak et al., 2015), and led to more cells having micronuclei when compared with cells that were treated with only a genotoxic agent. Finally, preventing checkpoint adaptation by co-treatment with a Cdk1 inhibitor reduced the number of cells that had micronuclei. These findings suggest that checkpoint adaptation is linked to the presence of micronuclei (Lewis & Golsteyn, 2016). The notion that HT-29 cells showed an increased number of micronuclei when deficient for Chk1 supports the previous observation (Petsalaki et al., 2014). These micronuclei, which possess a nuclear lamina, were able to replicate their genome independently and asynchronously compared with the main nucleus (Okamoto et al., 2012; Lewis & Golsteyn, 2016).

5. Chromothripsis

Stephens et al. first described chromothripsis in 2010 by identifying the event whereby hundreds of rearrangements occur in the genome (Stephens et al., 2011). It is a one-off catastrophic incident in which hundreds of extensive genomic rearrangements occur to one or few chromosomes after the random reattachment of the pulverised chromosomes. It is seen in about 3% of all cancers (Stephens et al., 2011), especially in brain and bone tumours (Storchova & Kloosterman, 2016). In the majority of the cases, chromothripsis will lead to cell death, but it is suggested that cells that survive do so because they have acquired a selection advantage due to their extensively altered genomes. These cells are characterised by three different advantageous genomic modifications: the loss of tumour suppressor genes, the gain of function oncogenes, and/or the formation of fusion genes. Chromothripsis can create mutations that can promote cancer development (Rode et al., 2015). Neuroblastoma, several myelomas, melanoma, and acute myeloid leukemia all show poor disease outcomes that are strongly associated with chromothripsis (Magrangeas et al., 2011; Molenaar et al., 2012; Rausch et al., 2012; Hirsch et al., 2013).

Crasta et al. studied micronuclei in cancer cells and found that DNA in these micronuclei was damaged during its replication. They also found that 7.6% of micronuclei contained pulverised chromosomes (Crasta et al., 2012). This pulverisation is part of a phenomena called chromothripsis. Micronuclei are proposed to be one of the main factors that cause chromothripsis (Zhang et al., 2015). In 2015, Zhang et al. provided a first indication of how chromothripsis can be acquired by using live cell imaging and single cell genome sequencing. They suggested that the enclosure of chromosomes in micronuclei is an important factor that contributes to the acquisition of the DNA lesions seen in chromothripsis (Zhang et al., 2015). These micronuclei are a result of cell division defects, and it was shown that whole chromosomes encapsulated in micronuclei acquire DNA damage. Subsequently, damaged chromosomes can re-enter daughter nuclei, and possibly integrate mutations into the genome (Crasta et al., 2012). Chromosomes in micronuclei are under-replicated, and accumulate damaged DNA (Crasta et al., 2012; Hatch et al., 2013). This under-replication of

chromosomes in the micronucleus causes an asymmetry in DNA copy number between the daughter nuclei, what identifies the missegregated chromosome and leads to de novo chromosome missegregation. This notion provides evidence for the suggestion that the rearrangements seen in micronucleated cells after division occur on the chromosome that is encapsulated in the micronucleus. Another piece of evidence is that only the missegregated chromosome accumulated chromosomal rearrangements after the division of the micronucleated cell. This feature has never been observed in normally segregated chromosomes after division in micronucleated cells, as well as control cells. To conclude, rearrangements are correlated with the chromatid that has been identified by the gained haplotype in the micronucleus (Zhang et al., 2015).

This intrachromosomal phenomenon, along with the encapsulation of one or more chromosomes into a micronucleus, affects genomic structure. This can result in translocations between the encapsulated chromosomes. Zhang et al. suggest that the reassembly of DNA fragments in a micronucleus can produce ring structures whose formation might be associated with chromothripsis. These ring structures are seen in a number of human cancers with missegregated chromosome origins (Garsed et al., 2014; Zhang et al., 2015). The formation of ring structures from fragmented chromosomes is a possible mechanism that is responsible for the production of double minute chromosomes (Carroll et al., 1988), which have been linked to chromothripsis (Zhang et al., 2013).

A consequence of chromothripsis is the loss of chromosomes fragments (Stephens et al., 2011). However, the precise mechanism is not yet understood. Research by Zhang et al. reported that the chromatid can indeed be shattered, with the distribution of DNA pieces between the daughter nuclei. Loss of DNA fragments was explained by the separation of these fragments into daughter nuclei that did not expand and did not become part of the final cell culture (Zhang et al., 2015).

Mechanisms That Might Lead to Chromothripsis

The mechanism that is proposed to be most plausible for chromosome pulverisation in micronuclei is entrance into mitosis before the DNA in the micronucleus has been completely replicated (Liu et al., 2011; Liu et al., 2012; Kinsella et al., 2014). The nuclear envelope of a micronucleus fails to disassemble during mitosis, which is crucial to maintain chromosome fragments. The nuclear envelope can be maintained because mitotic Cdks are unable to enter the micronucleus, nor phosphorylate lamins that are required for the disassembly of the nuclear envelope (Crasta et al., 2012). If the nuclear envelope of the micronucleus disassembles in mitosis, fragments would enter the cytoplasm and would be lost. This failure to disassemble leads to the segregation of intact nuclei to one of the daughter cells. The micronucleus then keeps these chromosome fragments enclosed in a compartment until the following cell cycle. It is suggested that the persistence of a micronucleus into the second interphase after its formation provides a repair mechanism to ligate the fragments that were formed randomly by incomplete DNA replication, and form rearranged chromosomes (Holland & Cleveland, 2012).

Pulverised and rearranged chromosomes can be reincorporated in the main nucleus to contribute to genomic instability, and thus cancer promotion. Although the fate of the micronucleus is still unknown, it is suggested that these micronuclei are excluded from the cell, degraded, or reincorporated in the main nucleus. The first two options result in the loss of these chromosomes, but the third option gives rise to genomic rearrangement (Crasta et al., 2012; Zhang et al., 2015).

6. Pharmacological Inhibition of Checkpoint Adaptation

There is now sufficient information available to test pharmacological approaches that can target adaptation to checkpoints in cancer cells. One of the checkpoints targeted is the spindle assembly checkpoint (SAC). The anaphase-promoting complex (APC) can be inhibited by a small molecule tosyl-L-arginine methyl ester (TAME) that displaces the IR tail of Cdc20 or Cdh1. It is suggested that the prodrug, proTAME, prevents the inactivation of SAC (Zeng et al., 2010). Another approach that is being investigated is the inhibition of the anaphase-promoting complex/cyclosome (APC/C). APC/C is an ubiquitin ligase that triggers the metaphase–anaphase shift and mitotic exit through the ubiquitin-dependent destruction of proteins such as securin and cyclin B1. The small molecule Apcin binds to Cdc20, and inhibits the APC/C-dependent proteolysis and mitotic exit by disrupting the interaction between the APC/C and Cdc20, which prevents the ubiquitination of D-box-containing substrates (Sackton et al., 2014). Anti-microtubule cancer drugs (AMCDs) can also be used to prevent mitotic exit with deformed spindles by targeting the Fcp1–Wee1–Cdk1 axis. During mitotic arrest induced by AMCDs, Fcp1 activates Wee1 by dephosphorylation, which in turn lowers the Cdk1 activity. This results in a weakened SAC-dependent mitotic arrest, and thus promotes mitotic exit and survival. The inhibition of Wee1 strengthens the SAC and extends mitosis, hence enhancing AMCD-induced cell death (Visconti et al., 2015).

Another checkpoint that is being targeted is the G2/M-checkpoint. One approach is targeting the DNA damage response (DDR). This response regulates DNA damage repair and signaling to cell cycle checkpoints (Hanahan & Weinberg, 2011). The dysregulation of the DDR has been associated with cancer, as it alters the response to DNA, damaging anti-cancer therapies. If a DNA repair pathway fails, its function might be taken over by another DDR pathway, which may be increased, and supports resistance to DNA damaging agents. The ATM and ATR pathways signal DNA damage and have multiple downstream targets. Therefore the inhibition of checkpoints is suggested to sensitise DNA-damaging agents. This can be done with an ATM inhibitor such as KU55933, Wee1, and Cdc25 inhibitors, or Chk1 inhibitor UCN-01. More recently two novel ATR

inhibitors, VE-821 and NU6027, have been identified to sensitise cells to various DNA damaging agents (Curtin, 2012). By inhibition of this pathway, the cells bypass the checkpoints, enter mitosis, and undergo mitotic catastrophe and, eventually, cell death (Visconti et al., 2016). Most of the inhibitors showed little impact on cell cycle distribution or viability. However, they prevented cell cycle arrest and increased the cytotoxicity of DNA damaging agents (Curtin, 2012).

7. Conclusions

We are proposing that checkpoint adaptation, micronuclei, and chromothripsis are distinct cancer cell phenomena that are linked by biological steps and enhance genomic instability (Figure 3). In experimental models, checkpoint adaptation provides an occasion for cells to produce micronuclei. The micronuclei isolate a portion of the genome from the main nucleus and create conditions that could lead to chromothripsis. Cells have checkpoints and DNA repair mechanisms as well as death pathways that greatly reduce the likelihood of genomic instability; however, examples of these events have been observed in experimental models. Checkpoint adaptation is a more frequent outcome than apoptosis when pharmacological concentrations of genotoxic agents are used in experimental models (Swift & Golsteyn, 2016a). Although most of these cells die in mitosis, a small number of cells survive and generate micronuclei that are prone to DNA damage and chromothripsis. All of the aforementioned processes may contribute to genomic instability, and thus are able to promote the development of resistance against treatments. As a new expanding field, we require a better understanding of the biochemical pathways that participate in these events. In the case of checkpoint adaptation, the role of mitotic kinases such as Cdk1 may be re-evaluated with a view on genomic instability in cancer cells. A better understanding of the acquisition of genomic instability in cancer cells will provide more insight in how cancer patients can be treated more effectively.

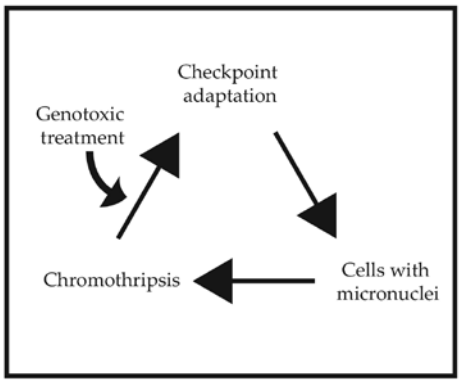

Figure 3. A schematic diagram of a relationship between checkpoint adaptation, micronuclei, and chromothripsis. A genotoxic treatment starts the cycle by initiating checkpoint adaptation.

CHAPTER II – MANUSCRIPT RESEARCH PAPER

Cancer cells that survive checkpoint adaptation (mitosis with damaged DNA) acquire major chromosomal rearrangements

1. Introduction

One of the hallmarks of cancer is genomic instability (Hanahan & Weinberg, 2011). Genomic instability can contribute to tumour heterogeneity, treatment resistance and poor patient outcomes and relapse. The tumour genomes of hundreds of patients with solid tumours have been sequenced by The Cancer Genome Sequencing Atlas project and showed that all tumours presented a different DNA sequence and chromosome organization. The cause of this variation is not known, however, it is suggested that it is caused by genomic instability (Network, 2008, 2012). A form of genomic instability is chromosome instability (CIN). CIN is considered a defect that includes gains or losses of whole chromosomes (numerical) (Tanaka & Hirota, 2016) and/or rearrangements, or gain or losses, of fractions of chromosomes (structural) (McClelland, 2017). These chromosomal changes might favour carcinogenesis and affect therapeutic response to anti-cancer agents (Birkbak et al., 2011; Bakhoum & Compton, 2012a; Tanaka & Hirota, 2016; McClelland, 2017). Therefore, a better understanding of how CIN and genomic complexities arise is needed (Vargas-Rondon et al., 2017).

One of the proposed mechanisms through which chromosome instability can arise is through checkpoint adaptation (Hunter et al., 2006; Ding et al., 2012; Lewis & Golsteyn, 2016). Checkpoint adaptation is a process in which cancer cells treated with a pharmacological concentration of a genotoxic agent arrest in G2/M phase, overcome the arrest and enter mitosis with damaged DNA (Toczyski et al., 1997; Syljuasen et al., 2006; Swift & Golsteyn, 2018). Histone γH2AX signals damaged DNA, which is activated by DNA damage kinases ATM/ATR. In addition, ATM/ATR phosphorylates checkpoint kinase 1 (Chk1) (Jazayeri et al., 2006), preventing the activation of the mitotic enzyme Cdk1, through the activation of Wee1 (Rothblum-Oviatt et al., 2001) and inhibition of Cdc25C (Dalal et al., 1999). Upon genotoxic treatment, it was thought that

cells would die by apoptosis due to extensive amounts of damaged DNA. However, it has been shown that cells can undergo another cell death pathway, which is checkpoint adaptation (Kubara et al., 2012; Swift & Golsteyn, 2016a). Cells undergoing checkpoint adaptation show dephosphorylated Chk1, allowing entrance into mitosis (Kubara et al., 2012; Jiang et al., 2017).

The majority of the cells undergoing checkpoint adaptation likely die by mitotic catastrophe. However, some cells are able to survive, with supposedly chromosomal changes due to their mitotic exit with damaged DNA (Brown & Attardi, 2005), and their acquisition of micronuclei (Lewis & Golsteyn, 2016). However, the consequences of checkpoint adaptation in cancer cells are not well understood. In this study, we used the human colorectal adenocarcinoma HT-29 cell experimental model to study the relationship between checkpoint adaptation and chromosome instability. HT-29 cells have previously been reported to undergo checkpoint adaptation in response to pharmacological concentrations of CPT (Kubara et al., 2012). We observed increased chromosome instability as one of the consequences of checkpoint adaptation, by studying chromosome structural and numerical aberrations in cells surviving checkpoint adaptation. More knowledge about the outcomes of checkpoint adaptation might provide insight into the biology behind treatment inefficiency seen in recurrent cancers.

2. Results

2.1 Cells treated with CPT acquire a rounded morphology

To induce checkpoint adaptation, we incubated HT-29 cells with 50 nM CPT, which is a pharmacological concentration (Rivory et al., 1997). Cells were either not treated or treated with 50 nM CPT and observed by phase-contrast light microscopy to analyze cell rounding, which is a marker for checkpoint adaptation (Kubara et al., 2012; Swift, 2015), at 24 and 48 hours after treatment. At 24 hours after treatment, the not-treated culture had few rounded cells. In the CPT-treated culture, nearly all cells were flat and adherent. At 48 hours after treatment, not-treated cells showed a similar cell morphology as those of 24 hours after treatment. By contrast, the CPT-treated culture showed an increase of rounded cells that was relatively large, compared to the not-treated culture (Figure 4A). The percentages of rounded cells in the not-treated culture were determined; 2.7% ± 0.6% of the cells showed a rounded morphology at 24 hours after treatment, which was similar to the 1.8% ± 0.3% observed after 48 hours. In the CPT-treated culture at 24 hours after treatment, 0.8% ± 0.7% of the cells showed a rounded morphology, compared to an increase to 11.4% ± 1% at 48 hours after treatment (Figure 4B). The increase in the number of rounded cells has been previously recognized as the process of checkpoint adaptation (Kubara et al., 2012).

2.2 Cells treated with CPT stain positive for histone γH2AX and pH3

To confirm that the rounded cells were undergoing checkpoint adaptation, we analyzed them for markers of damaged DNA (histone γH2AX) and mitosis (phospho-Ser^{10} histone H3 (pH3)). HT-29 cells were either not treated or treated with 50 nM CPT for 48 hours, and stained with DAPI, anti-histone γH2AX antibodies, and anti-pH3 antibodies. By immunofluorescence microscopy, we observed that few cells stained for histone γH2AX in the not-treated culture, compared to a large number of cells in the CPT-treated culture, as expected (Figure 5A). We determined that 0.5% ± 0.1% of the cells stained for histone γH2AX in the not-treated culture, compared to 98.3% ± 0.4% of the cells in the CPT-treated culture (Figure 5B). By immunofluorescence microscopy, we

observed that few cells stained for pH3 in the not-treated culture. In the CPT-treated culture, an increase in the number of pH3 signals were observed compared to the not-treated culture (Figure 5C). The percentage of cells staining for pH3 was 3.6% ± 0.3% in the not-treated culture, compared to 9.8% ± 1.4% in the CPT treated culture, as expected (Kubara et al., 2012) (Figure 5D). These observations confirmed that the cells treated with CPT have damaged DNA as they enter mitosis; hence, they are undergoing checkpoint adaptation.

2.3 Some cells survive checkpoint adaptation and proliferate

We collected cells that underwent checkpoint adaptation to be able to study the consequence of this phenomenon. Cells were either not treated or treated with 50 nM CPT. After 48 hours of treatment (TDC - total and DNA-damaged cells), a mechanical shake-off was performed to isolate the weakly adherent mitotic cells (MDC – mitotic and DNA-damaged cells) from the adherent flattened interphase cells (IDC – interphase and DNA-damaged cells). We recultivated the flattened cells (IDC) that remained attached after mechanical shake-off and observed that new rounded cells (MDC) appeared by 2 hours (Figure 6).

The ability to isolate MDCs from other cells enabled us to isolate cells that entered checkpoint adaptation. With these cells (MDCs) we could answer questions about chromosomes in cells that survive checkpoint adaptation. For subsequent experiments, we recultivated not-treated and 48 hour CPT-treated MDCs to study cell fate after checkpoint adaptation. Mock-treated cells and checkpoint adaptation survival (CAS) cells were observed by time-lapse light microscopy at the day of cell collection (0 d), 1, 2, 3, 6 and 10 days after checkpoint adaptation. We observed that mock-treated cells were able to settle in the culture flask and proliferate, forming colonies. In the CAS culture, we observed that cells were able to settle in the culture flask with abnormal cell morphologies, compared to mock-treated cells, but did not proliferate until day 6 of recultivation. We observed that the majority of CAS cells showed a multinuclear state at day 1, 2, and 3 of

recultivation, compared to the mononucleated mock-treated cells. After 6 days of recultivation of CAS cells, we observed cell morphologies similar to those of the mock-treated culture (Figure 7).

The number of cells that were able to survive after recultivation was determined. Not-treated and CPT-treated MDCs recultivated at 0 d were counted as well as the number of cells that survived for 10 days after recultivation. We determined that 59.8% ± 8.8% of not-treated MDCs were able to survive. By contrast, 1.9% ± 0.3% of CPT-treated MDCs survived checkpoint adaptation, as expected (Kubara et al., 2012) (Figure 8A). By phase-contrast light microscopy, we determined the number of CAS cells that showed abnormalities in the nucleus compared to the mock-treated culture (Figure 7). The percentages of multinucleated and mononucleated cells per culture were determined for 10 days. The mock-treated culture had very few multinucleated cells and reached a maximum of 0.4% of the total population at day 1 after recultivation. The number of multinucleated cells in the CAS culture was high and decreased from 94.7% ± 4.6% at day 1 to 8.4% ± 6.9% at day 6 after recultivation, after which the cells showed a mononucleated state (Figure 8B). These data showed that CAS cells acquired an abnormal nuclear state.

2.4 DNA damage signals decrease over time in survival cells

Knowing that cells that survived checkpoint adaptation acquired abnormal nuclei as compared to the mock-treated culture, we suspected that these cells might contain damaged DNA. We tested for damaged DNA signals in these survival cells by immunofluorescence microscopy. We either not treated cells or treated cells with 50 nM CPT, used as a genotoxic control, for 24 hours. In parallel, MDCs that were not treated and CPT treated for 48 hours, were recultivated for 1, 2 and 6 days (CAS). Cells were stained with DAPI and anti-histone γH2AX antibodies. Images of the CAS cultures are shown in Figure 9A. We observed that few not-treated cells stained for histone γH2AX, compared to a high number of cells staining in the CPT-treated culture. In the CAS 1 culture, we observed that the majority of cells stained for histone γH2AX. The number of cells staining for histone γH2AX was decreased in the CAS 2 culture compared to the CPT-treated and CAS 1

culture. After 6 days of recultivation (CAS 6), the number cells staining for histone γH2AX signals was low, similar to the not-treated culture (Figure 9A).

We determined the percentage of cells staining for histone γH2AX. In the not-treated and mock-treated cultures, the number of cells staining for histone γH2AX was approximately 2.4% ± 2.7%. In the CPT-treated culture, 95.3% ± 1.6% of the cells stained for histone γH2AX. In the CAS 1 culture the number of cells staining for histone γH2AX was 84.6% ± 8.2%, compared to 37.0% ± 16.5% in the CAS 2 culture and 1.3% ± 0.8% in the CAS 6 culture (Figure 9B). These data showed that cells surviving checkpoint adaptation signalled damaged DNA and that these signals decreased over time. Based on these observations, we decided to investigate if we could detect changes in chromosomes of cells undergoing checkpoint adaptation (48 hours of treatment), two days after surviving checkpoint adaptation (at the time the majority of the histone γH2AX signals were reduced) and ten days after surviving checkpoint adaptation.

2.5 Cells undergoing checkpoint adaptation show chromosome structure abnormalities

To study chromosomal changes during checkpoint adaptation, we observed chromosome configuration and chromosome structures in HT-29 cells. Cells were either not treated or treated with 50 nM CPT for 48 hours. MDCs were collected and stained with DAPI and nucleic acid probes to centromeres and telomeres. By immunofluorescence microscopy, we observed different chromosome configurations, which we categorized as follows: SCC (shattered chromosome configuration), ICC (intermediate chromosome configuration; both shattered and whole chromosomes), and WCC (whole chromosome configuration). In not-treated cells, we observed whole chromosomes, with centromeres localized in the center of the chromosomes and telomeres localized at the tips of the chromosomes, as expected. In CPT-treated cells, we observed that the majority had shattered chromosomes (SCC and ICC) with abnormally localized centromeres and telomeres, compared to not-treated cells (Figure 10A).

We determined the percentage of cells that fitted into each category. In the not-treated culture, 100% of the cells had a WCCs, whereas in the CPT-treated culture only 3.3% ± 2.2% had a WCC. The percentage of CPT-treated cells with an ICC was 53.3% ± 8.5%, and 43.3% ± 8.7% of the cells had SCCs. Of the cells that had an SCC, we observed that 64.5% ± 9.3% had clustered centromeres (as shown in Figure 10; CPT – SCC) (Figure 10B).

We then determined chromosome numbers per cell in cells that had an ICC or WCC. The average chromosome number per cell in the not-treated culture was 65.7 ± 0.7 with a range from 35 to 81 chromosomes per cell. In the CPT-treated culture, the average chromosome number per cell was 71.7 ± 8.0, with a wide range from 26 to 154 chromosome like structures per cell (Figure 11A).

To study chromosome structure rearrangements in the cells undergoing checkpoint adaptation, we counted dicentric chromosomes and acentric chromosomes by immunofluorescence microscopy (Figure 10). These structural rearrangements, dicentric and/or acentric chromosomes, were observed in 11.8% ± 1.5% of not-treated cells and in 89.6% ± 5.8% of CPT-treated cells (Figure 11B). Of the not-treated cells that had structural rearrangements, we observed that 65.5% ± 8.7% of the cells contained at least one dicentric chromosome and 42.8% ± 16.6% of the cells contained at least one acentric chromosome. No cells of the not-treated culture were observed to have both dicentric and acentric chromosomes. In the CPT-treated culture, we determined that that 60.0% ± 15.9% of the rearranged cells contained at least one dicentric chromosomes, 100% of the rearranged cells contained at least one acentric chromosome and 50.0% ± 12.4% of the rearranged cells acquired both dicentric and acentric chromosomes (Figure 11C). On average, a not-treated rearranged cell contained 0.5 ± 0.2 dicentric chromosomes and 0.4 ± 0.3 acentric chromosomes. A CPT-treated rearranged cell contained 1.6 ± 0.8 dicentric chromosomes and 15.6 ± 7.7 acentric chromosomes, on average (Figure 11D). These observations of changes in the chromosome configuration, chromosome number and increased structural rearrangements in cells undergoing checkpoint adaptation, supported the notion that these cells contained chromosomal changes.

2.6 Cells treated with CPT show abnormal chromosome configurations

The changes in chromosome structures in MDCs upon CPT treatment led us to ask if these cells contained interchromosomal rearrangements. We set to observe one chromosome, chromosome 7, in cells that undergo checkpoint adaptation. Chromosome 7 was chosen because of its relatively long length and there are four copies of it in HT-29 cells, instead of two copies as in normal cells (Kawai et al., 2002). Cells were either not treated or treated with 50 nM CPT for 48 hours. MDCs were collected and stained with DAPI and chromosome 7 specific probes. By immunofluorescence microscopy, we observed four chromosome 7 signals in not-treated cells on average. In CPT-treated cells, we observed a higher number of chromosome 7 signals, compared to not-treated cells (Figure 12A).

We determined the number of chromosome 7 signals per cell in each treatment and set a signal number threshold at 30. All cells with a higher signal number than 30 were considered to have a score of 30 to calculate the mean. We confirmed that not-treated cells contained 4.0 ± 0.1 chromosomes 7 signals per cell on average, as expected, with a range from 2 to 6 signals. Strikingly, we determined 19.6 ± 1.1 chromosome 7 signals per cell on average, in the CPT-treated culture, supporting the shattered and intermediate chromosome configuration. In this culture, the chromosome 7 signal number was widely distributed between 0 and 30 (Figure 12B). These data showed that cells undergoing checkpoint adaptation have a shattered and intermediate chromosome configuration, as confirmed by chromosome 7 staining.

2.7 CAS 2 cells acquire chromosome structure rearrangements

Knowing that cells undergoing checkpoint adaptation had chromosomal changes and that damaged DNA signals decreased over time, we asked whether cells surviving checkpoint adaptation still contained chromosomal changes. To study this, we recultivated MDCs of not-treated and CPT-treated cells for two days. Mitotic cells were collected from the mock-treated (mock-treated 2) and checkpoint adaptation survival (CAS 2) culture and stained with DAPI and with nucleic acid probes

to centromeres and telomeres. By immunofluorescence microscopy, we observed a WCC in the mock-treated culture, with centromeres localized in the center of the chromosomes and telomeres localized at the tips of the chromosomes, as expected. In CAS 2 culture, we observed that some cells contained shattered chromosomes (SCC or ICC), but the majority showed a WCC. Chromosomes of the cells in this culture showed abnormalities in their localization of centromeres and telomeres, compared to mock-treated cells (Figure 13A).

We determined the percentages of cells that fitted into the following configuration categories: SCC, ICC or WCC. In the mock-treated culture, 100% of the cells had a WCCs, compared to 69.6% ± 8.6% in the CAS 2 culture. The percentage of CAS 2 cells with an ICC was 26.0% ± 8.6%, and 4.4% ± 0.8% of the cells had SCCs. Of the cells that showed an SCC, we observed that 40.7% ± 5.5% had clustered centromeres.

We then counted chromosome numbers per cell in cells that had an ICC or WCC and observed that the average chromosome number per cell in the mock-treated culture was 67.7 ± 0.5 with a range from 38 to 80 chromosomes per cell. In the CAS 2 culture, the average chromosome number per cell was 38.8 ± 2.2, with a wide range from 8 to 128 chromosome like structures per cell (Figure 14A).

Structural rearrangements of chromosomes (i.e. dicentric and acentric chromosomes) were observed in 12.2% ± 0.4% of the cells in the mock-treated culture and in 86.3% ± 3.0% of the cells in the CAS 2 culture (Figure 14B). Of the mock-treated with structural rearrangements, we observed that 76.6% ± 14.5% of the cells contained at least one dicentric chromosome, 30.0% ± 10.0% of the cells contained at least one acentric chromosome, and 6.7% ± 6.7% of the cells contained both dicentric and acentric chromosomes. In the CAS 2 culture, we determined that that 71.9% ± 2.1% of the rearranged cells contained at least one dicentric chromosome, 77.3% ± 11.8% of the rearranged cells contained at least one acentric chromosome and 52.5% ± 12.7% of the rearranged cells contained both dicentric and acentric chromosomes (Figure 14C). On average, a mock-treated rearranged cell contained 0.8 ± 0.1 dicentric chromosomes and 0.3 ± 0.1 acentric chromosomes. A

CAS 2 rearranged cell contained 1.2 ± 0.2 dicentric chromosomes and 4.2 ± 1.4 acentric chromosomes, on average (Figure 14D). These data confirmed that cells that survived checkpoint adaptation for two days had readily observable structural and numerical chromosome changes, compared to mock-treated cells.

2.8 CAS 2 cells show abnormal chromosome configurations

We then investigated whether cells that survived for two days after checkpoint adaptation had interchromosomal rearrangements in chromosome 7. Cells were either not treated or treated with 50 nM CPT for 48 hours. MDCs were recultivated for two days. Mitotic mock-treated and CAS 2 cells were collected by mechanical shake-off and stained with DAPI and chromosome 7 specific probes. By immunofluorescence microscopy, we observed four chromosome 7 signals in mock-treated cells on average (Figure 15A). We determined the number of chromosome 7 signals per cell survival culture and set a signal number ceiling at 30. All cells with a higher signal number than 30 were considered to have a score of 30 to calculate the mean. We confirmed that mock-treated cells contained 4.0 ± 0.1 chromosomes 7 signals per cell on average, as expected, with a range from 3 to 5 signals. We determined 7.6 ± 0.1 chromosome 7 signals per cell on average, in the CAS 2 culture, which were widely distributed between 0 and 30 signals (Figure 15B).

Interchromosomal rearrangements and/or chromosome 7 signal number rearrangements (chromosome 7 signals different from four) were observed in 20.5% ± 5.6% of mock-treated cells and in 85.6% ± 7.2% of CAS 2 cells (Figure 15C). These data showed that, in addition to structure rearrangements, chromosomes had interchromosomal rearrangements at two days after checkpoint adaptation.

2.9 CAS 10 cells have a lower chromosome number per cell than mock-treated cells

Next, we studied the chromosomes of cells that survived checkpoint adaptation for ten days. Mitotic cells were collected from the mock-treated and checkpoint adaptation survival (CAS 10) culture and stained with DAPI and with nucleic acid probes to centromeres and telomeres. By

immunofluorescence microscopy, we observed a whole chromosome configuration, with centromeres localized in the center of the chromosomes and telomeres localized at the tips of the chromosomes, as expected, in the mock-treated culture. In CAS 10 culture, cells showed a similar chromosome configuration, and centromere and telomere localization as the mock-treated culture (Figure 16A). We determined the percentages of cells that fitted into the following configuration categories: SCC, ICC or WCC. In the mock-treated culture, 100% of the cells had a WCC. In the CAS 10 culture, 99.2% ± 0.8 of the cells had a WCC and the remaining cells had an ICC (Figure 16A).

We counted the number of chromosomes per cell and observed that the average chromosome number in mock-treated cells was 68.5 ± 0.6, with a distribution from 42 to 74 chromosomes. In the CAS 10 culture, the average chromosome number per cell was 51.1 ± 2.3, with a distribution from 7 to 72 chromosomes per cell (Figure 17A).

Structural rearrangements of chromosomes, dicentric and acentric chromosomes, were observed in 11.6% ± 1.6% of the cells in the mock-treated culture and in 18.7% ± 2.4% of the cells in the CAS 10 culture (Figure 17B). Of the cells that had structural rearrangements, we observed that in the mock-treated culture 23.3% ± 14.5% of the cells contained at least one dicentric chromosome, 57.5% ± 3.8% of the cells contained at least one acentric chromosome, and no cells contained both dicentric and acentric chromosomes. In the CAS 10 culture, we determined that 57.5 ± 3.8% of the rearranged cells contained at least one dicentric chromosome, 57.5% ± 10.9% of the rearranged cells contained at least one acentric chromosome, and 15.0% ± 7.6% of the rearranged cells contained both dicentric and acentric chromosomes (Figure 17C). On average, a mock-treated rearranged cell contained 0.2 ± 0.1 dicentric chromosomes and 0.8 ± 0.1 acentric chromosomes. A CAS 10 rearranged cell contained 0.6 ± 0.0 dicentric chromosomes and 0.7 ± 0.1 acentric chromosomes, on average (Figure 17D). These data showed that cells that survived checkpoint adaptation after ten days had fewer chromosomes than mock-treated cells, however, the percentage

of cells with chromosome structure rearrangements and the number of rearrangements (i.e. dicentric and acentric chromosomes) per cell were comparable to those of the mock-treated culture.

2.10 CAS 10 cells show chromosome 7 rearrangements

At day ten after checkpoint adaptation survival, cells showed similar levels of chromosome structure rearrangements as the mock-treated culture. We then asked if chromosome 7 signals were also similar in both cultures, by staining mitotic mock-treated and CAS 10 cells with DAPI and chromosome 7 specific probes. By immunofluorescence microscopy, we observed 4 chromosome 7 signals in mock-treated cells on average. In CAS 10 cells, we observed interchromosomal rearrangements and a lower number of chromosome 7 signals, compared to mock-treated cells. (Figure 18A). We determined the number of chromosome 7 signals per cell survival culture. We confirmed that mock-treated cells contained 4.0 ± 0.1 chromosomes 7 signals per cell on average, as expected, with a range from 3 to 6 signals. We determined 2.9 ± 0.3 chromosome 7 signals per cell on average, in the CAS 10 culture, which were distributed between 0 and 9 signals (Figure 18B). Interchromosomal rearrangements and/or chromosome 7 signal number rearrangements (chromosome 7 signals different from 4) were observed in 18.5% ± 1.9% of mock-treated cells and in 78.3% ± 4.6% of CAS 10 cells (Figure 18C). These data showed that cells, after ten days surviving checkpoint adaptation, had increased numbers of interchromosomal rearrangements of chromosome 7 and chromosome 7 signal number abnormalities, compared to mock-treated cells.

2.11 Confirmation of the outcomes of checkpoint adaptation in a second cell line

We then investigated whether our observations about the consequences of checkpoint adaptation upon chromosomes in HT-29 cells extended to a second, unrelated cell line, M059K. M059K cells were either not-treated or treated with 50 nM CPT for 72 hours to induce checkpoint adaptation. By phase-contrast light microscopy, we observed a cell morphology in the CPT-treated culture that was similar to that of not-treated cells at 24 and 48 hours after treatment. Few rounded cells were observed. At 72 hours after treatment, we observed an increase in number of rounded cells in the

CPT-treated culture, compared to not-treated cells, indicating checkpoint adaptation (Figure 19A). We determined that the number of rounded cells in the not-treated culture was approximately 2% ± 0.3% at all time points. In the CPT-treated culture we observed 0.6% ± 0.1%, 2.8% ± 0.3% and 5.8% ± 1.3% rounded cells, at 24, 48 and 72 hours after treatment, respectively (Figure 19B). These data confirmed that M059K cells can undergo checkpoint adaptation, as previously reported (Kubara et al., 2012; Lewis & Golsteyn, 2016).

To study whether M059K cells that undergo checkpoint adaptation had damaged chromosomes, we looked at the chromosome configuration in either not-treated or 72 hour CPT-treated cells. MDCs were collected by mechanical shake-off and stained with DAPI. By immunofluorescence microscopy, we observed a whole chromosome configuration in not-treated cells. In the CPT-treated culture, few cells with a whole chromosome configuration were observed and the majority of the cells contained shattered chromosomes (Figure 20A). We determined the chromosome configuration of both cultures and categorized them into SCC, ICC and WCC, as we had done for HT-29 cells. In the not-treated culture, 97.8% ± 2.2% of the cells had a WCC and the remaining 2.2% ± 2.2% of the cells had an ICC. In the CPT-treated culture, 4.5% ± 2.2% of the cells showed a WCC, 53.3% ± 1.9% showed an ICC, and 42.2% ± 1.1% of the cells showed an SCC (Figure 20B). These data were similar to those obtained from the experiments using the HT-29 cell line and revealed that CPT treatment changed the chromosome configuration in M059K cells.

We then determined whether the cells surviving checkpoint adaptation for four days had chromosomal changes. M059K cells have a longer cell cycle duration than HT-29 cells, therefore we recultivated these cells for four days instead of the two days as in HT-29, which allowed both cell lines to pass through two cell cycles before analysis. The cells were either not treated or treated with 50 nM CPT for 72 hours. MDCs were collected and recultivated for four days. Mitotic mock-treated and CAS 4 cells were collected by mechanical shake-off and stained with DAPI and chromosome 7 specific probes. By immunofluorescence microscopy, we observed 4 chromosome

7 signals on average in the mock-treated culture, with few cells showing interchromosomal rearrangements. In the CAS 4 culture, we observed an increase in the signal number and a decrease in the signal size, indicating broken chromosomes, and an increase of interchromosomal rearrangements compared to mock-treated cells (Figure 21A). We determined that mock-treated cells contained 4.4 ± 0.1 chromosome 7 signals per cell, on average, compared to 16.1 ± 1.6 signals in the CAS 4 culture. The signal number in the CAS culture was widely distributed between 2 and more than 30 signals per cell, compared to a range from 2 to 8 in the mock-treated culture (Figure 21B). These data acquired from a second cell line, M059K, were similar in trend as those using the HT-29 cell line.

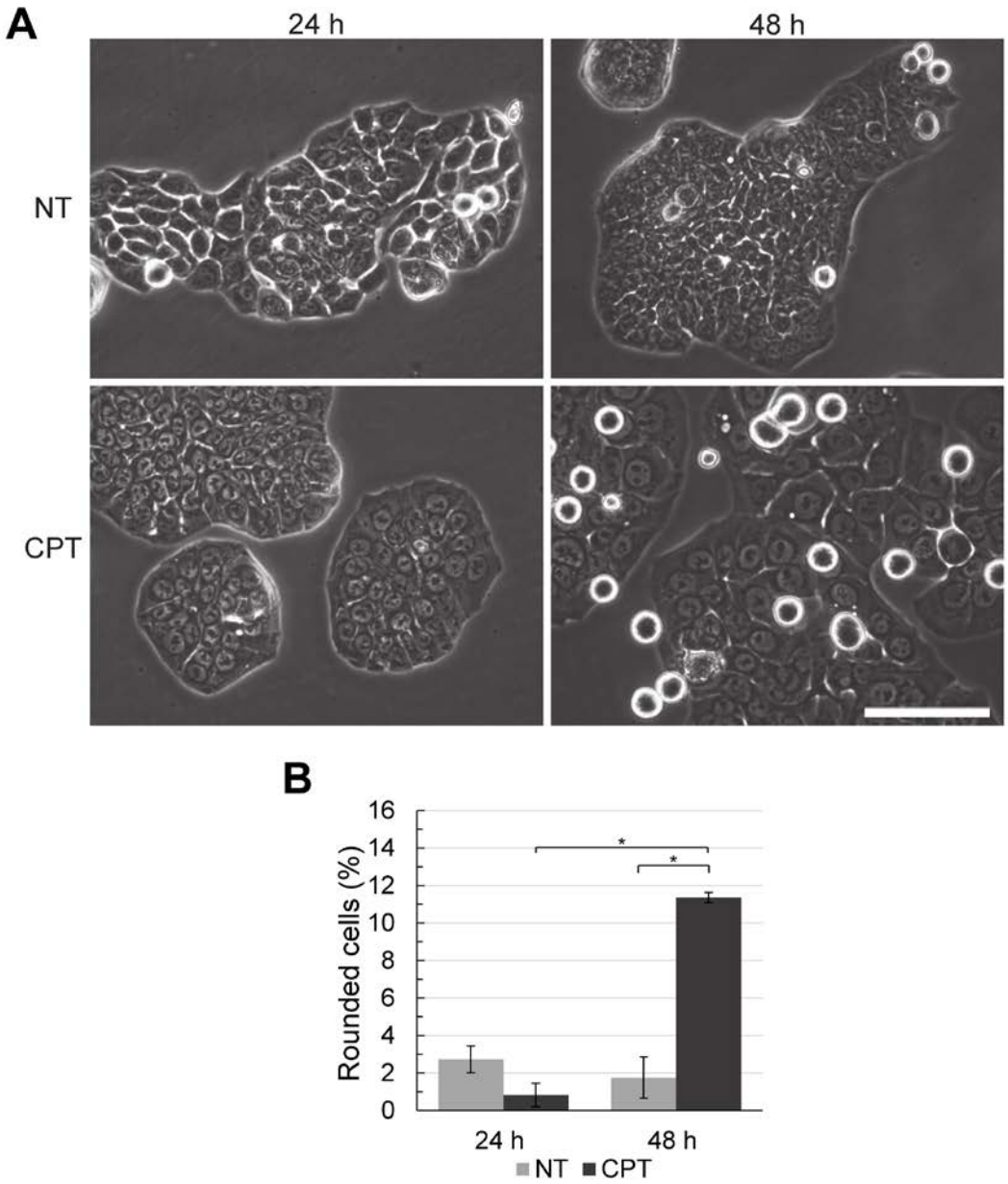

Figure 4. Cells treated with CPT acquire a rounded morphology. (A) HT-29 cells were either not treated (NT) or treated with 50 nM CPT (CPT) and observed by phase-contrast light microscopy at 24 and 48 h. Scale bar = 100 µm. (B) Cells were prepared and analyzed as described in A. The percentages of rounded cells were determined and compared between not-treated (NT) and CPT-treated (CPT) cultures at 24 and 48 h, and within treatments between time points. The mean percentages from three separate experiments ± standard error of the mean (SEM) are shown. The asterisks show significant differences, $p < 0.05$.

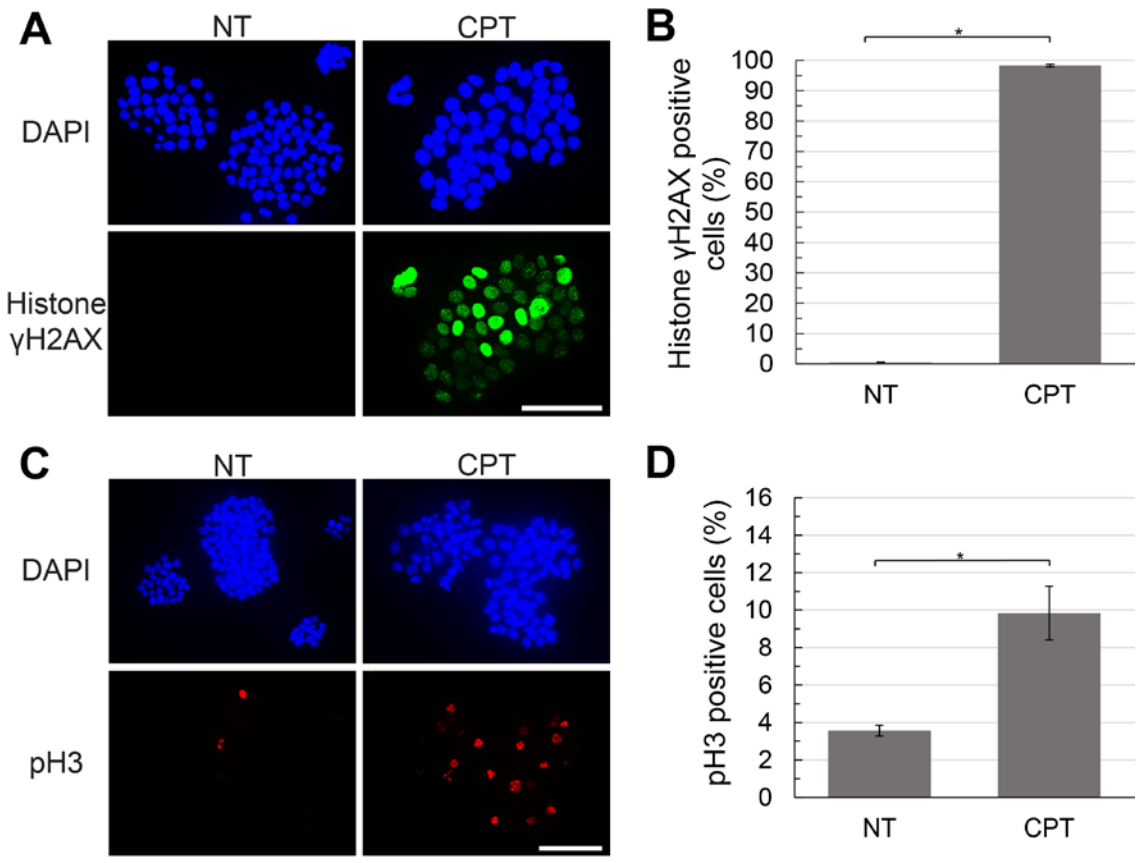

Figure 5. Cells treated with CPT have damaged DNA and enter mitosis. (A) HT-29 cells were either not-treated (NT) or treated with 50 nM CPT (CPT) for 48 h, and stained with DAPI (blue) to detect DNA and with anti-histone γH2AX antibodies (green). Cells were analyzed by immunofluorescence microscopy. Scale bar = 100 µm. (B) Cells were prepared and analyzed as described in A. The percentages of cells staining for histone γH2AX were determined for the not-treated (NT) and CPT-treated (CPT) culture, at 48 h. The mean percentages ± SEM from three separate experiments are shown. The asterisk shows significant difference, $p < 0.05$. (C) HT-29 cells were either not-treated (NT) or treated with 50 nM CPT (CPT) for 48 h, and stained with DAPI (blue) to detect DNA and with anti-phospho-Ser^{10} histone H3 antibodies (pH3 – red). Cells were analyzed by immunofluorescence microscopy. Scale bar = 100 µm. (D) Cells were prepared and analyzed as described in C. The percentage of cells staining for phospho-Ser^{10} histone H3 (pH3) was determined for the not-treated (NT) and CPT-treated (CPT) culture, at 48 h. The mean percentages ± SEM from three separate experiments are shown. The asterisk shows significant difference, $p < 0.05$.

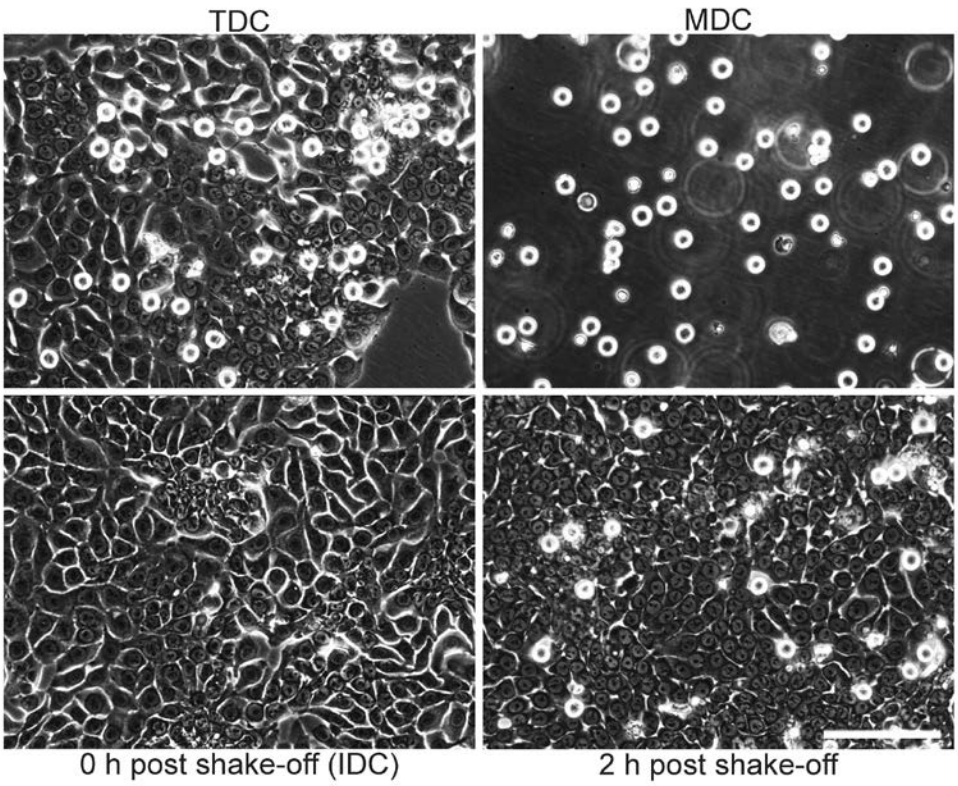

Figure 6. Cells that undergo checkpoint adaptation acquire a rounded morphology and can be collected by mechanical shake-off. HT-29 cells were treated with 50 nM CPT and observed by phase-contrast light microscopy. At 48 hours after treatment, the population of cells (TDC-total and DNA-damaged cells) contains a mix of interphase cells and cells in mitosis with a rounded morphology. Rounded cells were collected by mechanical shake-off (MDC – mitotic and DNA-damaged cells), leaving flattened interphase cells (IDC – interphase and DNA-damaged cells). New rounded cells appeared within 2 h in the IDC culture (2 h post-shake-off). Scale bar = 150 μm.

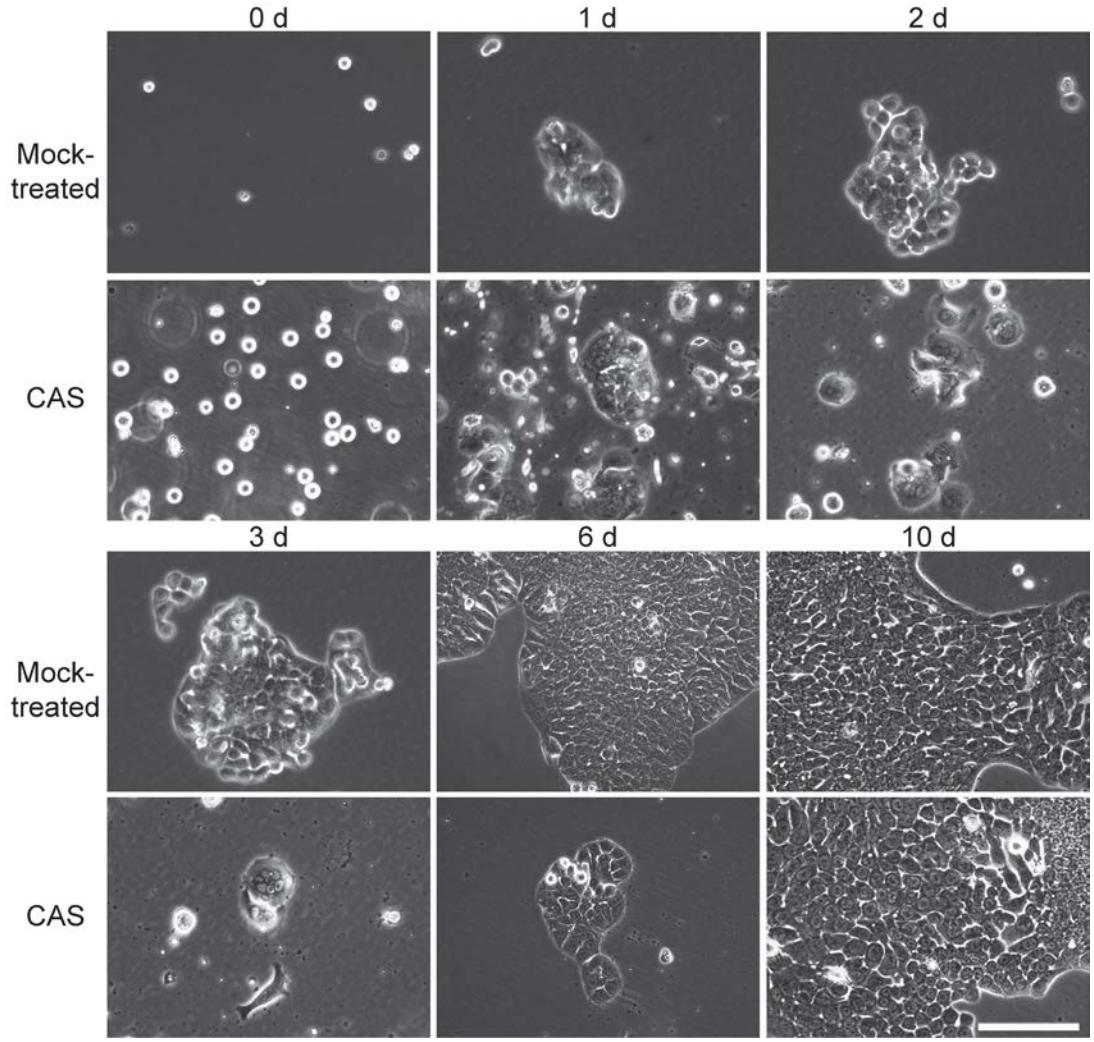

Figure 7. A low percentage of CPT-treated cells survive checkpoint adaptation and continue to proliferate. HT-29 cells were either not treated or treated with 50 nM CPT. After 48 hours, MDCs (mitotic and DNA-damaged cells) were collected by mechanical shake-off from the not-treated culture (Mock-treated) and the CPT-treated culture (CAS; checkpoint adaptation survival) and recultivated for 10 days. Cells were observed by time-lapse light microscopy at the moment of cell collection (0 d), and 1, 2, 3, 6 and 10 days (d) after checkpoint adaptation. Scale bar = 150 μm.

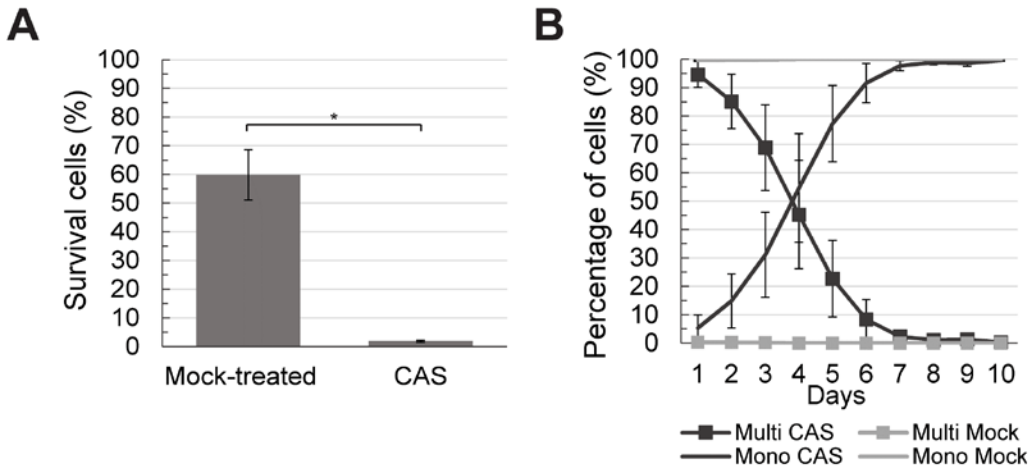

Figure 8. Cells that undergo checkpoint adaptation and survive show an abnormal nuclear state. (A) HT-29 cells were either not treated or treated with 50 nM CPT. After 48 hours, MDCs (mitotic and DNA-damaged cells) were collected by mechanical shake-off from the not-treated culture (Mock-treated) and the CPT-treated culture (CAS; checkpoint adaptation survival) and recultivated for 10 days. The percentage of cells surviving in each culture was determined. The mean percentages ± SEM from three separate experiments are shown. The asterisk shows significant difference, $p < 0.05$. (B) Cells were prepared and analyzed as described in A and were observed by time-lapse light microscopy for ten days. The percentage of cells with one nucleus (Mono) or more than one nuclear structure (Multi) was determined for each culture. The mean percentages ± SEM from three separate experiments are shown.

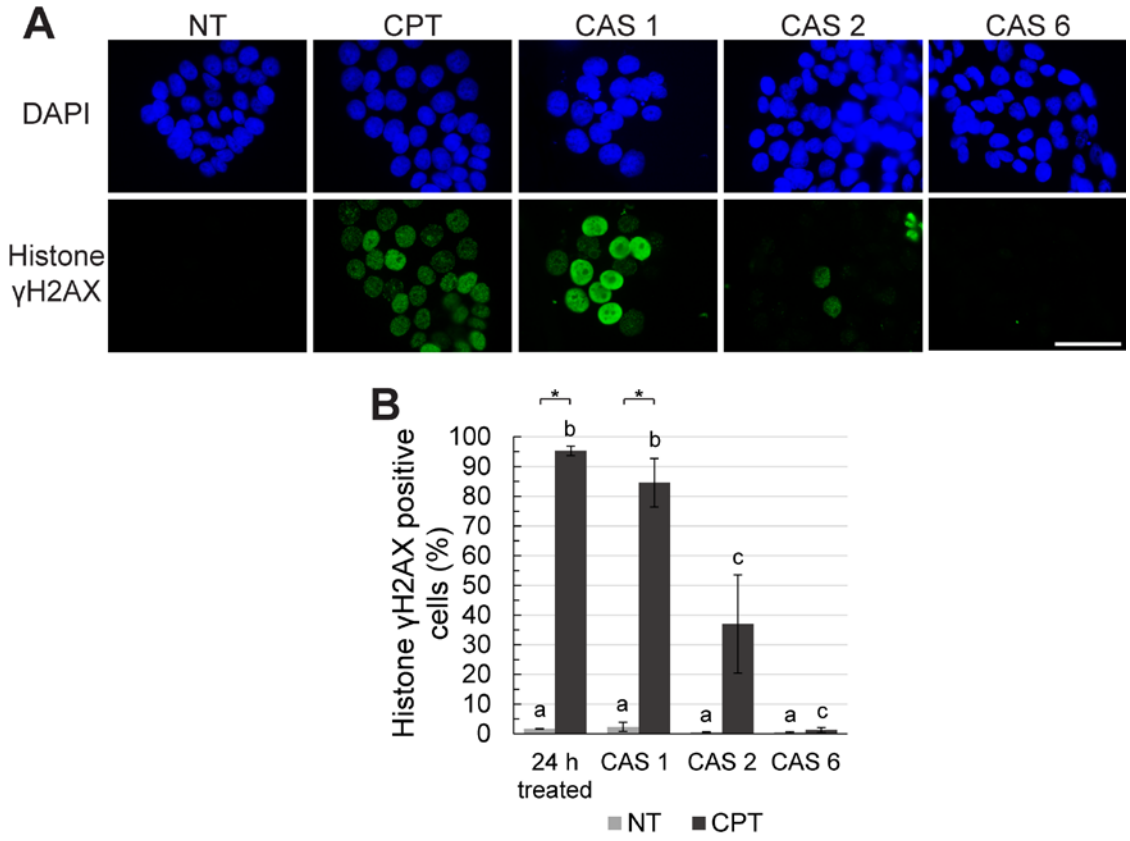

Figure 9. Damaged DNA signals decrease over time in cells that survive checkpoint adaptation. (A) HT-29 cells were either not treated (NT) or treated with 50 nM CPT (CPT) for 24 h, as controls, or treated with 50 nM CPT for 48 h and collected by mechanical shake-off. The MDCs (mitotic and DNA-damaged cells) were recultivated and analyzed at day 1 (CAS 1), 2 (CAS 2) and 6 (CAS 6). Cells were stained with DAPI (blue) to detect DNA and anti-histone γH2AX antibodies (green) and analyzed by immunofluorescence microscopy. Scale bar = 50 µm. (B) Cells were prepared and analyzed as described in A. The percentages of cells staining for histone γH2AX were determined for all cultures of A, including mock-treated cultures (NT – CAS 1, 2 and 6). The mean percentages ± SEM from three separate experiments are shown. The asterisks show significant differences between treatments within a time point, $p < 0.05$. The letters represent significant differences between time points within a treatment (NT – a, CPT – b and c), samples with different letters are significantly different from each other, $p < 0.05$.

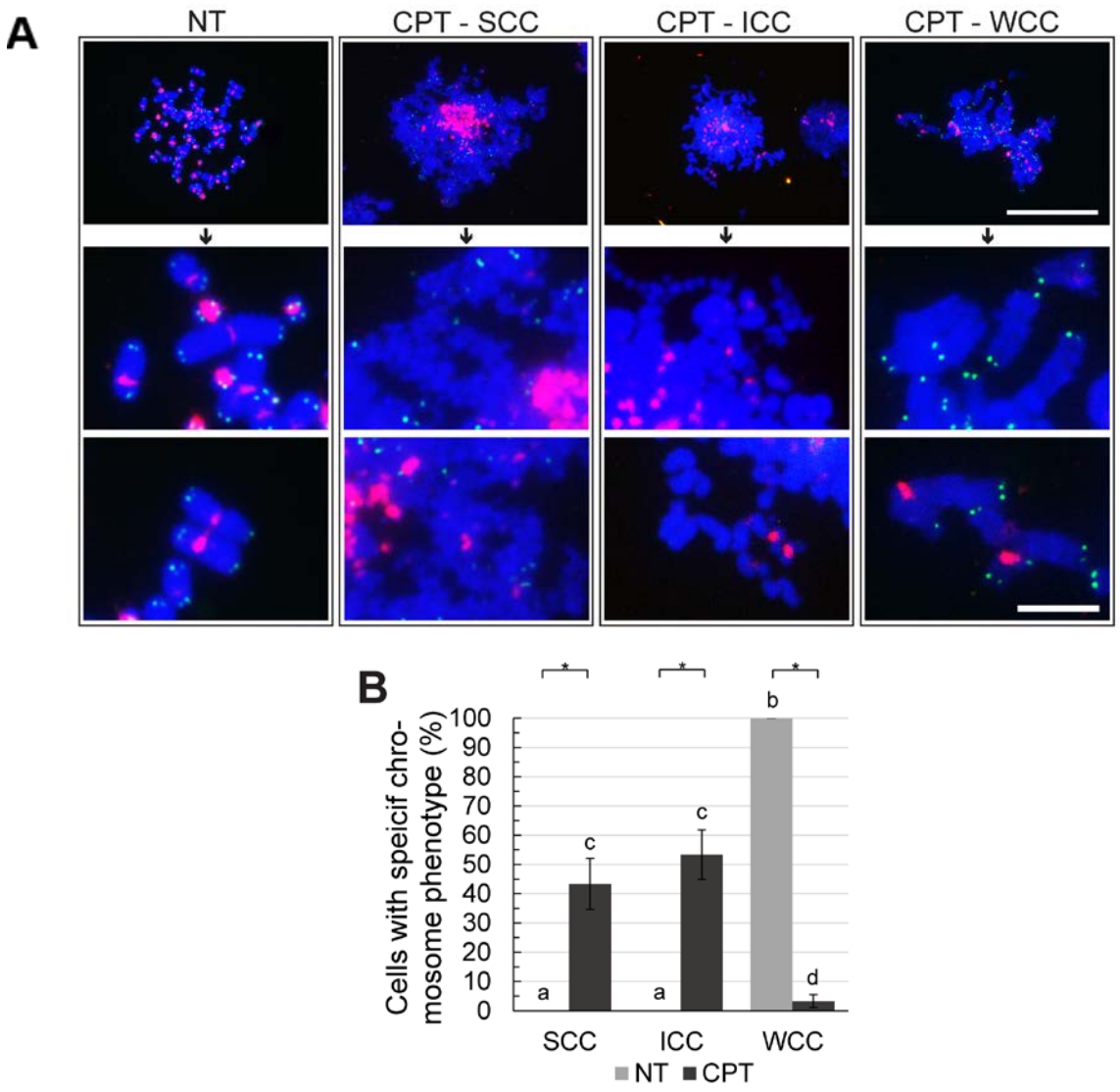

Figure 10. Cells that undergo checkpoint adaptation have abnormal chromosome configurations. (A) HT-29 cells were either not treated (NT) or treated with 50 nM CPT (CPT) for 48 h. MDCs (mitotic and DNA-damaged cells) were collected and stained with DAPI, (blue) to detect condensed chromosomes, centromere probes (red) and telomere probes (green), and observed by immunofluorescence microscopy. The top panel shows one mitotic cell per configuration (SCC – shattered chromosome configuration, ICC – intermediate chromosome configuration and WCC - whole chromosome configuration). Scale bar = 25 µm. Bottom panels show enlargements of chromosomal structures in the above shown mitotic cell. Scale bar = 5 µm. (B) Cells were prepared and analyzed as described in A. The percentages of cells with a SCC, ICC or WCC were determined. The mean percentages ± SEM from three separate experiments are shown. The asterisks show significant differences between treatments within each category, $p < 0.05$. The letters represent significant differences between categories within a treatment (NT – a and b, CPT – c and d), samples with different letters are significantly different from each other, $p < 0.05$.

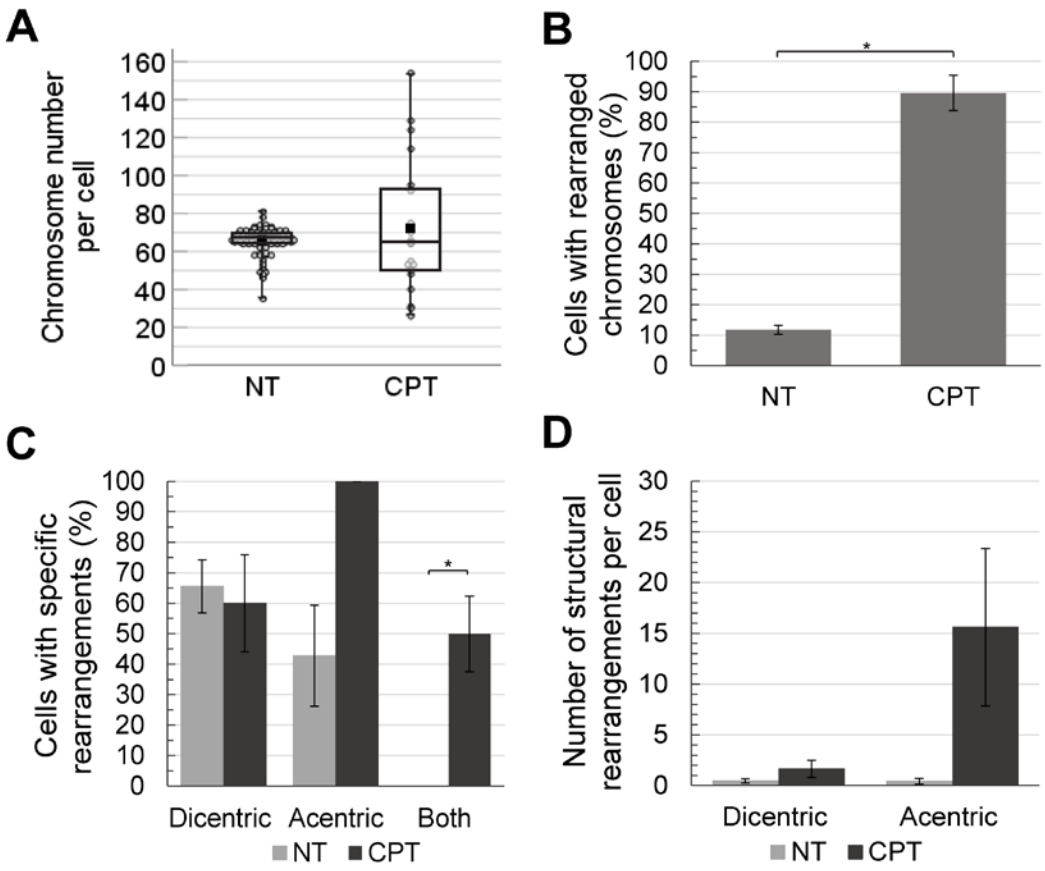

Figure 11. Cells that undergo checkpoint adaptation have changes in chromosome number and chromosome structure. (A) HT-29 cells were either not treated (NT) or treated with 50 nM CPT (CPT) for 48 h. MDCs (mitotic and DNA-damaged cells) were collected, and stained with DAPI (blue) to detect condensed chromosomes, centromere probes (red) and telomere probes (green), and observed by immunofluorescence microscopy. The number of chromosomes per cell were counted and the average (black marker), minimum and maximum (whiskers) are shown by the boxplot. The boxplot represents data from the total of non-SCC (shattered chromosome configuration) cells of three separate experiments taken together (NT n=104, CPT n=20), each cell is represented by a dot. No significant difference between the NT and CPT was measured, although the range in numbers differed greatly, $p < 0.05$. (B) Cells were prepared and analyzed as described in A. The percentages of non-SCC (shattered chromosome configuration) cells with rearranged chromosome structures (i.e. dicentric/acentric chromosomes) were determined. The mean percentages ± SEM from three separate experiments are shown. The asterisk shows significant difference, $p < 0.05$. (C) Cells were prepared and analyzed as described in A. The percentages of rearranged cells with dicentric chromosomes, acentric chromosomes, or both structural rearrangements were determined. The mean percentages ± SEM from three separate experiments are shown. The asterisk shows significant difference between treatments within a specific type of rearrangement, $p < 0.05$. (D) Cells were prepared and analyzed as described in A. The average number of specific rearrangements (dicentric or acentric) per cell was determined. The mean number of rearrangement per cell ± SEM from three separate experiments are shown. No significant difference was determined between treatments, $p < 0.05$.

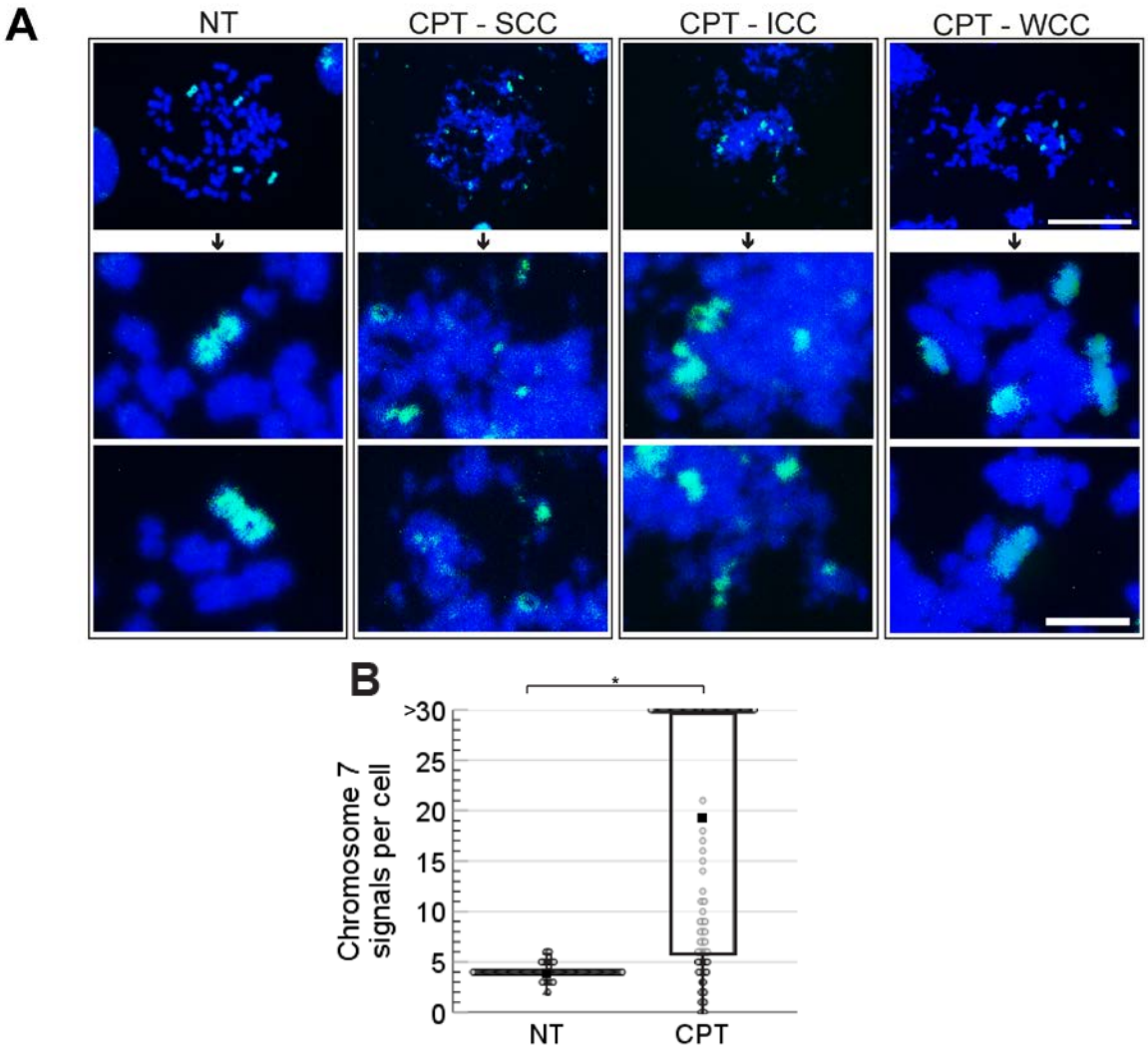

Figure 12. Analysis of chromosome 7 in cells undergoing checkpoint adaptation. (A) HT-29 cells were either not treated (NT) or treated with 50 nM CPT (CPT) for 48 h. MDCs (mitotic and DNA-damaged cells) were collected and stained with DAPI (blue), to detect condensed chromosomes and chromosome 7 probes (green). Cells were observed by immunofluorescence microscopy. The top panel shows one mitotic cell per configuration (SCC – shattered chromosome configuration, ICC – intermediate chromosome configuration and WCC – whole chromosome configuration). Scale bar = 25 µm. Bottom panels show enlargements of chromosome 7 in the above shown mitotic cell. Scale bar = 5 µm. (B) Cells were prepared and analyzed as described in A. The number of chromosome 7 signals were counted and the average (black marker), minimum and maximum (whiskers) are shown in the boxplot. The boxplot represents data from the total of cells of three separate experiments taken together (n=120), each cell is represented by a dot. When cells had more than 30 chromosomes 7 signals per cell, they were counted as 30. The asterisk shows significant difference, $p < 0.05$.

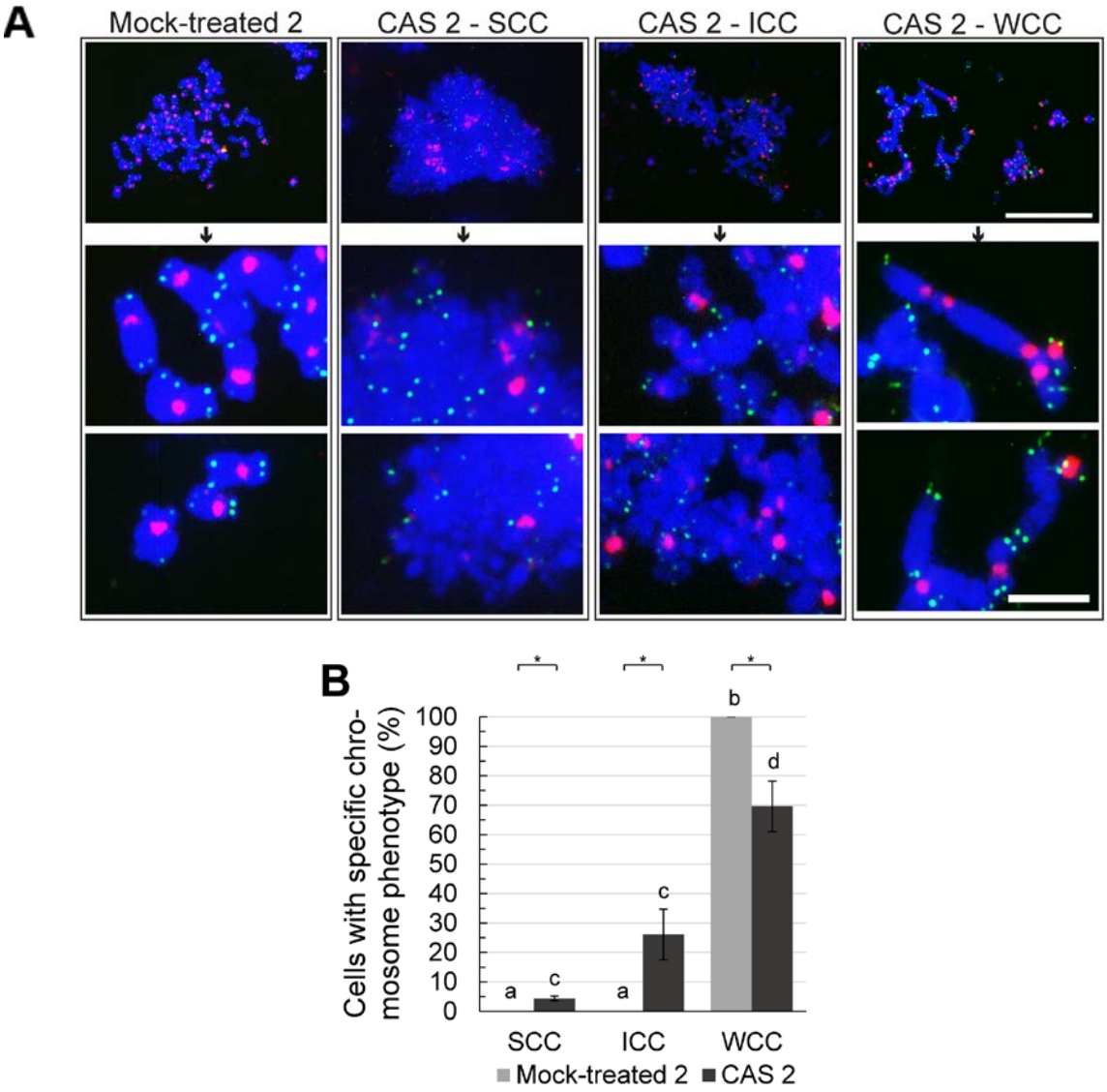

Figure 13. Cells that survive checkpoint adaptation after two days have abnormal chromosome configurations. (A) HT-29 cells were either not treated or treated with 50 nM CPT for 48 h. MDCs (mitotic and DNA-damaged cells) were collected by mechanical shake-off and recultivated for two days. Mitotic mock-treated (mock-treated 2) and checkpoint adaptation survival (CAS 2) cells were collected by mechanical shake-off and stained with DAPI (blue), to detect condensed chromosomes, centromere probes (red) and telomere probes (green), and were observed by immunofluorescence microscopy. The top panel shows one mitotic cell per configuration (SCC – shattered chromosome configuration, ICC – intermediate chromosome configuration and WCC - whole chromosome configuration). Scale bar = 25 µm. Bottom panels show enlargements of chromosomal structures in the above shown mitotic cell. Scale bar = 5 µm. (B) Cells were prepared and analyzed as described in A. The percentages of cells with a SCC, ICC or WCC were determined. The mean percentages ± SEM from three separate experiments are shown. The asterisks show significant differences between treatments within each category, $p < 0.05$. The letters represent significant differences between categories within a treatment (NT – a and b, CPT – c and d), samples with different letters are significantly different from each other, $p < 0.05$.

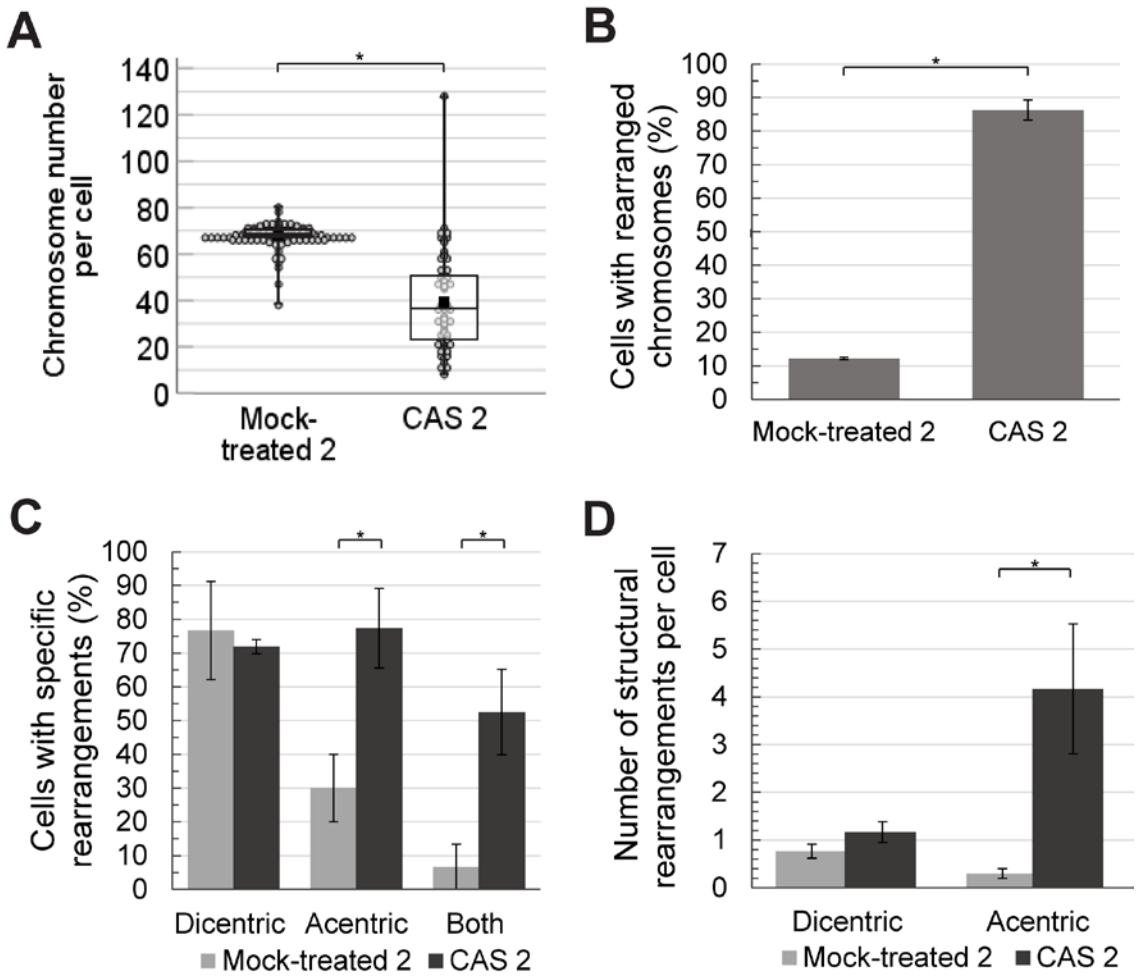

Figure 14. Cells that survive checkpoint adaptation after two days have abnormal chromosome structures. (A) HT-29 cells were either not treated or treated with 50 nM CPT for 48 h. MDCs (mitotic and DNA-damaged cells) were collected and recultivated for two days. Mitotic mock-treated (mock-treated 2) and checkpoint adaptation survival (CAS 2) cells were collected and stained with DAPI (blue) to detect condensed chromosomes, centromere probes (red) and telomere probes (green), and observed by immunofluorescence microscopy. The number of chromosomes per cell were counted and the average (black marker), minimum and maximum (whiskers) are shown by the boxplot. The boxplot represents data from the total of non-SCC (shattered chromosome configuration) cells of three separate experiments taken together (Mock-treated 2 n=115, CAS 2 n=60), each cell is represented by a dot. The asterisk shows significant difference, $p < 0.05$. (B) Cells were prepared and analyzed as described in A. The percentages of non-SCC (shattered chromosome configuration) cells with rearranged chromosome structures (i.e. dicentric/acentric chromosomes) was determined. The mean percentages ± SEM from three separate experiments are shown. The asterisk shows significant difference, $p < 0.05$. (C) Cells were prepared and analyzed as described in A. The percentages of rearranged cells, with dicentric chromosomes, acentric chromosomes, or both structural rearrangements, were determined. The mean percentages ± SEM from three separate experiments are shown. The asterisks show significant difference between treatments within a specific type of rearrangement, $p < 0.05$. (D) Cells were prepared and analyzed as described in A. The average number of specific rearrangements (dicentric or acentric) per cell was determined. The mean number of rearrangement per cell ± SEM from three separate experiments are shown. The asterisk shows significant difference, $p < 0.05$.

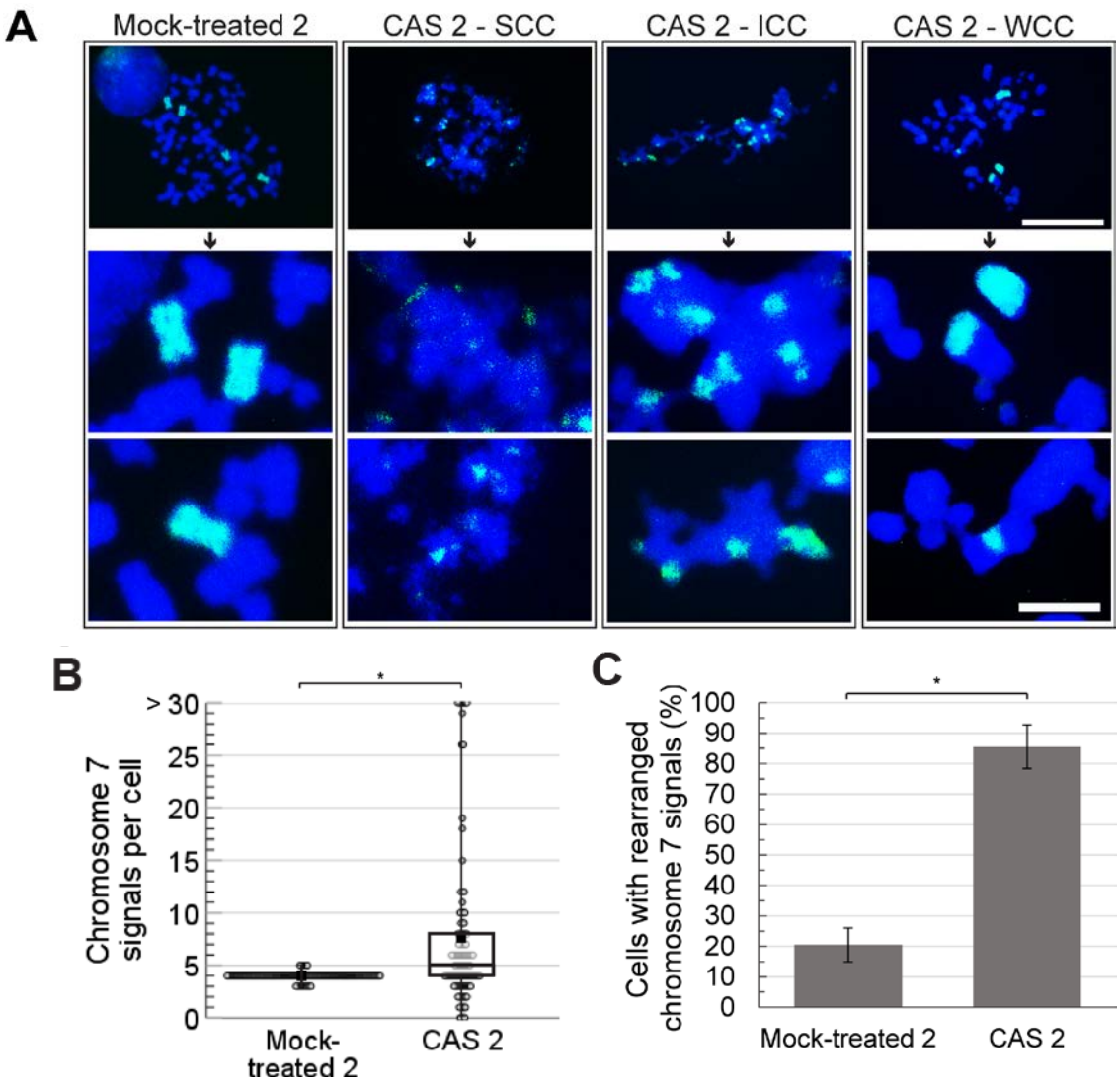

Figure 15. Analysis of chromosome 7 in cells that survived checkpoint adaptation after two days. (A) HT-29 cells were either not treated or treated with 50 nM CPT for 48 h. MDCs (mitotic and DNA-damaged cells) were collected and recultivated for two days. Mitotic mock-treated (mock-treated 2) and checkpoint adaptation survival (CAS 2) cells were collected and stained with DAPI (blue), to detect condensed chromosomes, and chromosome 7 probes (green). Cells were observed by immunofluorescence microscopy. The top panel shows one mitotic cell per configuration (SCC – shattered chromosome configuration, ICC – intermediate chromosome configuration and WCC – whole chromosome configuration). Scale bar = 25 µm. Bottom panels show enlargements of chromosome 7 in the above shown mitotic cell. Scale bar = 5 µm. (B) Cells were prepared and analyzed as described in A. The number of chromosome 7 signals were counted and the average (black marker), minimum and maximum (whiskers) are shown in the boxplot. The boxplot represents data from the total of cells of three separate experiments taken together (n=120), each cell is represented by a dot. When cells had more than 30 chromosomes 7 signals per cell, they were counted as 30. The asterisk shows significant difference, $p < 0.05$. (C) Cells were prepared and analyzed as described in A. The percentages of mock-treated (mock-treated 2) and checkpoint adaptation survival (CAS 2) cells with interchromosomal and/or chromosome 7 signal number rearrangements, were determined. The mean percentages ± SEM from three separate experiments are shown. The asterisk shows significant difference, $p < 0.05$.

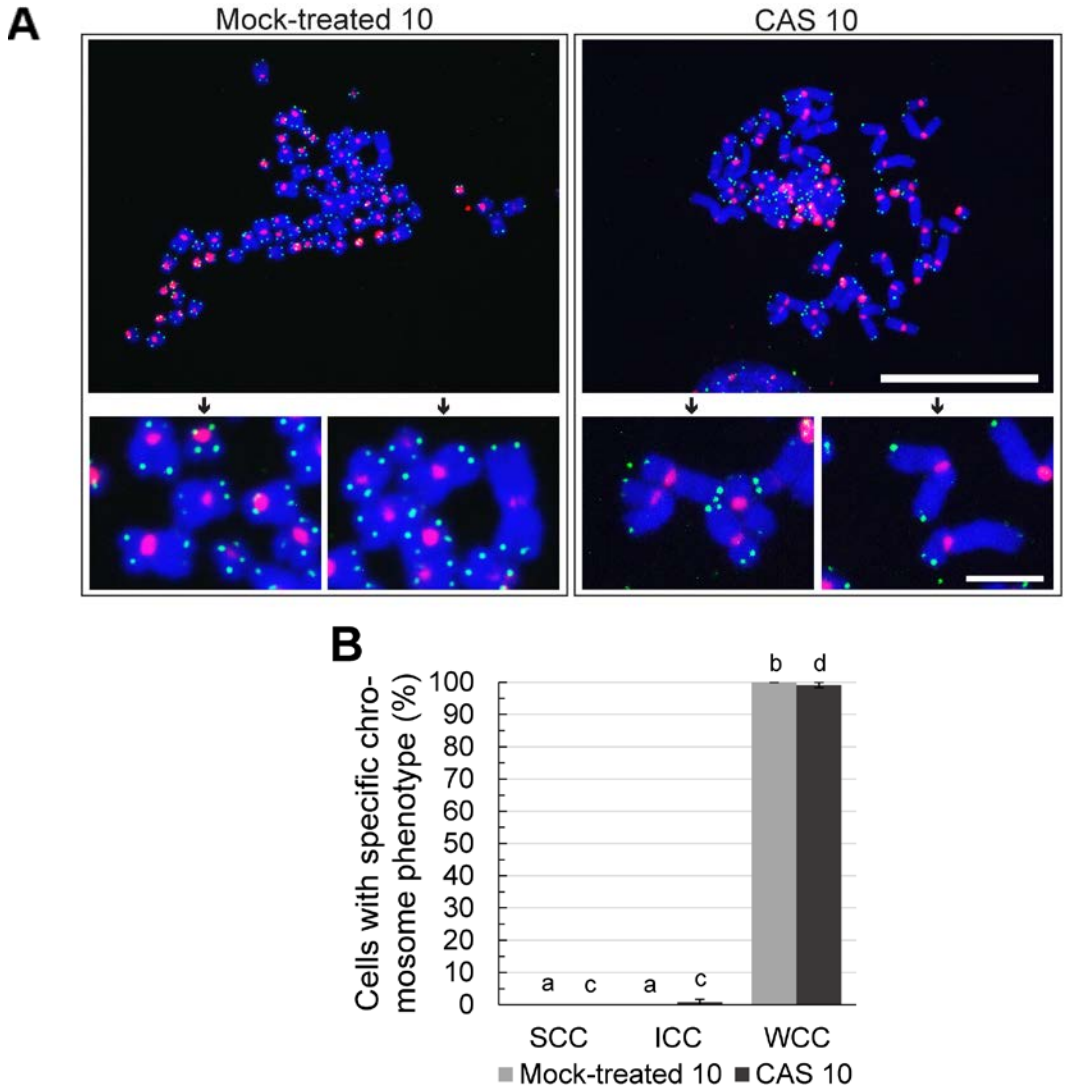

Figure 16. Cells that survive checkpoint adaptation after ten days have chromosome configurations similar to mock-treated cells. (A) HT-29 cells were either not treated or treated with 50 nM CPT for 48 h. MDCs (mitotic and DNA-damaged cells) were collected by mechanical shake-off and recultivated for ten days. Mitotic mock-treated (mock-treated 10) and checkpoint adaptation survival (CAS 10) cells were collected by mechanical shake-off and stained with DAPI (blue), to detect condensed chromosomes, centromere probes (red) and telomere probes (green), and observed by immunofluorescence microscopy. The top panel shows one mitotic cell per culture. Scale bar = 25 µm. Bottom panels show enlargements of chromosomal structures in the above shown mitotic cell. Scale bar = 5 µm. (B) Cells were prepared and analyzed as described in A. The percentages of cells that fitted into the following configuration categories: SCC (shattered chromosome configuration), ICC (intermediate chromosome configuration) or WCC (whole chromosome configuration) were determined. The mean percentages ± SEM from three separate experiments are shown. The letters represent significant differences between categories within a treatment (NT – a and b, CPT – c and d), samples with different letters are significantly different from each other, $p < 0.05$.

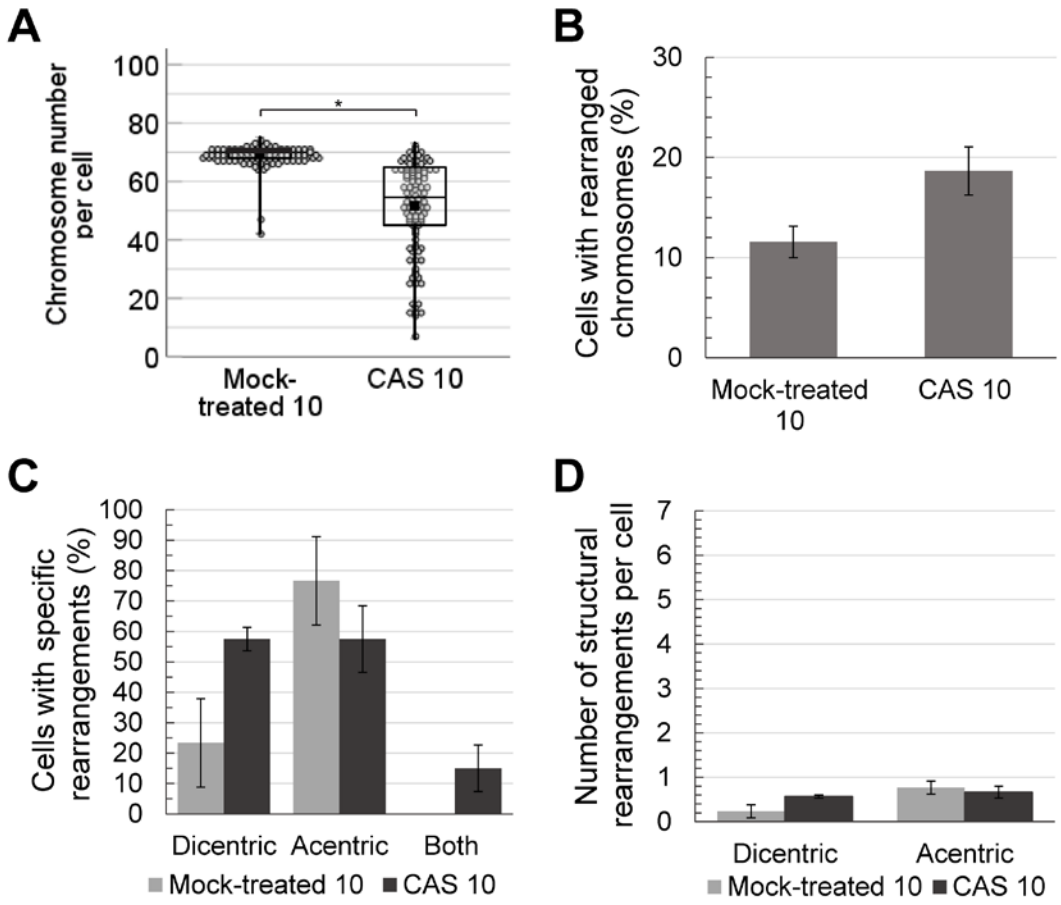

Figure 17. Cells that survive checkpoint adaptation after ten days have chromosome structures similar to mock-treated cells. (A) HT-29 cells were either not treated or treated with 50 nM CPT for 48 h. MDCs (mitotic and DNA-damaged cells) were collected and recultivated for ten days. Mitotic mock-treated (mock-treated 10) and checkpoint adaptation survival (CAS 10) cells were collected and stained with DAPI (blue) to detect condensed chromosomes, centromere probes (red) and telomere probes (green), and observed by immunofluorescence microscopy. The number of chromosomes per cell were counted and the average (black marker), minimum and maximum (whiskers) are shown by the boxplot. The boxplot represents data of three separate experiments taken together (mock-treated 10 n=116, CAS 10 n=117), each cell is represented by a dot. The asterisk shows significant difference between cultures, $p < 0.05$. (B) Cells were prepared and analyzed as described in A. The percentages of cells with rearranged chromosome structures (i.e. dicentric/acentric chromosomes) were determined. The mean percentages ± SEM from three separate experiments are shown. No significant difference was determined, $p < 0.05$. (C) Cells were prepared and analyzed as described in A. The percentages of rearranged cells with dicentric chromosomes, acentric chromosomes, or both structural rearrangements, were determined. The mean percentages ± SEM from three separate experiments are shown. No significant difference between treatments within a specific type of rearrangement was determined, $p < 0.05$. (D) Cells were prepared and analyzed as described in A. The average number of specific rearrangements (dicentric or acentric) per cell was determined. The mean number of rearrangement per cell ± SEM from three separate experiments are shown. No significant difference was determined, $p < 0.05$.

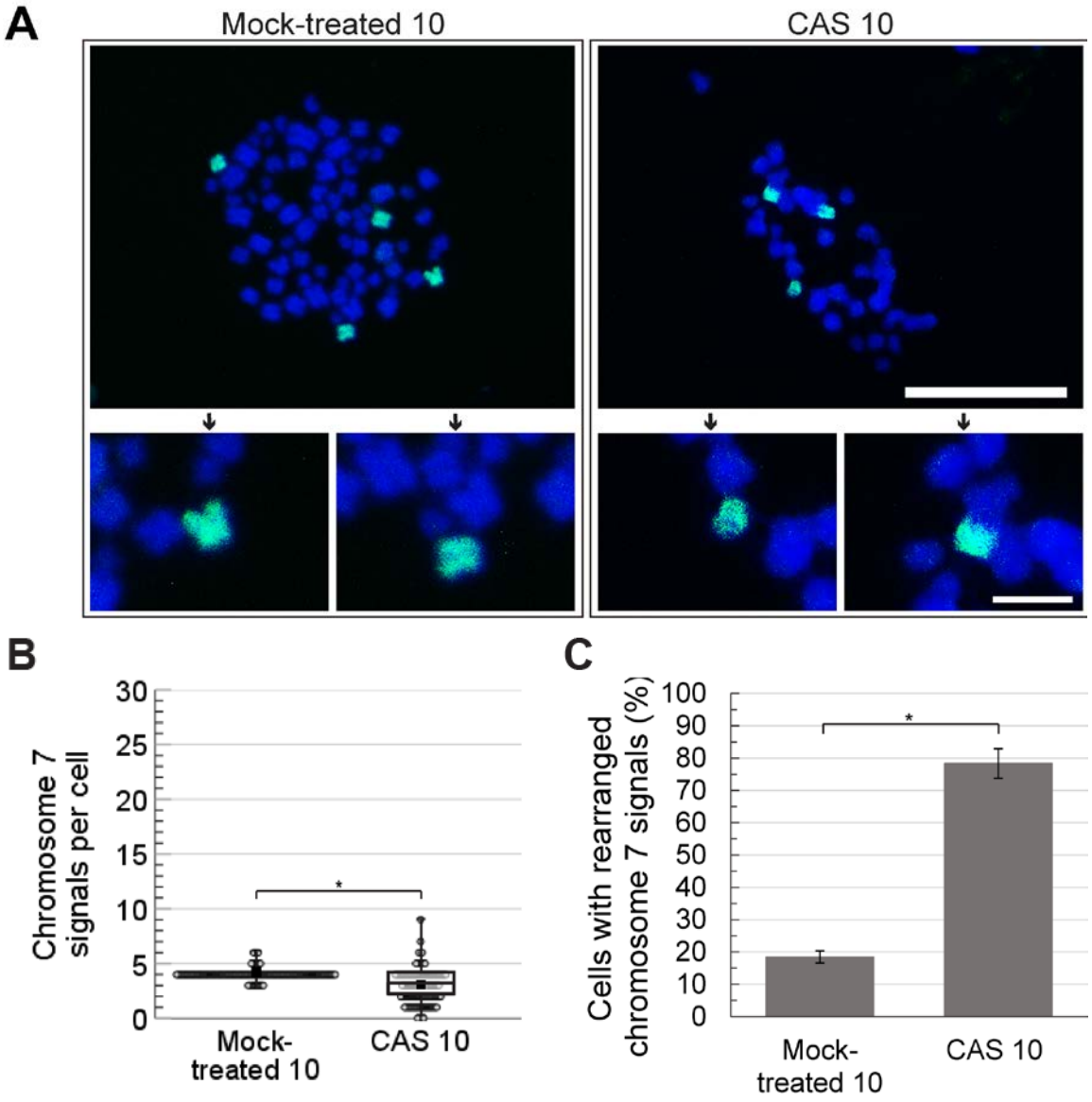

Figure 18. Analysis of chromosome 7 in cells that survived checkpoint adaptation after ten days. (A) HT-29 cells were either not treated or treated with 50 nM CPT for 48 h. MDCs (mitotic and DNA-damaged cells) were collected and recultivated for ten days. Mitotic mock-treated (mock-treated 10) and checkpoint adaptation survival (CAS 10) cells were collected and stained with DAPI (blue), to detect condensed chromosomes, and chromosome 7 probes (green). Cells were observed by immunofluorescence microscopy. The top panel shows one mitotic cell per culture. Scale bar = 25 µm. Bottom panels show enlargements of chromosome 7 in the above shown mitotic cell. Scale bar = 5 µm. (B) Cells were prepared and analyzed as described in A. The number of chromosome 7 signals were counted and the average (black marker), minimum and maximum (whiskers) are shown in the boxplot. The boxplot represents data from the total of cells of three separate experiments taken together (n=120), each cell is represented by a dot. The asterisk shows significant difference, $p < 0.05$. (C) Cells were prepared and analyzed as described in A. The percentages of cells with interchromosomal and/or chromosome 7 signal number rearrangements, were determined. The mean percentages ± SEM from three separate experiments are shown. The asterisk shows significant difference, $p < 0.05$.

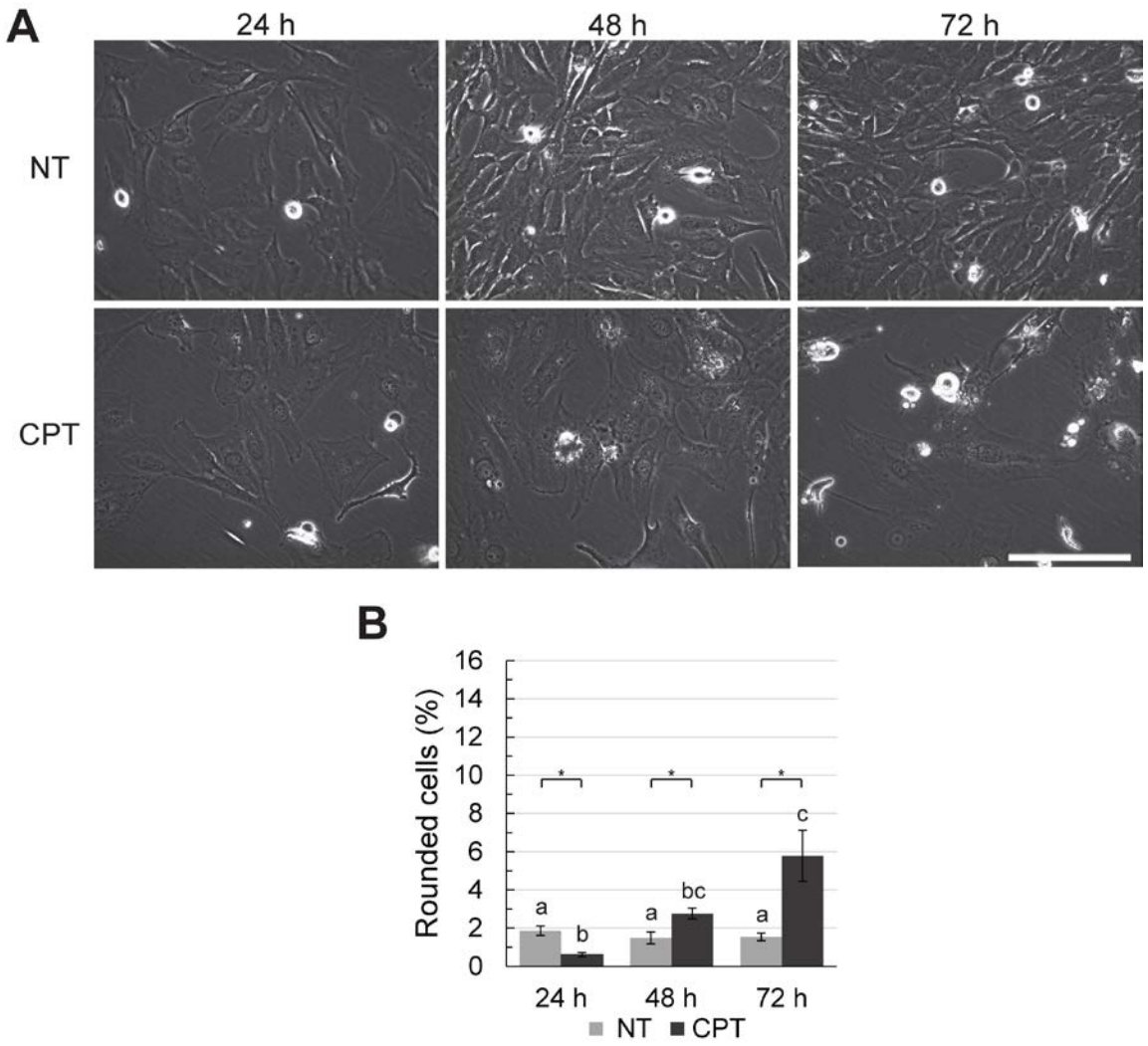

Figure 19. M059K cells treated with CPT acquire a rounded morphology. (A) M059K cells were either not treated (NT) or treated with 50 nM CPT (CPT) and observed by phase-contrast light microscopy at 24, 48 and 72 h. Rounded cells were visible in non-treated samples, but rarely at 24 and 48 h after treatment and commonly by 72 h of CPT treatment. Scale bar = 200 µm. (B) Cells were prepared and analyzed as described in A. The percentages of rounded cells were determined and compared between not-treated (NT) and CPT-treated (CPT) cultures at 24, 48 and 72 h. The mean percentages ± SEM are shown from three separate experiments. The asterisks show significant differences between treatments within each time point, $p < 0.05$. The letters represent significant difference between time points within a culture (NT – a, CPT – b and c). Samples with different letters are significantly different from each other, $p < 0.05$.

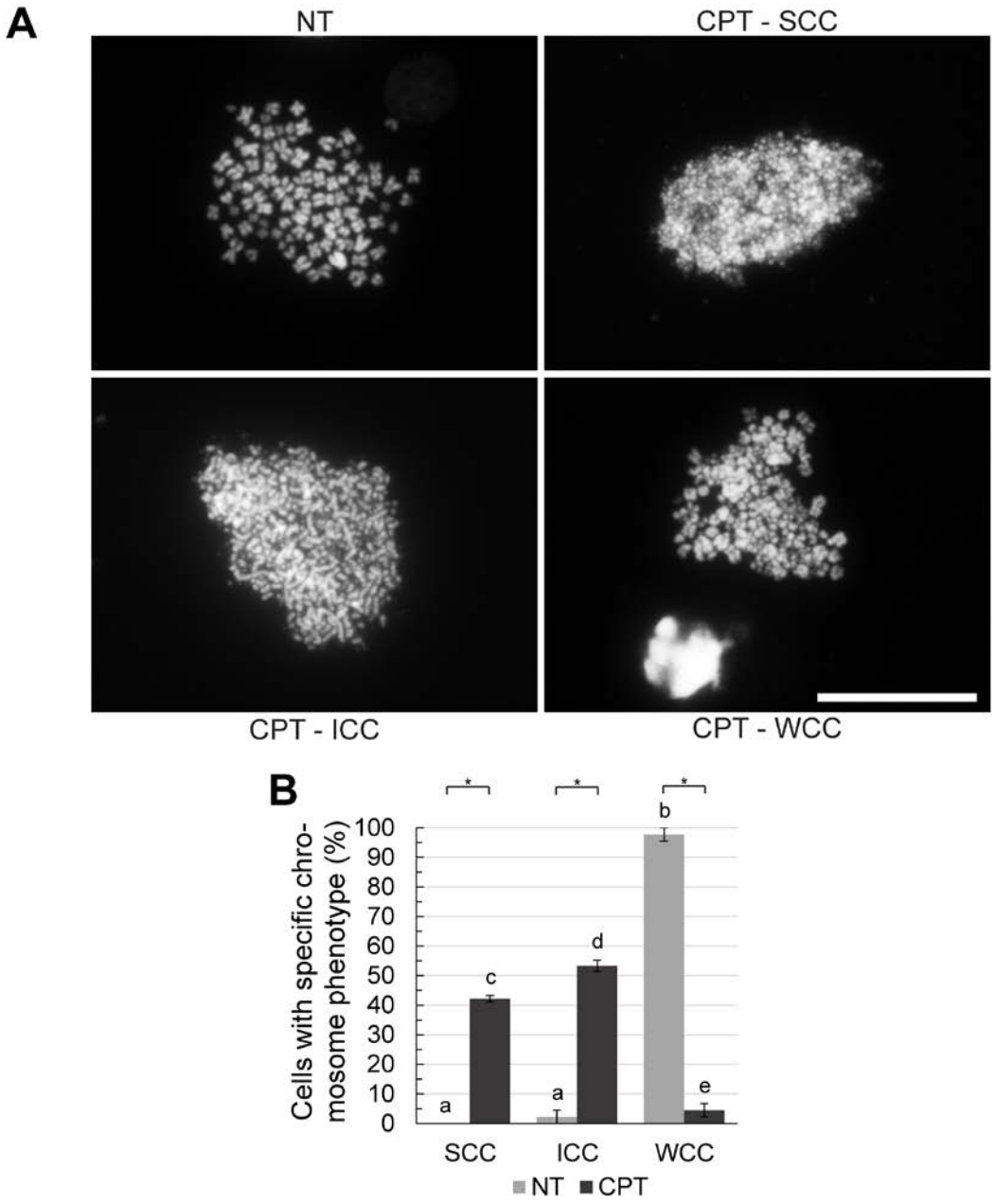

Figure 20. M059K cells that undergo checkpoint adaptation show an abnormal chromosome configuration. (A) M059K cells were either not treated (NT) or treated with 50 nM CPT (CPT) for 72 h and stained with DAPI (blue) to detect condensed chromosomes. Cells were observed by immunofluorescence microscopy and were categorized into: SCC (shattered chromosome configuration), ICC (intermediate chromosome configuration) or WCC (whole chromosome configuration). Scale bar = 25 μm. (B) Cells were prepared and analyzed as described in A. The percentages of M059K cells with the following chromosome configurations: SCC, ICC or WCC were determined. The mean percentages ± SEM from three separate experiments are shown. The asterisks show significant differences between treatments within categories, $p < 0.05$. The letters represent significant differences between categories within each treatment (NT – a and b, CPT – c, d and e), samples with different letters are significantly different from each other, $p < 0.05$.

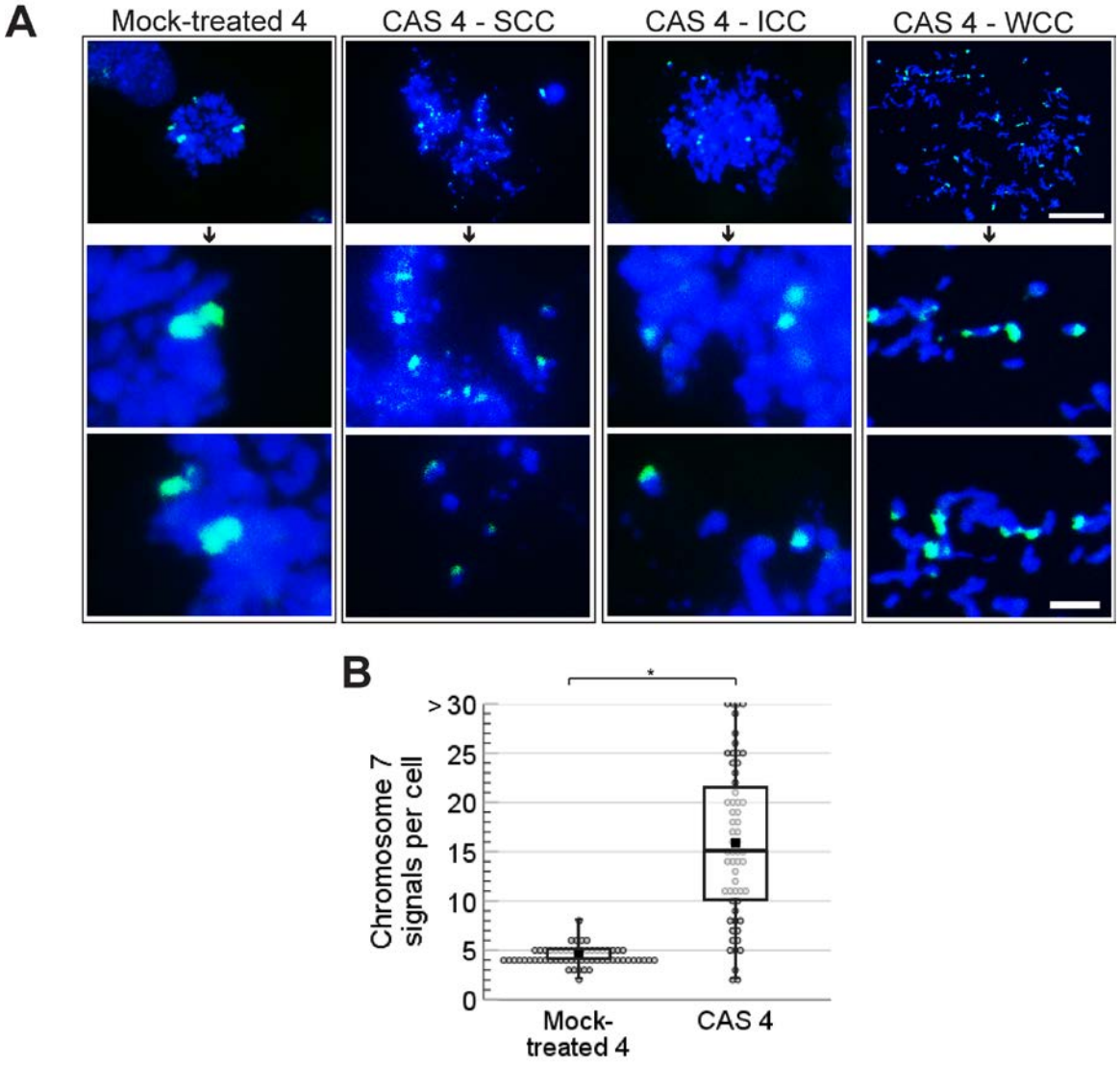

Figure 21. Analysis of chromosome 7 in M059K cells that survived checkpoint adaptation after four days. (A) M059K cells were either not treated or treated with 50 nM CPT for 72 h. MDCs (mitotic and DNA-damaged cells) were collected and recultivated for four days. Mitotic mock-treated (mock-treated 4) and checkpoint adaptation survival (CAS 4) cells were collected and stained with DAPI (blue), to detect condensed chromosomes, and chromosome 7 probes (green). Cells were observed by immunofluorescence microscopy. The top panel shows one mitotic cell per chromosome configuration (SCC – shattered chromosome configuration, ICC – intermediate chromosome configuration and WCC – whole chromosome configuration). Scale bar = 25 µm. Bottom panels show enlargements of chromosome 7 in the above shown mitotic cell. Scale bar = 5 µm. (B) Cells were prepared and analyzed as described in A. The number of chromosome 7 signals were counted per cell and the average (black marker), minimum and maximum (whiskers) are shown in the boxplot. The boxplot represents data from the total of cells of three separate experiments taken together (n=120), each cell is represented by a dot. When cells had more than 30 chromosomes 7 signals per cell, they were counted as 30. The asterisk shows significant difference, $p < 0.05$.

3. Discussion

CIN is one of the hallmarks of cancer (Hanahan & Weinberg, 2011). It can drive intratumour heterogeneity, which is known to contribute to metastasis, treatment inefficiency and treatment resistance (Cahill et al., 1999; Burrell et al., 2013; McClelland, 2017; Bakhoum et al., 2018). However, the molecular pathways that are involved in CIN and how it drives oncogenesis remains largely unknown. One proposed mechanism through which CIN can be promoted in cancer cells is checkpoint adaptation (Syljuasen et al., 2006; Bartek & Lukas, 2007; Lewis & Golsteyn, 2016; Swift & Golsteyn, 2016a; Kaddour et al., 2017; Kalsbeek & Golsteyn, 2017). Checkpoint adaptation is a process in which cells enter mitosis with damaged DNA. Most cells die after entering checkpoint adaptation, however, a small number can exit mitosis and continue to proliferate (Kubara et al., 2012). It has been previously shown that cells surviving checkpoint adaptation acquire micronuclei, which is a marker for CIN (Chang et al., 1999; Lewis & Golsteyn, 2016). Those data suggest that checkpoint adaptation and CIN are linked. Using our experimental model, we have shown that cancer cells that survive checkpoint adaptation acquire interchromosomal and numerical rearrangements. These new results reveal that chromosomes can undergo major rearrangements by the process of checkpoint adaptation.

We have developed the HT-29 cell experimental model that enables one to collect and recultivate cells that undergo checkpoint adaptation, to more easily observe the fate. Mitotic HT-29 cells have a unique and rounded, weakly adherent morphology and unlike many other cell lines, they can remain in mitotic arrest for long periods (Gascoigne & Taylor, 2008; Kubara et al., 2012). HT-29 is a near-triploid cell line that contains 4 copies of chromosome 7, which is relatively long in length, thereby providing sufficient material and making it a valuable tool to study interchromosomal rearrangements (Kawai et al., 2002; Roschke et al., 2002). Lastly, treatment of colorectal cancer cells with CPT has been commonly used in the clinic and cytotoxicity can be achieved at pharmacological concentrations in cell culture conditions (Pizzolato & Saltz, 2003; Kubara et al., 2012; Swift & Golsteyn, 2014). These above mentioned features makes our

experimental model a valuable tool to study checkpoint adaptation. An additional cell line, M059K, was used to confirm that the increased level of chromosomal rearrangements upon checkpoint adaptation is a general consequence of this process.

To test for CIN as an outcome of checkpoint adaptation, we first confirmed that we were able to induce checkpoint adaptation in our cell model. Of the cells undergoing checkpoint adaptation, 1.9% of these cells were able to exit mitosis and proliferate for ten days. We observed that the majority of cells undergoing checkpoint adaptation had an SCC or ICC and more than 60% of the cells with an SCC showed clustered centromeres. Very few cells undergoing checkpoint adaptation had a chromosome configuration comparable to a not-treated cell. The shattered chromosomes observed were expected upon excessive DNA damage induced by the genotoxic agent CPT (Ryan et al., 1994). Ten days after surviving checkpoint adaptation almost all cells had a similar chromosome configuration as the mock-treated culture. This suggests that cells that were able to survive for ten days were the cells that had the least damage upon treatment or that the damage was repaired over the course of time.

Previous studies have described chromosome shattering after genotoxic treatment and proposed it as a form of mitotic catastrophe, as a consequence of unrepaired DNA damage during interphase (Chu, 1965; Stevens et al., 2007; Hubner et al., 2009). Shattering of all chromosomes within a cell was derived from an abnormal mitotic cell consisting of non-condensed chromatin with a normally shaped spindle apparatus (Hubner et al., 2009). Non-condensed chromatin was proposed to be a consequence of a factor depletion model in which a limited number of proteins in both chromatin condensation and DNA repair is involved. The exhaustion of this pool might result in condensation failure (Cremer & Cremer, 2006). It was shown that the spindle apparatus was able to bind centromeres and extracted chromatin fibres from the bulk chromatin to one side of the apparatus, resulting in clustered centromeres (Hubner et al., 2009), what might be an explanation for clustered centromeres we observed in cells with an SCC. The abnormal chromosome

configuration of cells undergoing checkpoint adaptation supported the suggestion that cells surviving checkpoint adaptation have chromosomal changes.

Previous studies have shown that cells with a shattered chromosome configuration exited mitosis and proceeded to interphase with highly abnormal, multilobulated nuclear configuration and entered apoptosis several hours after mitotic exit (Hubner et al., 2009). This might be an explanation for the multinucleated cells observed after surviving checkpoint adaptation. We showed that cancer cells that underwent checkpoint adaptation presented a multinucleated state in the first days after surviving checkpoint adaptation. After 6 days, the cells showed a mononucleated state, comparable to the mock-treated culture. Multinucleated cells are considered giant cells and are a form of chromosome instability and used as a marker for aggressive and chemoresistant tumour behaviour. It is an outcome of genotoxic treatment and is one of the most important characteristics of mitotic catastrophe and thought to cause apoptotic or necrotic cell death in the majority of cells (Weihua et al., 2011; Bhatia & Kumar, 2014; ZhangWu et al., 2015). However, multinucleated giant cells have been shown to be capable of continuously generating rapidly proliferating mononucleated cells in higher eukaryotes, by the process of nuclear budding (Solari et al., 1995). Knowing that cells that underwent and survived checkpoint adaptation showed abnormal chromosome configurations and nuclear states, we were interested to know whether these cells presented abnormalities in the key features of chromosomes, centromeres and telomeres.

We stained chromosomes with centromere and telomere probes to study chromosome structure and numerical rearrangements. We observed that cells undergoing checkpoint adaptation, and two days after surviving checkpoint adaptation, showed a 70% increase in the number of cells with structural rearrangements, compared to not-treated and mock-treated cells. However, two days after surviving checkpoint adaptation, the number of dicentric and/or acentric chromosomes per cell was reduced compared to the number of these aberrations in cells undergoing checkpoint adaptation. Ten days after surviving checkpoint adaptation, the levels of structural rearrangements were similar to those of mock-treated cells. Surviving checkpoint adaptation after two days resulted

in a reduction from 67.7 to 38.8 chromosomes per cell, on average. Cells surviving for ten days showed a reduction from 68.5 to 51.1 chromosomes per cell, on average, as a consequence of checkpoint adaptation.

In addition to chromosome structure rearrangement, we stained for chromosome 7, as a representation of all chromosomes, to observe interchromosomal rearrangements in cells undergoing checkpoint adaptation. During the process of checkpoint adaptation, chromosome 7 signal numbers were high and dispersed compared to not-treated cells, confirming the shattered chromosome configuration that was observed. Cells surviving checkpoint adaptation after two days showed an average increase in chromosome 7 signal number of 3.6 per cell and the number of cells with a signal number and/or interchromosomal rearrangement of chromosome 7 increased by approximately 60%, compared to the mock-treated culture. By ten days after surviving checkpoint adaptation cells had lost one chromosome 7 signal, on average, and strikingly, almost 60% of the cells observed contained a rearrangement in chromosome 7. These data confirm that even though structural rearrangement levels decreased over time in checkpoint adaptation survival cells, the level of interchromosomal and numerical rearrangements was increased, compared to the mock-treated culture. This confirms that cells that survive checkpoint adaptation acquired major chromosomal rearrangements.

One explanation for the reduction of chromosome structure rearrangements and chromosome number over time, may be chromosome missegregation during mitosis. Segregation errors can lead to increased aneuploidy and chromosome instability. The erroneous rejoining of broken chromosomes by double-strand DNA break repair, can lead to chromosome structure rearrangements, which are prone to chromosome missegregation during mitosis (Carrano & Heddle, 1973). Lagging acentric or dicentric chromosomes can be incorporated into a micronucleus in one of the daughter cells, where the chromosome is prone to damage (Terradas et al., 2009; Xu et al., 2011; Terradas et al., 2012; Santaguida & Amon, 2015; Kalsbeek & Golsteyn, 2017). The micronucleus can be degraded or reincorporated into the daughter nucleus, resulting in loss of the

chromosome(s) or the reincorporation of damaged and/or rearranged chromosome(s) into the main nucleus, promoting chromosome instability or aneuploidy (Stephens et al., 2011; Crasta et al., 2012). Lewis & Golsteyn (2016) have shown that micronuclei are acquired in cells that survived checkpoint adaptation, suggesting that the reduction in chromosome structure rearrangements we have observed might be caused by chromosome missegregation during mitosis.

Our result is supported by several studies that showed that cancer cells have increased numbers of chromosomal changes after surviving genotoxic treatment. Kaddour et al. (2017) showed that after IR *in vitro* of lymphocytes of Hodgkin Lymphoma patients, cells had increased numbers of dicentric and acentric chromosomes. These levels decreased over cell cycle progression. Variability of chromosomes was reduced over progression of cell cycles, suggesting stabilization of the genome. Another study focused on lymphocytes of Hodgkin Lymphoma patients before, during and after genotoxic treatment (Ramos et al., 2018). This study *in vivo* showed that during treatment, the number of chromosome structure rearrangements in lymphocytes doubled compared to the levels before treatment. One year after treatment, the number of chromosome rearrangements, mostly non-clonal rejoined chromosome structure rearrangements and aneuploidy, were almost 10-fold higher than before treatment, which indicated that new rearrangements formed continuously. This study also showed that several chromosome rearrangements observed could be linked to cancer secondary to treatment (Ramos et al., 2018).

In our experiments, we observed fewer cells with nuclear structure abnormalities ten days after surviving checkpoint adaptation, compared to cells undergoing or surviving checkpoint adaptation after two days. In addition, we observed fewer cells with shattered chromosomes and fewer chromosome structure rearrangements per cell, compared to cells undergoing or surviving checkpoint adaptation after two days. Chromosome numbers as well as structural, and numerical rearrangements of chromosome 7 per cell were widely distributed in the checkpoint adaptation surviving cultures, suggesting checkpoint adaptation as a contributor to intratumoural heterogeneity. It has been shown that absence of functional p53 is required for cells to tolerate these

genomic changes. In cells with functional p53, CIN led to durable cell cycle arrest (Thompson & Compton, 2010; Rausch et al., 2012). This is supported by the finding that non-cancerous cells do not undergo checkpoint adaptation (Lewis & Golsteyn, 2016). Taking this together with the study showing that intermediate levels of CIN were associated with poor patients outcomes, rather than extreme CIN levels, suggests that there is a threshold of damaged DNA or CIN that can be tolerated in cells, and when exceeded will induce cell death (Birkbak et al., 2011; Thompson et al., 2017).

We speculate that cells surviving checkpoint adaptation go through a cycle of chromosome instability promoting mechanisms. Chromosome structure rearrangements can lead to chromosome missegregation during mitosis, which in turn could lead to incorporation into a micronucleus or loss of the chromosome (aneuploidy). The micronucleus is a structure that can promote further change by degradation (aneuploidy) or reincorporation into the main nucleus after chromothripsis, with chromosome structures rearrangement, closing the cycle.

By using our experimental model, we observed that cells that survived checkpoint adaptation acquired major chromosomal rearrangements compared to not-treated parental cells. This model can be used to focus on the molecular pathways that are involved in the formation of rearranged chromosomes after genotoxic treatment. DNA repair pathways likely have a major role in the rejoining of the broken chromosomes, which might lead to these rearranged chromosomes. It is possible that the DNA repair might lower the level of damaged DNA and hence the proposed damaged DNA threshold required for cell death might not be reached. Understanding the biochemical pathways driving chromosomal change and its relation to tumour development might provide knowledge to the development of successful combinational therapies that can target those pathways and reduce carcinogenesis.

4. Materials and methods

4.1 Cell culture

The human cell lines HT-29 (ATCC HTB-38) and M059K (ATCC CRL-2365) were obtained from the American Type Culture Collection (ATCC). HT-29 cells were maintained in Roswell Park Memorial Institute (RPMI) 1640 medium (ThermoFisher; 21870092) supplemented with 10% (v/v) heat-inactivated fetal bovine serum (FBS) (ThermoFisher; 12484028) and 2 mM GlutaMAX (ThermoFisher; 35050061). M059K cells were maintained in Dulbecco's Modified Eagle Medium (DMEM)/F-12 (ThermoFisher; 11320082) supplemented with 10% (v/v) heat inactivated FBS, 2 mM Modified Eagle Medium non-essential amino acids (ThermoFisher; 11140050) and 15 mM HEPES (4-(2-hydroxyethyl)-1-piperazineethanesulfonic acid) (FisherScientific; BP310500), pH 7.4. Cells were grown at 37°C in 5% CO_2 and media were changed every 3-4 days. HT-29 cells were plated at a density of 3.0 x 10^5cells/25 cm^2 flask or 6.0 x 10^5/6 well culture plate and cultured for 48 or 72 h prior to treatment. M059K cells were plated at a density of 6.0 x 10^5/75 cm^2 flask or 3.0 x 10^5/6 well culture plate and cultured for 24 or 48 h prior to treatment. The compound CPT (Sigma; 7689034) was dissolved in dimethyl sulfoxide (DMSO) (MilliporeSigma; D2438) to a concentration of 10 mM. The compound was stored at -20°C until use. Not-treated cells were treated with the solvent only (DMSO) in a volume equal to the highest volume of the compound tested, and never adding more than 1% (v/v).

4.2 Cell morphology assay

HT-29 cells were seeded at 6.0 x 10^5/6 well culture plate and incubated at 37°C for 48 or 72 h prior to treatment, M059K cells were seeded at 3.0 x 10^5/6 well culture plate and incubated for 24 or 48 h prior to treatment to reach a cell confluency of 50-70%. Images were captured at 24 and 48 h in HT-29 cells, and 24, 48, and 72 h in M059K cells, with an Infinity 1 camera powered by Infinity Capture imaging software (Lumenera Corporation) on an Olympus CKX41 inverted microscope. Images were processed using Adobe Photoshop (CC 2017.0.1) software. Interphase cells and

rounded cells were manually counted using Image J (1.47v) or Adobe Photoshop (CC 2017.0.1) software and the percentage of rounded cells in the total sample was determined. A minimum of 200 cells were counted for each treatment and the mean and standard error of the mean of at least three independent experiments were calculated.

4.3 Immunofluorescence microscopy

HT-29 cells were plated on glass coverslips at 6.0 x 10^5/6 well culture plate and incubated at 37°C for 48 or 72 h prior to treatment. After 48 h of treatment, cells were fixed at room temperature for 20 min in 3% (v/v) paraformaldehyde (Fisher Scientific; 30525894) diluted in phosphate buffered saline (PBS) (137 mM NaCl, 3 mM KCl, 100 mM Na_2HPO_4, 18 mM KH_2PO_4). Cells were quenched for 10 min with 50 mM NH_4Cl in PBS, permeabilized for 5 min using 0.2% (v/v) Triton X-100 in PBS and blocked for 1 h with 3% (w/v) bovine serum albumin (BSA) (Fisher Scientific; J6465522) in PBS-T (0.1% (v/v) Tween-20 (MilliporeSigma; CAEM9480) diluted in PBS). Cells were then incubated with primary antibodies as described: anti-histone γH2AX (MilliporeSigma; 05-636; 1:400) for 1 h at room temperature or anti-pH3 (MilliporeSigma; 06-570; 1:1000) overnight at 4°C. After washing with PBS-T, cells were incubated with secondary antibodies for 45 min at room temperature as follows: Alexa Fluor 488-conjugated anti-mouse (ThermoFisher; A11059; 1:400) for anti-histone γH2AX and Alexa Fluor 594 AffiniPure goat anti-rabbit (Jackson ImmunoResearch; 111585003; 1:400) for anti-pH3. Nuclei were stained with 300 nM 4’,6-diamidino-2-phenylindole (DAPI) (FisherScientific; LSD1306) in PBS for 15 min and coverslips were mounted onto microscope slides using ProLong Gold Antifade reagent (FisherScientific; P36934). Cells were observed on an Olympus BX41 microscope and images were captured using an Infinity 3 camera operated by Infinity Capture imaging software (Lumenera Corporation). The signal for not-treated cells was set to zero using the exposure settings of the microscope camera. Cells staining for pH3 and histone γH2AX and the total number of cells (DAPI stained) were counted with Adobe Photoshop (CC 2017.0.1). Cells were considered positive when they exhibited

a staining intensity greater than background levels. Images were prepared using Adobe Photoshop (CC 2017.0.1) software. A minimum of 100 cells were counted for each treatment and the mean and standard error of the mean of at least three independent experiments were calculated.

4.4 Mechanical shake-off

HT-29 and M059K cells were plated at 1 x 10^6 cells/75 cm^2 flask and 2 x 10^6 cells/75 cm^2 flask respectively and incubated at 37°C for 48 or 72 h prior to treatment. After 48 h of HT-29 treatment or 72 h of M059K treatment, medium was aspirated and cells were gently washed with PBS. Fresh medium was added at 3 ml/75 cm^2 and the flask was tapped with medium force on all edges to extract rounded cells from flattened cells (Swift & Golsteyn, 2018).

4.5 Time-lapse video microscopy for analysis of survival cells

HT-29 cells were plated at 1 x 10^6/75 cm^2 flask and incubated at 37°C for 48 or 72 h prior to treatment. Cells undergoing checkpoint adaptation were collected by mechanical shake-off and re-cultivated. Time-lapse video microscopy images were taken using Cytation™ 5 Cell Imaging Multi-mode Reader using Gen5 software (BioTek Instruments, USA) to collect phase-contrast images every 30 min for 10 days post checkpoint adaptation, using a 10x objective in a controlled chamber at 37°C and 5% CO_2. Medium was changed every 3-4 days. Cells were manually scored for morphology. At least 300 cells were observed per treatment and the mean and standard error of the mean of at least three independent experiments were calculated. The figure has been constructed by combining images of two separate, but identical experiments.

4.6 Survival assay

HT-29 and M059K cells were plated at 1 x 10^6 cells/75 cm^2 flask and 2 x 10^6 cells/75 cm^2 flask respectively and cultivated for 48 or 72 h hours prior to treatment. At 48 h after treatment of HT-29 cells, a mechanical shake off was performed to collect rounded cells. M059K cells were treated for 72 h prior to mechanical shake-off. Collected rounded cells were counted using hemocytometer and cell viability was confirmed by vital dye exclusion. Cells were re-plated in a 25 cm^2 flask and

placed in the incubator at 37ºC until the desired time for survival analysis. At desired times, cells were collected by trypsinization and counted using a hemocytometer to determine the number of cells that survived. The percentage of re-cultivated cells that survived was estimated using the following formula:

$$N0 = 10^{\{\log NT-(\log 2/tg)\ T\}}$$

In the formula; NT = number of cells collected at the end of the survival assay, N0 = number of cells that were able to proliferate (i.e., survival cells), tg = generation time in hours, and T = time of culture in hours. Then, the percentage of surviving cells was calculated using the following formula:

$$P = (N0 / N) \times 100$$

In the formula; N = number of cells placed in the flask at the beginning of the survival assay and N0 = number of cells that were able to proliferate (i.e. survival cells) (Leibovitz & Mazur, 1977). Experiments were repeated at least three times.

4.7 Mitotic cell fixation

HT-29 and M059K cells were plated at 1.5 x 10^6/75 cm^2 and 3 x 10^6/150 cm^2 flask respectively for 48 or 72 h prior to treatment. HT-29 cells were treated with 50 nM CPT for 48 h and M059K cells were treated with 50 nM CPT for 72 h followed by treatment of KaryoMAX colcemid (10 μg/ml) (Gibco; 15210-040) for 1 h at 37 ºC. Colcemid was used to increase the number of metaphase cells in a culture. Next, freshly prepared warm hypotonic solution (0.075 M KCl (MilliporeSigma; CAPX1405-1) in distilled H_2O was added to the cells for 30 min to make nuclei swell osmotically. Then, cells were fixed by adding Carnoy's fixative 3:1 methanol (FisherScientific; A4524) and acetic acid (MilliporeSigma; CAAX0073-9) solution and incubated for 10 min on ice followed by a mechanical shake-off to collect mitotic cells. Cells were placed into a pre-cooled 15 mL Falcon tube and centrifuged for 5 min at 220 rcf. The supernatant was removed and cells were resuspended

in 5 mL cold fixative and incubated on ice for 5 min followed by 5 min centrifugation at 220 rcf. This was repeated three times and after the last centrifugation cells were resuspended in 0.5 mL of fixative and the cell suspension was dropped on a cold, clean glass slide and blown to disperse the chromosomes.

4.8 Fluorescent in situ hybridization – centromeres and telomeres

Slides were prepared as described in the mitotic cell fixation method. Additionally, the slides were fixed with 3% (v/v) paraformaldehyde (Ted Pella Inc; 18505) for 2 min and washed twice in PBS for 2 min each followed by RNase solution (100 µg/ml RNase A (MilliporeSigma; R6513) in PBS) and incubated for 20 min at 37^{o}C. After two PBS washes the slide was dehydrated by incubation for 2 min in 70%, 85% and 100% cold ethanol. Mixture of peptide nucleic acid (PNA) probes (Alexa488 labelled PNA TelC probe (AF488-OO CCCTAACCCTAACCCTAA) (PNA Bio; F1004) and Cy3 labelled PNA centromere probe (ATTCGTTGGAAACGGGA) (PNA Bio; F3003)) and hybridization buffer (20 mM Tris, pH 7.4, 60% formamide (MilliporeSigma; F9037), 0.1 µg/ml UltraPure salmon sperm DNA solution (ThermoFisher; 15632-011), and distilled water, final pH 7.4) was added to the slide followed by denaturation at 85^{o}C for 10 min. Next, the slide was placed in the dark at room temperature for 2 h for hybridization. The slides were immersed in 2x SSC (distilled water, NaCl (BDH chemicals), sodium citrate (MilliporeSigma), HCl (FisherScientific) and 0.1% Tween-20 (MilliporeSigma; CAEM9480)) twice at 55-60^{o}C for 15 min, once at room temperature for 15 min. The slide was stained with 300 nM DAPI (FisherScientific; LSD1306) solution for 10 min followed by three washes with 2x SSC, 1x SSC and water, respectively. Cells were observed on an Olympus BX41 microscope and images were captured using an Infinity 3 camera operated by Infinity Capture imaging software (Lumenera Corporation). Chromosome structures were observed and images prepared with Adobe Photoshop (CC 2017.0.1) software. A minimum of 35 cells per treatment were observed and analyzed for chromosome structure rearrangements. Experiments were repeated at least three times.

4.9 Fluorescent in situ hybridization - chromosome 7

Slides were prepared according to the mitotic cell fixation method, where after flushed with fresh fixative when still damp. The slides were transferred to 2x SSC (distilled water, NaCl (BDH chemicals), sodium citrate (MilliporeSigma), HCl (FisherScientific)) pH 7 for 2 min at room temperature and dehydrated by incubation for 2 min in 70%, 85% and 100% cold ethanol. Whole chromosome probe, specific for chromosome 7 (Cytocell; LPP07G). Chromosome 2 and 12 specific probes (Cytocell; LPP02G and LPP12R) were also tested, but we proceeded only with chromosome 7 probes. The sample slide was prewarmed at 37 ^{o}C for 5 min. The probe was added to the slide, covered with cover glass, and sealed with rubber cement followed by denaturation at 80^{o}C for 2 min. Next, the slide was placed in a hermetically closed humidified chamber at 37 ^{o}C overnight for hybridization. Rubber cement was removed and coverslip removed and washed in 2x SSC at 37 ^{o}C for 2 min and transferred to 0.4X SSC at 70 ^{o}C for 2 min, followed by a wash in 2x SSC 0.05% Tween-20 at 22 ^{o}C for 30 seconds. Next, slides were stained with DAPI (FisherScientific; LSD1306) for 10 min and washed with 2x SSC 0.05% Tween-20 (MilliporeSigma; CAEM9480) for 5 min. Coverslips were mounted onto microscope slides using ProLong Gold Antifade reagent (FisherScientific; P36934). Cells were observed on an Olympus BX41 microscope and images were captured using an Infinity 3 camera operated by Infinity Capture imaging software (Lumenera Corporation). Chromosome 7 signals were determined and images prepared with Adobe Photoshop (CC 2017.0.1) software. The ceiling for chromosome 7 signals was set to 30, more than 30 signals per cell were considered as 30 to calculate the mean. A minimum of 40 and 20 cells per treatment were observed for HT-29 and M059K, respectively. Experiments were repeated at least three times.

4.10 Statistical analysis

Data were analysed using Microsoft Excel 2010 and SPSS software. Data are presented as means from three independent experiments ± SEM. One-way analysis of variance (ANOVA) with Tukey's post hoc test and/or a two-sample or paired t-test was used to analyse results. A probability level of $p < 0.05$ was considered significant.

CHAPTER III

PNKP inhibitor A12B4C50 induces DNA repair complex dissociation but does not affect checkpoint adaptation

1. Introduction

Cancer cells have hallmarks that differentiate them from normal cells. One of the hallmarks is a sustained proliferative signal, which can be targeted by genotoxic treatment to inhibit DNA replication (Helleday et al., 2008; Hanahan & Weinberg, 2011). Topoisomerases are an example of enzymes that play an important role in DNA replication and are used as therapeutic targets. Topoisomerases release the topological restraints that emerge from DNA strand separation during replication and transcription (Pommier et al., 2010). There are five known human topoisomerases, one of them is topoisomerase 1 (Topo1). Topo1 nicks one DNA strand to initiate DNA relaxation and forms a Topo1-DNA cleavage complex with a covalent bond to the 3'-phosphate (P) break end. Upon resolving the topological restraint, Topo1 re-ligates the nick (Champoux, 2001).

CPT is a Topo1 inhibitor and has been used to treat colon cancer patients. CPT stabilizes the Topo1-DNA cleavage complex, which prevents the re-ligation of the nick, leaving an SSB (Koster et al., 2007; Xu & Her, 2015). These SSBs are converted to DSB during S phase when the replication fork collides with the Topo1-DNA cleavage complex (Strumberg et al., 2000; Pommier et al., 2003). DSBs activate repair pathways to maintain genome stability, however, when there is too much damage to be repaired, cells will initiate a cell death programme, achieving the therapeutic goal of chemical induced cell death (Hartwell et al., 1994; Jekimovs et al., 2014).

The capacity of tumour cells to repair damaged DNA could influence the clinical response to many genotoxic treatments. As a result, inhibitors of several DNA repair enzymes, are being investigated for their ability to sensitize cells to radiation and chemotherapeutic drugs (Pilie et al., 2018). We are focussing on the DNA repair enzyme PNKP, which functions as both phosphatase and kinase in the processing of DNA ends produced by topoisomerase inhibitors. These 3’-P and

5’-OH ends cannot be ligated and are processed by PNKP to generate 3'-OH and 5'-P termini that are accessible for ligation by DNA ligase III (LIG3) (Figure 22) (Pheiffer & Zimmerman, 1982; Habraken & Verly, 1988). PNKP is involved in SSB repair and the non-homologous end joining (NHEJ) repair pathway (Weinfeld et al., 2011), whereas homologous recombination (HR) is independent from PNKP and requires DNA end resection for homology sequence searching in sister chromatids (Symington & Gautier, 2011). PNKP is regulated by complex formation with the DNA repair scaffold proteins XRCC1 and XRCC4 for SSB repair and NHEJ, respectively (Weinfeld et al., 2011). Like several other DNA repair proteins, PNKP, has become of increasing clinical interest for the sensitization of cancer cells to IR or chemotherapeutic agents (Zhu et al., 2009; Allinson, 2010). The inhibition of PNKP has been shown to sensitize cancer cells to CPT (Freschauf et al., 2009; Freschauf et al., 2010).

In this chapter, we studied whether the inhibition of PNKP would affect checkpoint adaptation entrance or survival. Checkpoint adaptation is a mechanism in which cancer cells treated with pharmacological concentrations of chemotherapeutic drugs enter mitosis with damaged DNA (Syljuasen, 2007; Kubara et al., 2012). It has been suggested that checkpoint adaptation might contribute to genomic instability (Lewis & Golsteyn, 2016; Swift & Golsteyn, 2016b) and may be involved in tumour resistance and relapse (Burrell et al., 2013). We have developed an experimental model, in which HT-29 cells that are treated with 50 nM CPT undergo checkpoint adaptation and have shown that some of these cells are able to proliferate, but with striking chromosomal rearrangements (chapter 2). It is reasonable to assume that these chromosomal rearrangements are formed by the joining of broken chromosomes. Therefore, we investigated whether PNKP might participate in chromosomal changes or the steps of checkpoint adaptation, by using PNKP inhibitors. To study the effect of PNKP inhibition on checkpoint adaptation, we tested three new PNKP inhibitors, A12B4C3 (H5), A12B4C50 and A83B4C63.

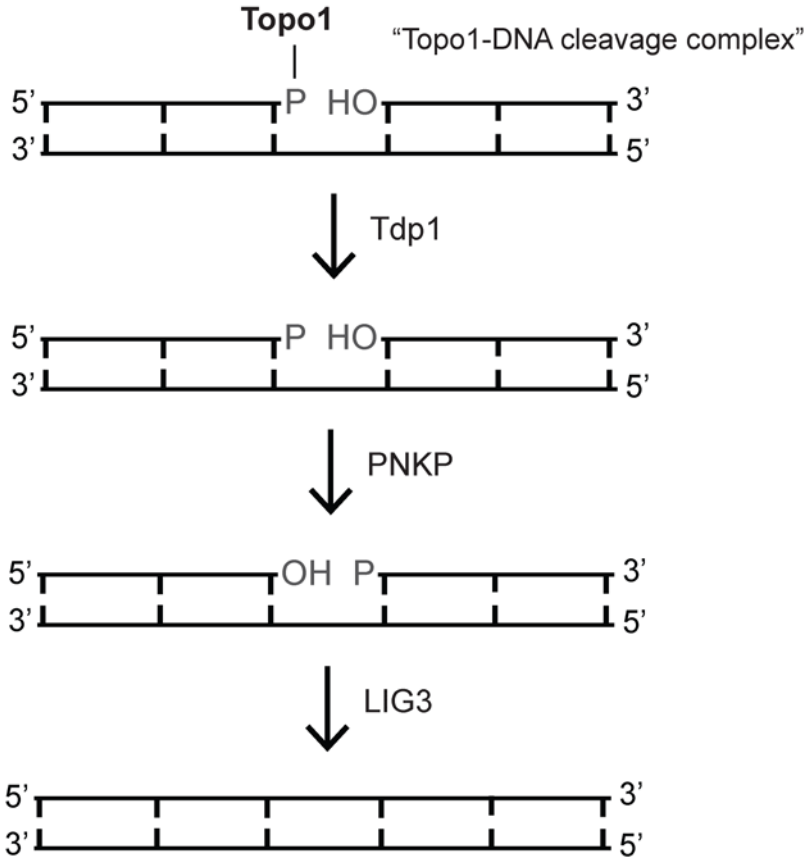

Figure 22. DNA break termini induced by CPT treatment. CPT stabilizes the Topo1-DNA cleavage complex, preventing nick ligation. Tdp1 can cleave the covalent bond between 3'-P and Topo1, allowing PNKP to process DNA termini to 3'-OH and 5'-P, which can be rejoined by LIG3 (Weinfeld et al., 2011).

2. Results

2.1 Morphology assay of novel PNKP inhibitors

To study PNKP inhibitors in relation to checkpoint adaptation, we first investigated the morphological effect of PNKP inhibitors on HT-29 cells. In a morphology assay, we tested the three new PNKP inhibitors, H5, A12B4C50 and A83B4C63, which were provided by Dr. M. Weinfeld from the University of Alberta. Cells were either not treated, treated with 50 nM CPT, used as a genotoxic control, or treated with H5, A12B4C50 or A83B4C63 at 1.5 µM, 5 µM and 15 µM, for 48 hours. By phase-contrast light microscopy, no differences in cell morphology were observed between the not-treated and the PNKP inhibitor-treated cultures at 1.5 and 5 µM. Cells treated with 15 µM H5 did not display a morphological change compared to not-treated cells, whereas cells treated with 15 µM A12B4C50 or A83B4C63 showed a weakly or not adherent morphology, membrane blebbing and cell-cell detachment. Cells treated with 50 nM CPT showed an increase in cell rounding, compared to the not-treated and PNKP inhibitor-treated cultures, as expected (Figure 23). For subsequent experiments, we decided to continue with A12B4C50 as our PNKP inhibitor, which was being investigated by several other laboratories studying PNKP, at a concentration at which no effect on cell morphology was detected, which was 5 µM.

2.2 Inhibition of DNA repair complex PNKP-XRCC1 by A12B4C50

We investigated whether the proteins PNKP and XRCC1 were present and co-localized in our experimental model. HT-29 cells were either not treated, treated with 50 nM CPT, treated with 5 µM A12B4C50, or co-treated with 50 nM CPT and 5 µM A12B4C50 for 24 hours. Cells were stained with DAPI and anti-PNKP (Figure 24) or anti-XRCC1 (Figure 25) antibodies. Immunofluorescence microscopy showed that PNKP was localized both inside and outside the nucleus, with a higher signal within the nucleus. No differences were observed between the not-treated and treated cultures (Figure 24). XRCC1 was observed to be localized mainly in the nucleus

and at low levels outside the nucleus. No differences were observed between the not-treated and treated cultures (Figure 25). These data showed that PNKP and XRCC1 co-localized in our model.

We tested whether A12B4C50 interaction with PNKP could be detected by the Cellular Thermal Shift Assay (CETSA). Cells were either not treated, treated with 10 μM of the Cdk4 inhibitor PD0332991, or treated with 5 μM A12B4C50 for 24 hours. To set conditions for the CETSA, we used cyclin-dependent kinase 4 **(**Cdk4) protein stabilization upon PD0332991 ligand binding as the positive control. Cells were collected and heated to different temperatures ranging from 39.7 ℃ to 67.0 ℃, whereafter cells were lysed and extracts prepared. These extracts were analyzed by western blotting for Cdk4 and PNKP. In not-treated cells, Cdk4 showed a gradual decrease in protein levels from 39.7 ℃ to 67.0 ℃. Upon treatment with PD0332991, the intensity of protein levels increased at 39.7 ℃ compared to not-treated cells at this temperature. This intensity was maintained until a temperature of 49.2 ℃, where after Cdk4 levels gradually decreased to not-treated levels. PNKP showed protein levels that remained stable from 39.7 ℃ to 43.9 ℃ in not-treated cells, where after it decreased at 46.5 ℃, and was undetectable from 49.2 ℃ onwards. Upon treatment with A12B4C50, no differences were detected upon PNKP protein levels, compared to not-treated cells. (Figure 26A). By dosimetry scanning, we determined that PD0332991 treatment led to significant thermal stabilization of Cdk4 at 46.5 ℃ and 49.2 ℃, compared to not treated cells. No thermal stabilization of PNKP was detected upon A12B4C50 treatment, compared to not-treated cells (Figure 26B). These data showed that A12B4C50 did not thermally stabilize PNKP in vitro at 5 μM.

We next sought to determine whether A12B4C50 addition to cells would have an effect upon the interaction between PNKP and its binding partner XRCC1. To test this, we performed a XRCC1 immunoprecipitation from cells that were either not treated, treated with 50 nM CPT, treated with 5 μM A12B4C50, or co-treated with 50 nM CPT and 5 μM A12B4C50 for 24 hours. Cell extracts were prepared and each extract was either mock-treated (whole cell extract) or incubated with anti-XRCC1 antibodies. The immune-complex was analyzed by western blotting

with anti-XRCC1 and anti-PNKP antibodies. Anti-actin antibodies were used as a control for the amount of protein loaded. The supernatant remaining after isolation of the immuno-complex was also analyzed (Figure 27). We observed that XRCC1 was present in the whole cell extract, which we were able to isolate with immunoprecipitation (IP XRCC1), resulting in lower levels of XRCC1 remaining in the supernatant. PNKP was present in the whole extract at lower levels than XRCC1. We compared levels of XRCC1 to PNKP in each treatment to determine complex formation. Cells either not treated and A12B4C50 treated showed low levels of PNKP that co-immunoprecipitated with XRCC1. CPT-treated cells showed an increase in XRCC1 levels compared to not-treated and A12B4C50-treated cells, which co-immunoprecipitated PNKP, as expected (Whitehouse et al., 2001). Co-treatment of CPT with A12B4C50 resulted in a lower XRCC1 band intensity than CPT-treated cells, but stronger compared to not-treated and A12B4C50-treated cells. We also observed a reduction of the co-immunoprecipitation of PNKP with XRCC1, compared to CPT-treated cells, confirming its intended function (Freschauf et al., 2009). This result showed that A12B4C50 was able to reduce the PNKP-XRCC1 interaction in our experimental model.

2.3 PNKP inhibitors do not affect cell rounding

To determine whether PNKP inhibitors would affect the process of checkpoint adaptation, we co-treated HT-29 cells with CPT and one of the three PNKP inhibitors to test for cell rounding, which is a marker for checkpoint adaptation (Kubara et al., 2012; Swift & Golsteyn, 2014). Cells were either not treated, treated with 5 μM H5, A12B4C50 or A83B4C50, treated with 50 nM CPT, or co-treated with 50 nM CPT and 5 μM of one of the inhibitors. The cells were observed and scored for cell rounding by phase-contrast light microscopy 48 hours after treatment. The not-treated culture showed few rounded cells. The cultures treated with the inhibitors showed a similar cell morphology as the not-treated culture. In the CPT-treated culture, we observed an increase in rounded cells compared to the not-treated culture. No morphological differences were observed

between the culture treated with CPT and the cultures co-treated with CPT and the PNKP inhibitors (Figure 28A).

We determined the percentages of rounded cells in the cultures 48 hours after treatment and found that the percentages of rounded cells were 1.7% ± 0.4% in the not-treated culture, 1.8% ± 0.6% in the H5-treated culture, 1.4% ± 0.4% in the A12B4C50-treated culture, and 0.9% ± 0.2% in the A83B4C63-treated culture. By contrast, the percentages were 11.0% ± 1.4% in the CPT-treated culture, 8.4% ± 1.3% in the co-treated culture of CPT with H5, 10.1% ± 1.7% in the co-treated culture of CPT with A12B4C50, and 8.8% ± 0.4% in the co-treated culture of CPT with A83B4C63 (Figure 28B). These results showed that percentages of rounded cells after CPT treatment were not affected by the presence of a PNKP inhibitor.

2.4 Cells co-treated with CPT and A12B4C50 stain for histone γH2AX and pH3

We determined that the co-treatment of CPT with A12B4C50 was able to reduce PNKP-XRCC1 interaction, but did not affect the number of rounded cells compared to CPT treatment alone. We then tested whether A12B4C50 co-treated cells still produced the checkpoint adaptation phenotype of mitosis with damaged DNA, using immunofluorescence microscopy. Cells were either not treated, treated with 50 nM CPT, treated with 5 μM A12B4C50, or co-treated with 50 nM CPT and 5 μM A12B4C50, and were stained with DAPI, histone γH2AX and pH3 antibodies, at 48 hours after treatment. In the not-treated and A12B4C50-treated culture, few cells stained for histone γH2AX and pH3. The CPT-treated culture showed many cells staining for histone γH2AX and an increase in the number of cells staining for pH3, compared to the not-treated and A12B4C50-treated culture (Figure 29A). Co-treatment of CPT with A12B4C50 resulted in a cell phenotype similar to that of the CPT-treated culture.

The percentages of cells staining for histone γH2AX were determined. In the not-treated culture 0.4% ± 0.3% of the cells stained for histone γH2AX, compared to 95.3% ± 4.5% in the CPT-treated culture, 0.6% ± 0.2% in the A12B4C50-treated culture, and 71.8% ± 7.7% in the co-treated

culture of CPT with A12B4C50 (Figure 29B). Next, we determined the percentages of cells staining for pH3. We observed that 3.7% ± 0.4% of not-treated cells stained for pH3, which was similar to the percentage of cells in the A12B4C50-treated culture (3.3% ± 0.2%). By contrast, in the CPT-treated culture 9.1% ± 3.5% of the cell stained for pH3, consistent with checkpoint adaptation as previously reported (Kubara et al., 2012), In the co-treated culture the percentage of pH3 staining cells was 7.1% ± 1.8% (Figure 29C). These data supported the cell rounding data and confirmed that cells co-treated with CPT and A12B4C50 underwent checkpoint adaptation. We observed no effect of A12B4C50 on the number of cells entering checkpoint adaptation.

2.5 Chromosome configuration was not affected by A12B4C50

Although our results showed that A12B4C50 had little effect upon entry into mitosis, we sought to identify whether it affected two of the key outcomes of checkpoint adaptation, changes in chromosome structure and survival rate. We compared the karyotypes of cells either not treated, treated with 50 nM CPT, treated with 5 μM A12B4C50, or co-treated with 50 nM CPT and 5 μM A12B4C50 for 48 hours. Mitotic cells were collected by mechanical shake-off, stained with DAPI, and observed by immunofluorescence microscopy. We observed that not-treated cells and A12B4C50-treated cells showed similar chromosome configurations. In CPT-treated and co-treated cells we observed that the majority of these cells contained shattered chromosomes, compared to the not-treated and A12B4C50-treated cultures. No difference between CPT treatment and co-treatment was observed (Figure 30A).

We scored the number of cells that fitted into each of the following categories: SCC, ICC; or WCC. In the not-treated or A12B4C50-treated cultures, no cells with an SCC were observed. By contrast, the percentage of cells with an SCC was 44.4% ± 2.9% in the CPT-treated culture and 53.7% ± 3.5% in the CPT with A12B4C50 co-treated culture. The percentages of cells with an ICC were 2.2% ± 1.1% in the not-treated culture, 50.0% ± 1.9% in the CPT-treated culture, 3.7% ± 2.2% in the A12B4C50-treated culture, and 42.6% ± 3.4% in the co-treated culture of CPT with

A12B4C50. The percentages of cells with a WCC were 97.8% ± 1.1% in the not-treated culture, 5.6% ± 2.2% in the CPT-treated culture, 96.3% ± 4.5% in the A12B4C50-treated culture, and 3.7% ± 0.3% in the co-treated culture of CPT with A12B4C50 (Figure 30B). These results suggested that the chromosome configuration after co-treatment was similar to that of CPT treatment alone.

2.6 A12B4C50 does not affect checkpoint adaptation survival rates

We next determined whether the co-treatment of CPT with A12B4C50 affected the survival rate of cell that underwent checkpoint adaptation. Cells were either not treated, treated with 50 nM CPT or 50 nM CPT with 5 µM A12B4C50 (TDC – total and DNA-damaged cells) or treated with 5 µM A12B4C50 alone. Images are shown for CPT treatment and the co-treatment 48 hours after treatment. We performed a mechanical shake-off to isolate the weakly adherent mitotic cells (MDC – mitotic and DNA-damaged cells) from the adherent flattened interphase cells (IDC – interphase and DNA-damaged cells) (Figure 31).

The MDC's were then re-cultivated for ten days. No morphological differences were observed by phase-contrast light microscopy between the survival cultures that were cultivated from cells either not-treated, treated with 50 nM CPT, treated with 5 µM A12B4C50, or co-treated with 50 nM CPT and 5 µMA12B4C50, after ten days (Figure 32A). This result was consistent with previously described data (chapter 2). In the not-treated culture, 65.2% ± 26.1% of the re-cultivated cells survived, similar to the 64.7% ± 30.5% that was observed in the A12B4C50-treated culture. After CPT treatment, cell survival was 0.8% ± 0.5%, which was similar to the value of 2.5% ± 0.9% after co-treatment of CPT with A12B4C50 (Figure 32B). These data showed that A12B4C50 addition to CPT treatment did not affect survival rate after checkpoint adaptation.

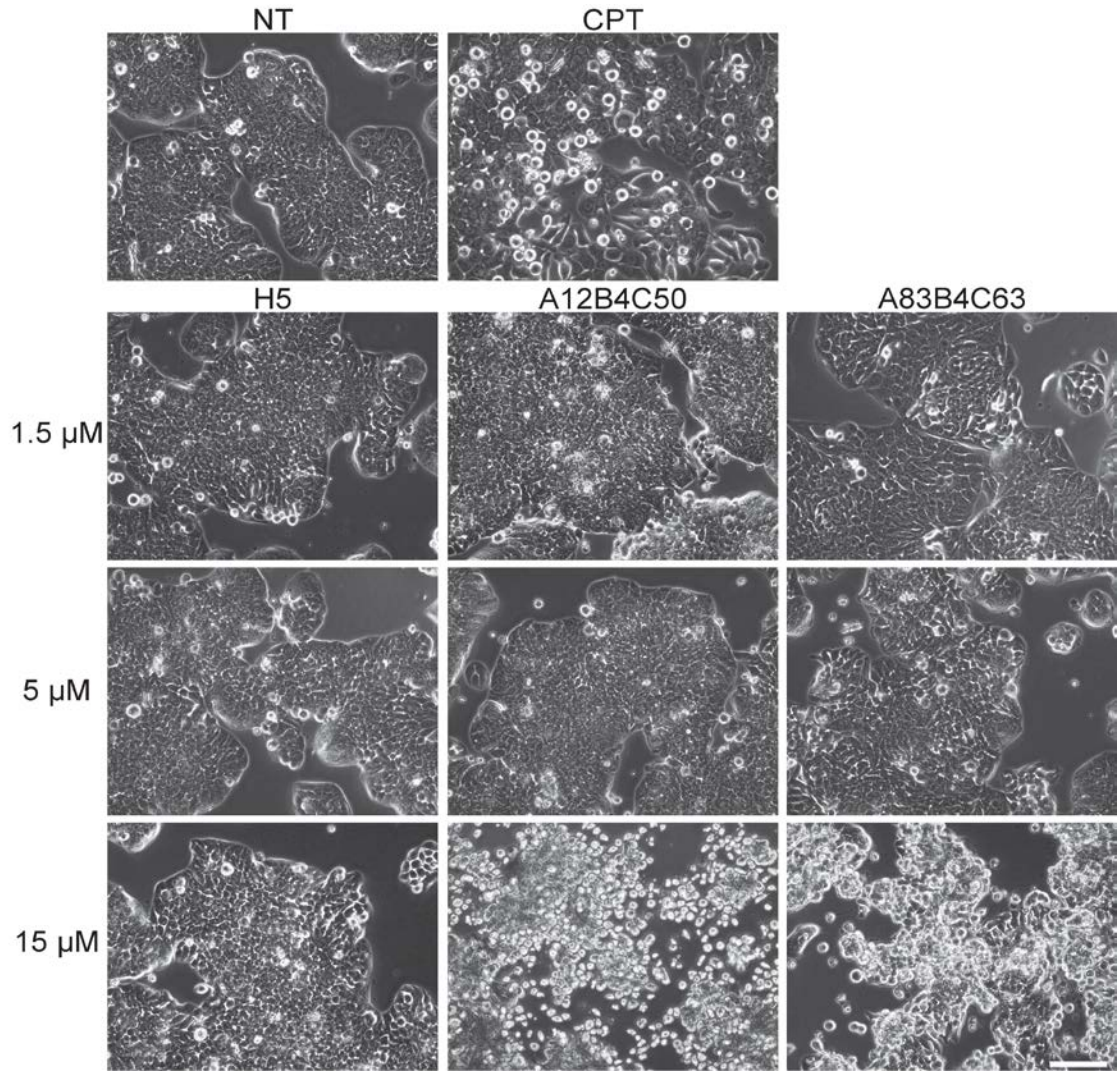

Figure 23. Cells treated with different concentrations of PNKP inhibitors. HT-29 cells were not treated (NT), treated with 50 nM CPT (CPT), or treated with different concentrations (1.5, 5, and 15 µM) of the PNKP inhibitors, H5, A12B4C50, and A83B4C63. Cells were observed by phase-contrast light microscopy at 48 h after treatment. Scale bar = 150 µm.

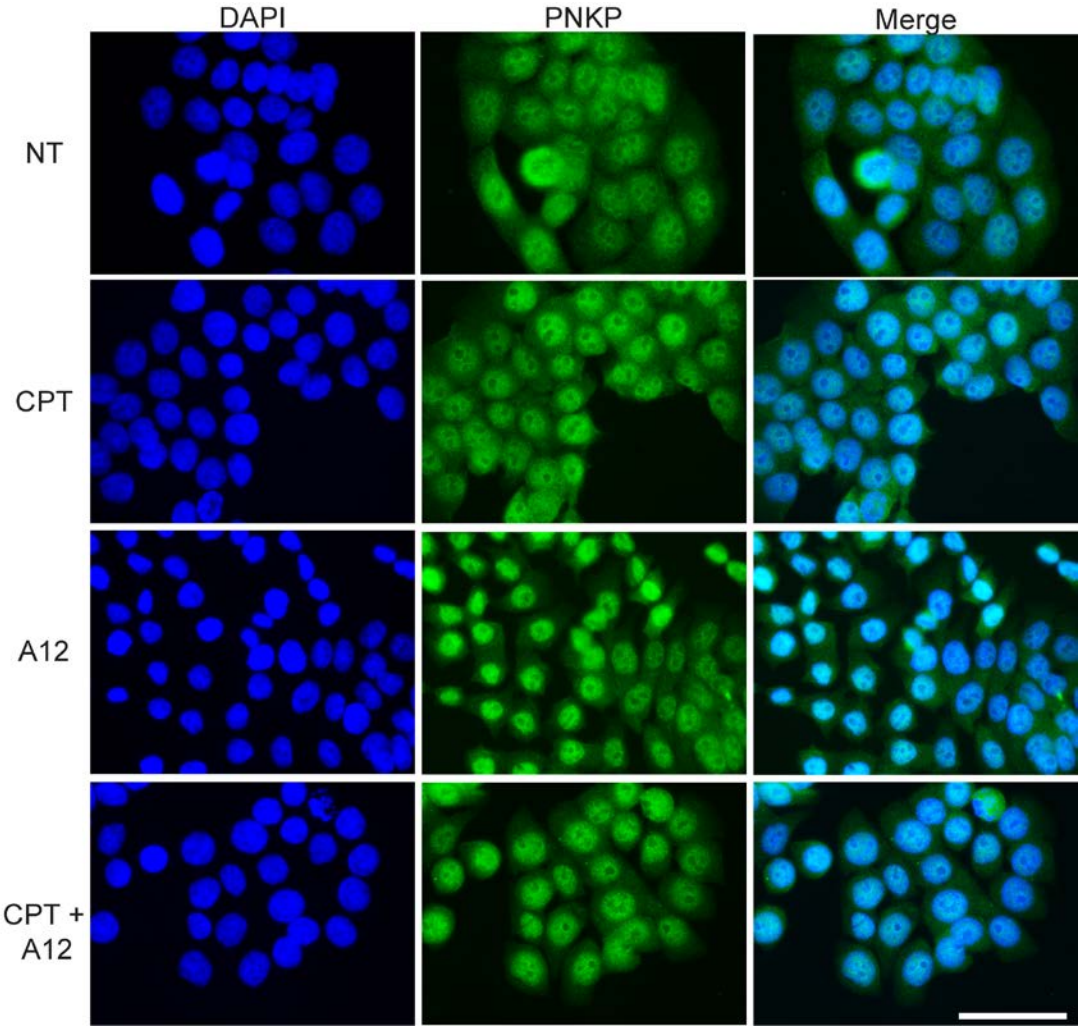

Figure 24. The cellular location of PNKP does not change after treatment with the PNKP inhibitor A12B4C50. HT-29 cells were not treated (NT), treated with 50 nM CPT (CPT), treated with 5 μM A12B4C50 (A12), or co-treated with 50 nM CPT and 5μM A12B4C50 (CPT + A12) for 24 h, and stained with DAPI (blue) to detect DNA and anti-PNKP antibodies (green). Cells were observed by immunofluorescence microscopy. Scale bar = 50 μm.

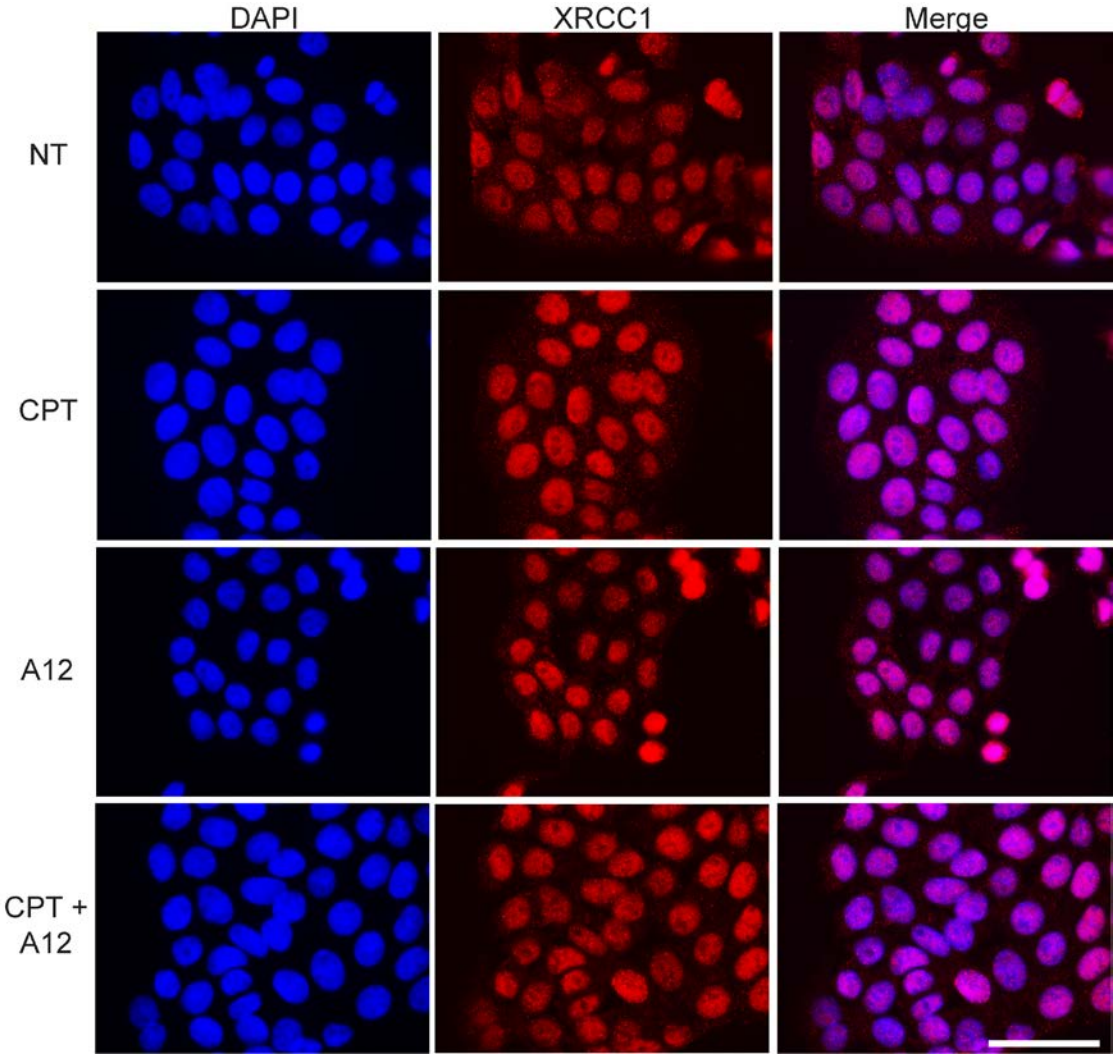

Figure 25. The cellular location of a protein partner of PNKP, XRCC1, does not change after treatment with the PNKP inhibitor A12B4C50. HT-29 cells were not treated (NT), treated with 50 nM CPT (CPT), treated with 5 µM A12B4C50 (A12), or co-treated with 50 nM CPT and 5µM A12B4C50 (CPT + A12) for 24 h, and stained with DAPI (blue) to detect DNA and anti-XRCC1 antibodies (red). Cells were observed by immunofluorescence microscopy. Scale bar = 50 µm.

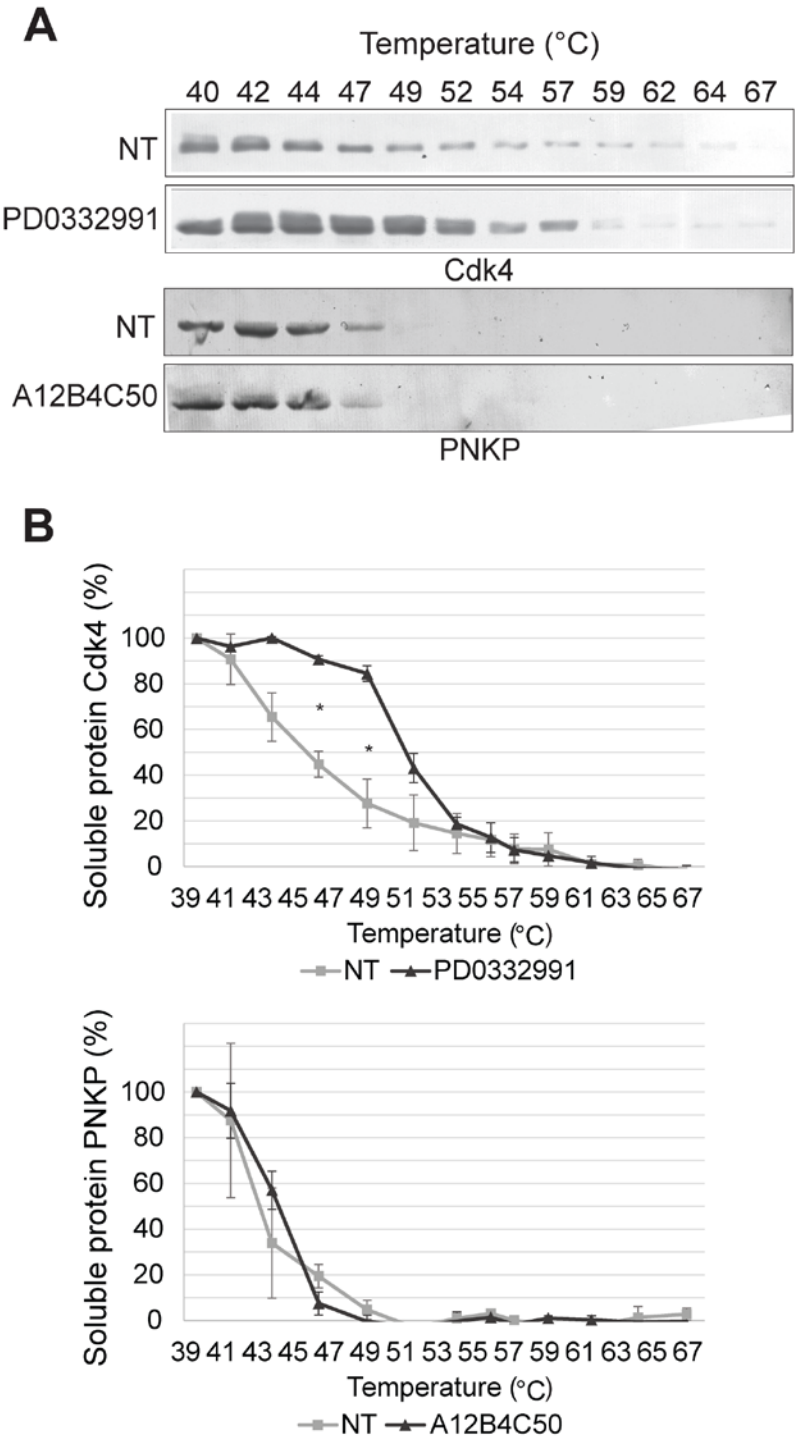

Figure 26. Analysis of cells treated with A12B4C50 by CETSA. (A) HT-29 cells were not treated (NT), treated with 10 µM PD0332991 (a Cdk4 inhibitor), or treated with 5 µM A12B4C50 for 24 h. Cell were processed at temperatures ranging from 39.7 °C to 67.9 °C and analyzed by western blotting with either Cdk4 (top panels) or PNKP (bottom panels) antibodies. (B) The western blots in A were analyzed and the percentage of soluble protein determined by dosimetry scanning per sample. The mean percentages ± SEM are shown from three separate experiments. The asterisks show significant differences between not-treated and PD0332991-treated samples, $p < 0.05$.

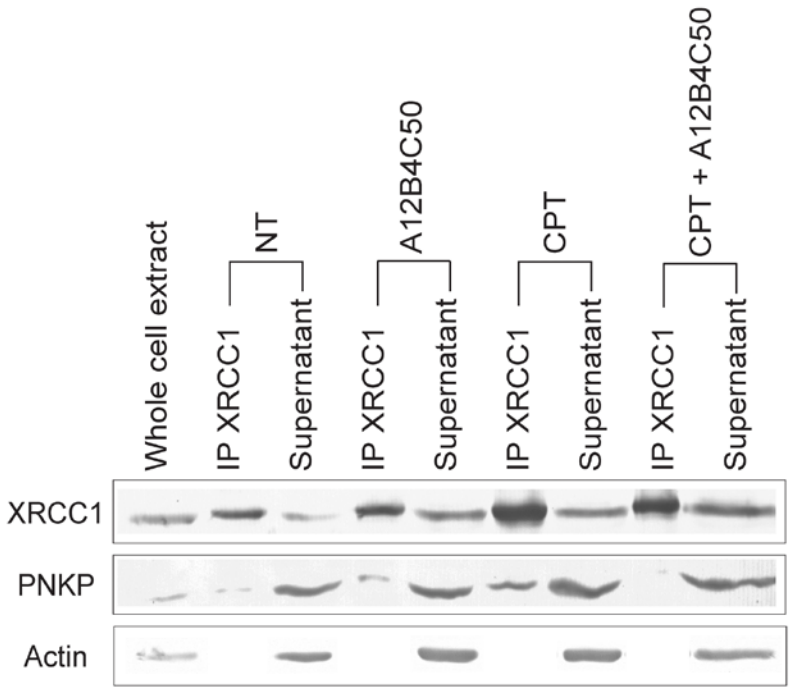

Figure 27. Analysis of the PNKP-XRCC1 complex in cells treated with A12B4C50. HT-29 cells were either not treated (NT), treated with 5 μM A12B4C50, treated with 50 nM CPT, or co-treated with 50 nM CPT and 5 μM A12B4C50 (CPT + A12B4C50) for 24 h. Cell extracts were prepared and XRCC1 was isolated by immunoprecipitation with anti-XRCC1 antibodies. The whole cell extract, immunoprecipitated samples (IP XRCC1), and supernatants after immunoprecipitation were analyzed by western blotting with anti-XRCC1, anti-PNKP or anti-actin antibodies (control).

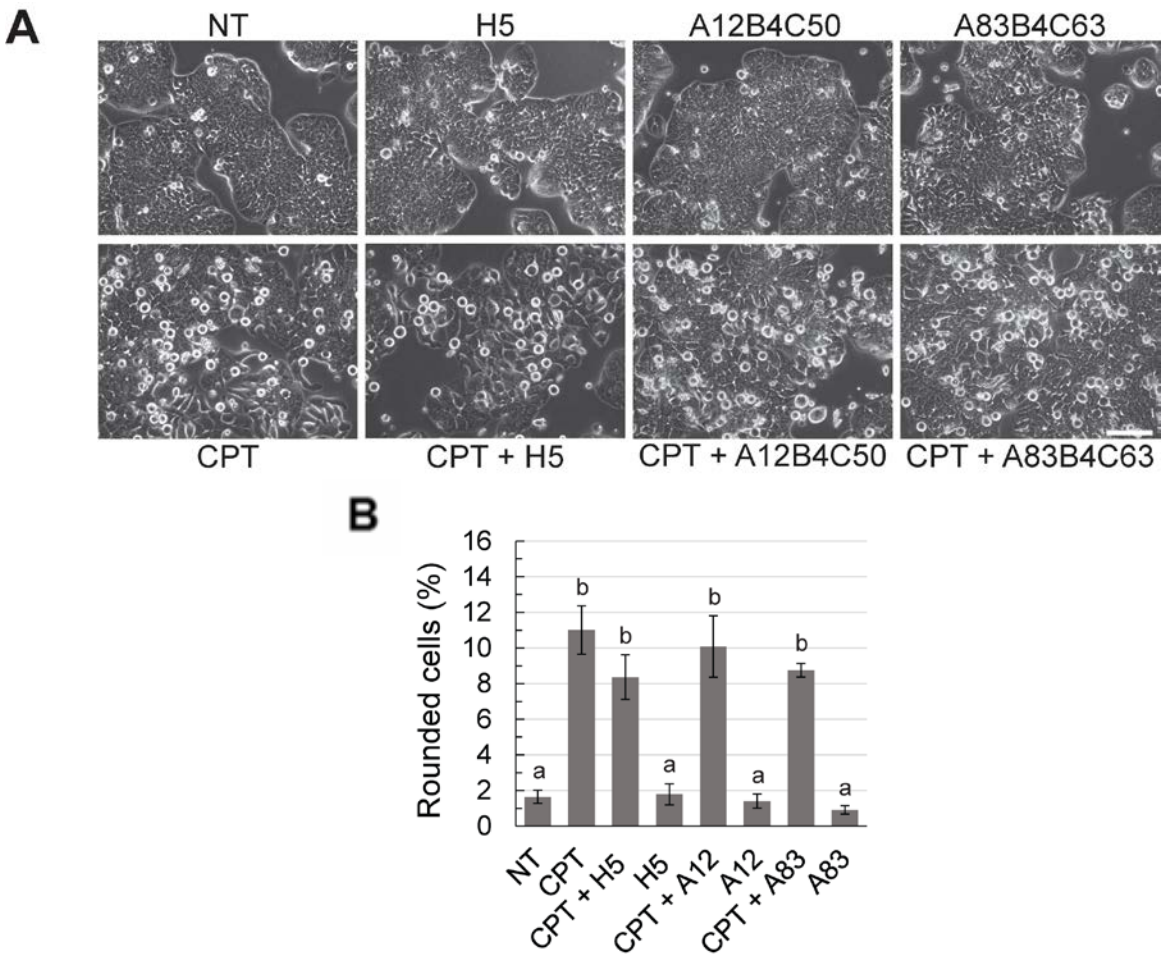

Figure 28. Cells co-treated with CPT and A12B4C50 acquire a rounded morphology. (A) HT-29 cells were either not treated (NT), treated with one of the PNKP inhibitors at 5 μM (H5, A12B4C50, or A83B4C63), treated with 50 nM CPT, or co-treated with 50 nM CPT and one of the PNKP inhibitors at 5 μM (H5, A12B4C50, or A83B4C63). Cells were observed by phase-contrast light microscopy 48 h after treatment. Scale bar = 100 μm. (B) Cells were prepared and analyzed as described in A and the percentages of rounded cells were determined. The mean percentages ± SEM from three separate experiments are shown. The letters show significant differences, different letters represent significant difference, $p < 0.05$.

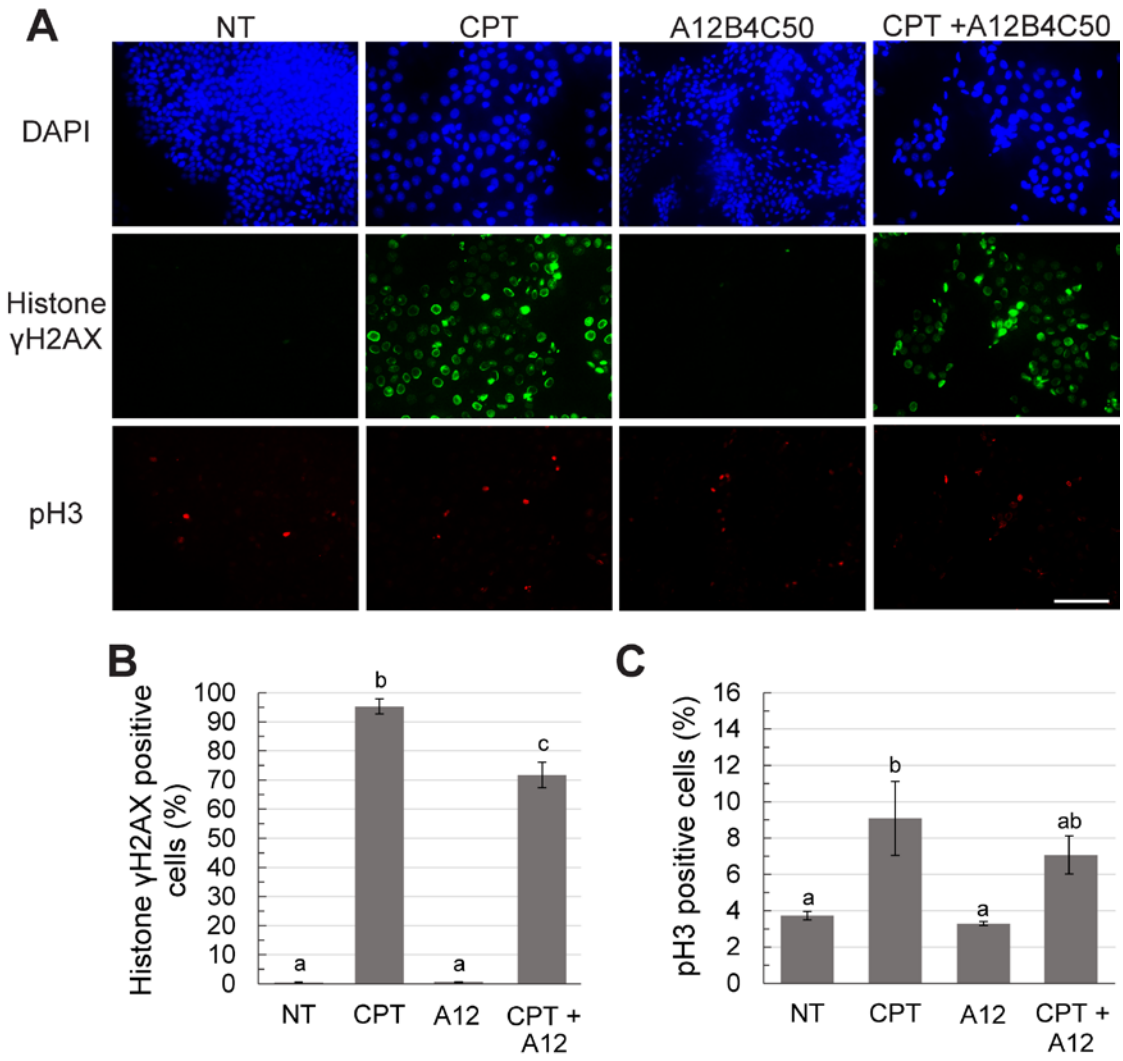

Figure 29. Cells co-treated with CPT and A12B4C50 have damaged DNA and enter mitosis. (A) HT-29 cells were either not treated (NT), treated with 50 nM CPT (CPT), treated with 5 µM A12B4C50 (A12B4C50), or co-treated with 50 nM CPT and 5µM A12B4C50 (CPT + A12B4C50) for 48 h. Cells were stained with DAPI (blue) to detect DNA, anti-histone γH2AX (green), and anti-phospho-Ser^{10} histone H3 (pH3 - red) antibodies. Cells were observed by immunofluorescence microscopy. Scale bar = 100 µm. (B) Cells were prepared and analyzed as described in A. The percentages of cells staining for histone γH2AX were determined. The mean percentages ± SEM from three separate experiments are shown. The letters show significant differences, different letters represent significant difference, $p < 0.05$. (C) Cells were prepared and analyzed as described in A. The percentage of cells staining for phospho-Ser^{10} histone H3 (pH3) was determined. The mean percentages ± SEM from three separate experiments are shown. The letters show significant differences, different letters represent significant difference, $p < 0.05$.

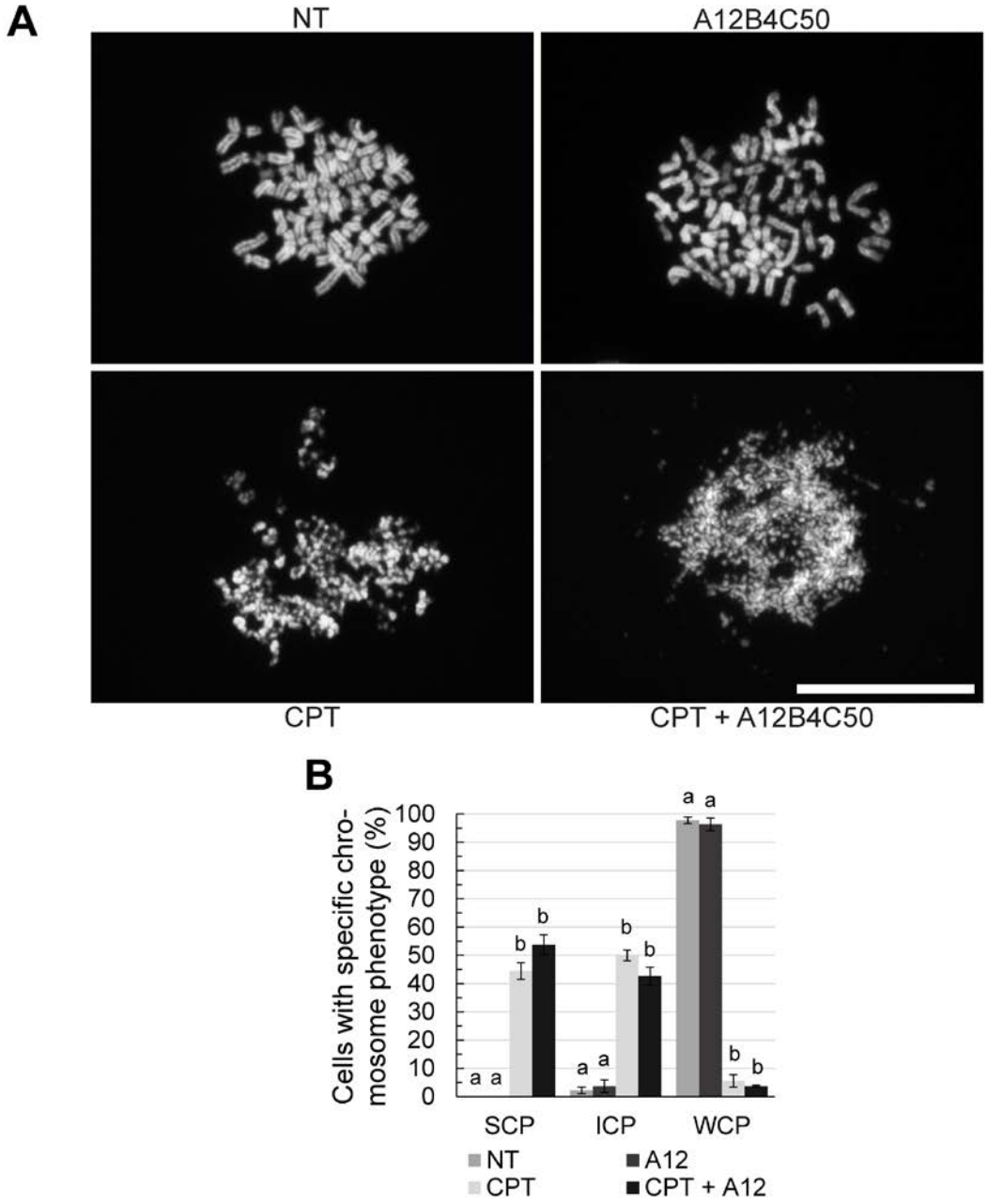

Figure 30. Cells undergoing checkpoint adaptation with or without A12B4C50 show abnormal chromosome configurations. (A) HT-29 cells were either not treated (NT), treated with 5 μM A12B4C50 (A12B4C50), treated with 50 nM CPT (CPT), or co-treated with 50 nM CPT and 5μM A12B4C50 (CPT + A12B4C50) for 48 h. MDCs (mitotic and DNA-damaged cells) were collected and stained with DAPI (blue) to detect condensed chromosomes. Cells were analyzed by immunofluorescence microscopy. Scale bar = 25 μm. (B) Cells were prepared and analyzed as described in A. The chromosome configurations of cells were determined and categorized into: SCC, ICC or WCC. The percentages of cells in each category was determined. The mean percentages ± SEM from three separate experiments are shown. The letters represent significant differences within configurations, samples with different letters are significantly different, $p < 0.05$.

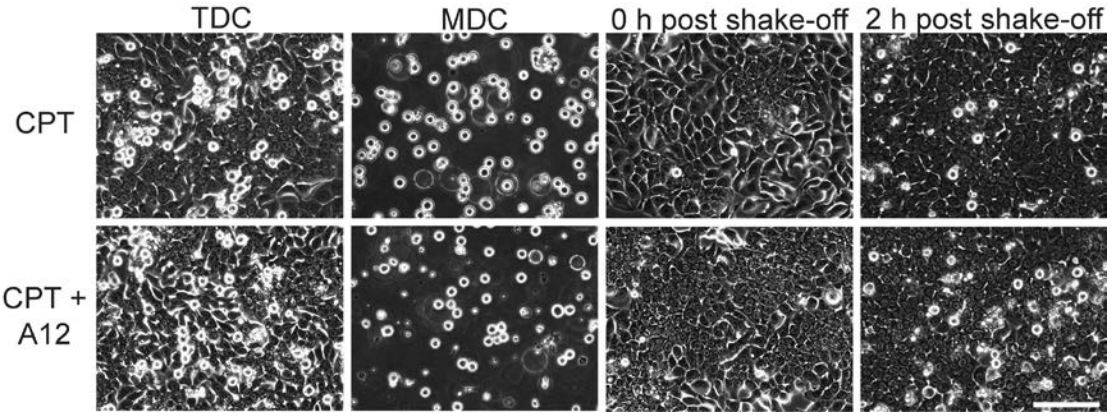

Figure 31. Cells that undergo checkpoint adaptation with or without A12B4C50 acquire a rounded morphology and can be collected by mechanical shake-off. HT-29 cells were treated with 50 nM CPT (CPT) or co-treated with 50 nM CPT and 5 μM A12B4C50 (CPT + A12B4C50) and observed by phase contrast light microscopy. At 48 hours after treatment, the population of cells (TDC- total and DNA-damaged cells) contain a mix of interphase cells and cells in mitosis with a rounded morphology. Rounded cells were collected by mechanical shake-off (MDC – mitotic and DNA-damaged cells), leaving flattened interphase cells (IDC – interphase and DNA-damaged cells). New rounded cells appeared within 2 h in the IDC culture (2 h post-shake-off). Scale bar = 100 μm.

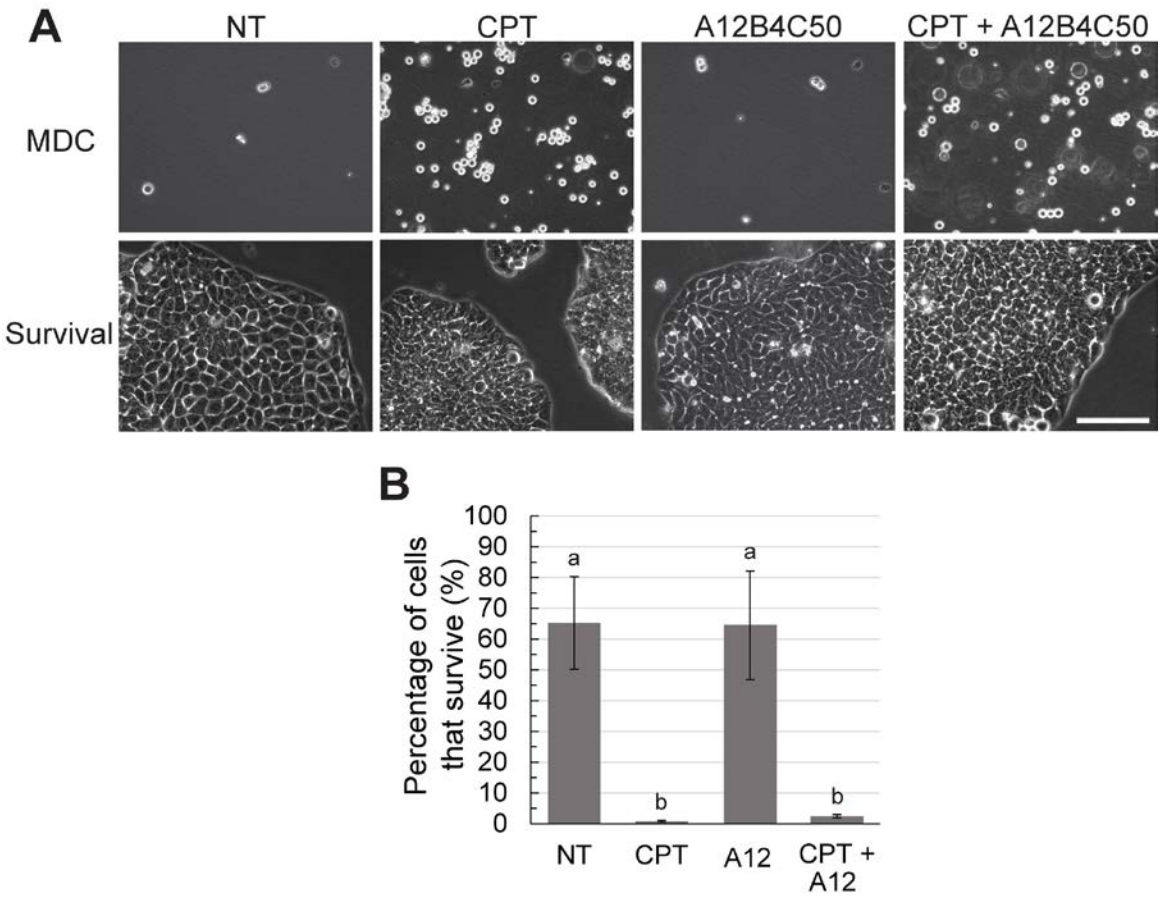

Figure 32. Cells that undergo checkpoint adaptation with or without PNKP inhibitors have similar survival percentages.(A) HT-29 cells were not treated (NT), treated with 50 nM CPT (CPT), treated with 5 µM A12B4C50 (A12), or co-treated with 50 nM CPT and 5 µM A12B4C50 (CPT + A12). MDCs (mitotic and DNA-damaged cells) were collected by mechanical shake-off and recultivated for 10 days (survival). Cells were observed by phase contrast light microscopy. Scale bar = 100 µm. (B) Cells were prepared and analyzed as described in A. Cells were counted at the time of collection (MDC) and after 10 days of re-cultivation (survival) to determine the percentage of cells surviving checkpoint adaptation. The mean percentages ± SEM from three separate experiments are shown. The letters show significant differences, different letters represent significant difference, $p < 0.05$.

3. Discussion

Clinical response of many genotoxic treatments has been shown to be affected by the capacity of tumour cells to repair damaged DNA. Therefore, inhibitors of several DNA repair enzymes, such as Chk1, PARP1 and PNKP, are being studied for the sensitization of cancer cells to genotoxic agents (Pilie et al., 2018). Inhibition of PNKP phosphatase activity has been shown to increase sensitivity of cancer cells to CPT (Freschauf et al., 2009; Freschauf et al., 2010). The purpose of our study was to investigate whether PNKP inhibitors would modify the process or outcome of checkpoint adaptation. Because PNKP has already been demonstrated to increase cytotoxicity in a CPT model, we proposed to test if we could increase cytotoxicity in a checkpoint adaptation model, which uses a lower, yet cytotoxic concentration of CPT. In this study, we showed that the PNKP inhibitor A12B4C50 was able to inhibit the PNKP interaction with XRCC1, however, no effect of A12B4C50 on checkpoint adaptation outcome was detected.

To begin to test the role of a PNKP inhibitor in our model, we selected A12B4C50 as the inhibitor, for the reason that it was being investigated by several other laboratories studying PNKP. We decided to study A12B4C50 at a concentration of 5 μM, as 15 μM induced changes in cell morphology that has not previously been reported and may be due to its effect on secondary targets in cells. Next, we confirmed that A12B4C50 had a biological effect when added to cells. We co-immunoprecipitated PNKP with XRCC1 and observed a reduction of PNKP-XRCC1 interaction after co-treatment with CPT and A12B4C50, compared to CPT treatment alone. These data show that A12B4C50 was able to inhibit PNKP and thereby reducing the DNA repair complex PNKP-XRCC1 interaction, which is involved in SSB repair. This result suggests that the DNA repair protein complex PNKP-XRCC4, which is involved in NHEJ, might also be reduced upon A12B4C50 treatment.

Knowing that A12B4C50 was able to reduce PNKP-XRCC1 interaction, we tested the relationship between this inhibitor and checkpoint adaptation. By immunofluorescence microscopy, we confirmed that the cells co-treated with CPT and A12B4C50 entered mitosis with damaged

DNA. The percent of cells staining for damaged DNA decreased after co-treatment of CPT with A12B4C50, compared to treatment with CPT alone. We did not observe a change in the percentage of cells entering mitosis after CPT treatment upon a co-treatment with A12B4C50. A suggestive explanation might be that inhibition of PNKP reduced DNA repair, thereby maintaining high damage DNA levels in cells, reaching a damage threshold that induces apoptosis. There is a small number of cells that did not respond to CPT treatment. In the co-treatment, the total number of cells might have decreased due to apoptosis, whereas the number of cells that were unaffected by CPT treatment remains untouched. Therefore, it appears that damaged DNA signals decreased in cells upon co-treatment with A12B4C50, when actually CPT cytotoxicity was increased.

These obtained data suggest that the A12B4C50 likely alters PNKP function in our model. We explored other methods to test the PNKP inhibitor, such as the CETSA, but we were unable to observe an effect on thermal PNKP stabilization in not-treated and A12B4C50-treated cells. It has been proposed that small molecule inhibitors of PNKP, such as A12B4C50, disrupt its secondary structure, thereby preventing interaction with XRCC1 (Freschauf et al., 2010). However, it is possible that this structural change might not stabilize the protein or only causes a very small structural change that does not affect the overall stability detectable by the CETSA in our laboratory (Martinez et al., 2018). We also tested PNKP and XRCC1 localization in our model. By immunofluorescence microscopy, we observed that the proteins were mainly co-localized in the nucleus and that the localization was independent of the treatment. It has been previously reported that PNKP is localized in the nucleus and mitochondria (Tahbaz et al., 2012), and that XRCC1 is primarily localized in the nucleus but also at low levels in the cytoplasm (Kirby et al., 2015), which is consistent with our data.

We then tested the effect of A12B4C50 upon the outcome of checkpoint adaptation. Chromosome configuration of cells undergoing checkpoint adaptation was determined, but we were unable to detect a difference between chromosome configurations of cells treated with CPT and co-treated with A12B4C50. Additionally, the number of cells surviving after checkpoint adaptation

was also not affected by a co-treatment with A12B4C50. This suggest that A12B4C50 does not affect checkpoint adaptation outcomes. We reason that CPT induced damage may be primarily repaired by HR instead of NHEJ. DSBs that are induced by Topo1 poisons, such as CPT, are one-ended DSBs, caused by replication fork collision in S phase, which are mainly repaired by HR (Arnaudeau et al., 2001; Chapman et al., 2012; Xu & Her, 2015). In addition, it has been shown that NHEJ deficiency or inhibition can lead to cell death resistance in CPT treated cells. A proposed mechanisms how this could occur is that NHEJ has a negative role in Topo1 damage repair. Repair of CPT-induced DSBs by NHEJ would lead to erroneous rejoining of these breaks and promote cell death. Therefore, inhibition of NHEJ by inhibition of PNKP may remove this negative role and promote HR, which is less error prone and hence likely to promote cell survival through checkpoint adaptation (Adachi et al., 2004).

The increase in sensitivity of cells to CPT after PNKP inhibition that has been previously observed, might be explained by the higher concentration of CPT that was used in those cells, compared to our experimental model. The concentration that was used in this previous study ranged from 1 to 6 μM, which is about 20-120 fold higher than our experimental concentration and 13 fold higher than the peak plasma concentration used in the clinic (75 nM) (Raymond et al., 2002). CPT is an S phase-specific toxicant but it has been shown that at higher concentrations of CPT, non-S-phase cells can also be killed by CPT, due to the utilization of different DDR pathways in response to low or high dosages of CPT. A low dosage (0.1 μM) of CPT caused replication initiated processing of the Topo1-DNA cleavage complex, which is S phase-specific, mainly triggering replication protein A (RPA) phosphorylation, supposedly leading to cell cycle arrest. A high dosage (10 μM) of CPT caused transcription initiated processing of the Topo1-DNA cleavage complex, triggering activation of ATM, p53 and Chk1/2 activation, which is S phase independent, supposedly leading to apoptosis (Goldwasser et al., 1995; Huang et al., 2010). Therefore, the sensitivity to CPT upon PNKP inhibition previously observed by Freschauf (2009) might be affected by the utilization of a different DDR pathway than in our model.

We conclude that we are unable to detect an effect of A12B4C50 treatment on checkpoint adaptation outcomes. This might suggest that checkpoint adaptation is dependent on a threshold of damaged DNA and that the primary DNA repair pathway involved in the rejoining of broken chromosomes in checkpoint adaptation is PNKP independent. Previous studies have shown that HR and its downstream pathway play important roles in cell survival promotion after CPT treatment (Arnaudeau et al., 2001; Malik & Nitiss, 2004). Future studies would need to focus on DNA repair pathways involved in checkpoint adaptation in order to reduce chromosomal rearrangements that might contribute to chromosome instability and hence contribute to poor patient outcomes.

4. Materials and methods

4.1 Cell culture

The human cell line HT-29 (ATCC HTB-38) was obtained from the American Type Culture Collection (ATCC). HT-29 cells were maintained in Roswell Park Memorial Institute (RPMI) 1640 medium (ThermoFisher; 21870092) supplemented with 10% (v/v) heat-inactivated fetal bovine serum (FBS) (ThermoFisher; 12484028) and 2 mM GlutaMAX (ThermoFisher; 35050061). Cells were grown at 37°C in 5% CO_2 and media were changed every 3-4 d. HT-29 cells were plated at a density of 3.0 x 10^5cells/25 cm^2 flask or 6.0 x 10^5/6 well culture plate and cultured for 48 or 72 h prior to treatment. The compounds CPT (Sigma; 7689034), H5, A12B4C50 and A83B4C63 (Dr. M. Weinfeld) were dissolved in dimethyl sulfoxide (DMSO) (MilliporeSigma; D2438) to a concentration of 10 mM. The compounds were stored at -20°C until use. Not-treated cells were treated with the solvent only (DMSO) in a volume equal to the highest volume of the compound tested, and never adding more than 1% (v/v), and used as a negative control. CPT was used as a positive control for checkpoint adaptation.

4.2 Cell rounding morphology assay

HT-29 cells were seeded at 6.0 x 10^5/6 well culture plate and incubated at 37°C for 48 or 72 h prior to treatment to reach a cell confluency of 50-70%. Images were captured at 24 and 48 h in HT-29 cells, with an Infinity 1 camera powered by Infinity Capture imaging software (Lumenera Corporation) on an Olympus CKX41 inverted microscope. Images were processed using Adobe Photoshop (CC 2017.0.1) software. Interphase cells and rounded cells were manually counted using Adobe Photoshop (CC 2017.0.1) software and the percentage of rounded cells in the total sample was determined. Not-treated cells were used as a negative control, and CPT treated cells as genotoxic control. A minimum of 200 cells were counted for each treatment and each experiment was performed at least three times. The mean and standard error of the mean of the percentages of rounded cells were calculated.

4.3 Immunofluorescence microscopy

HT-29 cells were plated on glass coverslips at 6.0 x 10^5/6 well culture plate and incubated at 37°C for 48 or 72 h prior to treatment. After 48 h of treatment, cells were fixed at room temperature for 20 min in 3% (v/v) paraformaldehyde (PFA) (Fisher Scientific; 30525894), diluted in PBS (137 mM NaCl, 3 mM KCl, 100 mM Na_2HPO_4, 18 mM KH_2PO_4). Cells were quenched for 10 min with 50 mM NH_4Cl in phosphate buffered saline (PBS), permeabilized for 5 min using 0.2% (v/v) Triton X-100 in PBS and blocked for 1 h with 3% (w/v) bovine serum albumin (BSA) (Fisher Scientific; J6465522) in PBS-T (0.1% (v/v) Tween-20 (MilliporeSigma; CAEM9480) diluted in PBS). Cells were then incubated with primary antibodies as described: anti-histone γH2AX (MilliporeSigma; 05-636; 1:400) for 1 h at room temperature or anti-pH3 (MilliporeSigma; 06-570; 1:1000), monoclonal mouse anti-XRCC1 (Abcam; ab1838; 1:200) or polyclonal rabbit anti-PNKP (Dr. M. Weinfeld, University of Alberta; 1:500) overnight at 4°C. After washing with PBS-T cells were incubated with secondary antibodies for 45 min at room temperature as follows: Alexa Fluor 488-conjugated anti-mouse (ThermoFisher; A11059; 1:400) for anti-histone γH2AX and anti-XRCC1. Alexa Fluor 594 AffiniPure goat anti-rabbit (Jackson ImmunoResearch; 111585003; 1:400) for anti-pH3 and anti-PNKP. Nuclei were stained with 300 nM DAPI (FisherScientific; LSD1306) in PBS for 15 min and coverslips were mounted onto microscope slides using ProLong Gold Antifade reagent (FisherScientific; P36934). Cells were observed on an Olympus BX41 microscope and images were captured using an Infinity 3 camera operated by Infinity Capture imaging software (Lumenera Corporation). The signal for not-treated cells was set to zero using the exposure settings of the microscope camera and staining greater than the background level was detected. Cells staining for pH3 and histone γH2AX and the total number of cells (DAPI stained) were counted with Adobe Photoshop (CC 2017.0.1). XRCC1 and PNKP signals in cells were localized. Images were prepared using Adobe Photoshop (CC 2017.0.1) software. A minimum of 100 cells were counted for each treatment and the mean and standard error of the mean percentage of at least three independent experiments were calculated.

4.4 CETSA

HT-29 cells were plated at 1 x 10^6 cells/75 cm^2 flask for 48 or 72 h after which they were treated for 24 h. Cells were collected by trypsinization and resuspended in 1.5 mL PBS and ¼ tablet protease inhibitor (Roche; 11836170001). The cell suspension was aliquoted into 16 PCR tubes. The tubes were placed into the PCR machine (Eppendorf Mastercycler Pro) and each tube was heated at a different temperature in a gradient from 39.7 °C – 67.0 °C for 3 min. Next, the tubes were kept at room temperature for 3 min before freezing the tubes in liquid nitrogen. The cells are lysed by snap-freezing three times by thawing the tubes at 25°C and freezing them in liquid nitrogen. The lysate was centrifuged for 25 min at 16.000 X g at 4°C. The supernatant was transferred to a microcentrifuge tube and prepared for electrophoresis and western blotting by adding 2x SDS Sample Buffer (1:1) (20% (v/v) glycerol, 10% (v/v) DTT, 6% (w/v) SDS, 500 mM Tris, pH 6.8) and heated at 95°C for 5 min. The samples were loaded on the SDS-PAGE gel and western blotting procedure was performed. Experiments were performed three times.

4.5 Cell extraction

HT-29 cells were plated at 1 x 10^6 cells/75 cm^2 flask and incubated at 37°C for 48 or 72 hours prior to treatment. After 24 h treatment cells were trypsinized and washed with cold PBS (137 mM NaCl, 3 mM KCl, 100 mM Na_2HPO_4, 18 mM KH_2PO_4). Cells were resuspended in cold lysis buffer (50 mM HEPES, pH 7.4, 50 mM NaF, 10 mM EGTA (ethylene glycol-bis(beta-aminoethyl ether)-N,N'-tetraacetic acid), 50 mM β-glycerophosphate, 1 mM ATP, 1 mM DTT (dithiothreitol), 1% Triton X-100 (v/v), 10 µg/ml RNase A (MilliporeSigma; R6513), 0.4 U/ml DNase I (Life Technologies; AM2235) and protease inhibitor cocktail (Roche; 11836170001)) at a concentration of 20.000 cells/µL lysis buffer, passed through a 26-gauge needle for five passages and incubated on ice for 30 min. The suspension was centrifuged at 10,000 x g for 10 min at 4°C and the solution was aliquoted into 1.5 mL microcentrifuge tubes and stored at -80°C. Extracts were prepared three times and used for immunoprecipitation.

4.6 Immunoprecipitation

HT-29 cell extracts (200 µL per sample), 24 h treated, were incubated with the primary antibodies monoclonal mouse anti-XRCC1 (Abcam; ab1838; 1:50) or polyclonal rabbit anti-PNKP (Dr. M. Weinfeld, University of Alberta; 1:50) at 4°C overnight. The cell lysate and antibody were centrifuged at 4°C for 10 min at 10.000 x g and supernatant was transferred into a tube containing washed magnetic beads (BioRad; 1614023, 1614013; Protein G beads for anti-mouse IgG pull down, Protein A for anti-rabbit IgG pulldown) and incubated for 1 h at 4°C with gentle rocking. The tubes containing the magnetic beads were placed in a magnetic separation rack (BioRad; 1614916) for 15 seconds. The supernatant was separated from the pellet. The pellet was gently washed 3 times in 1x TBS-T (Tris-buffered saline, 0.1 % Tween-20 (MilliporeSigma; CAEM9480)) and resuspended in 40 µL 2x SDS sample buffer (20% (v/v) glycerol, 10% (v/v) DTT, 6% (w/v) SDS, 500 mM Tris, pH 6.8) and vortexed. The samples were heated at 95°C for 5 min and centrifuged for 1 minute at 14.000 X g. The samples were loaded onto an SDS-PAGE gel and western blotting procedure was performed. Experiments were performed three times.

4.7 Electrophoresis and western blot analysis

Extracts used for electrophoresis were heated at 95°C for 5 min in the presence of 2x SDS sample buffer (20% (v/v) glycerol, 10% (v/v) DTT, 6% (w/v) SDS, 500 mM Tris, pH 6.8). Cell extracts were separated on 10% (v/v) SDS-polyacrylamide gels with 4% (v/v) stacking gels by running at 200 volts for 45 min. Precision Plus Dual Colour marker (BioRad; 161039) was used to determine molecular weight in kilodaltons (kDa). Proteins were transferred onto nitrocellulose membranes (FisherScientific; 10600003) by semi-dry transfer (BioRad) for 45 min at 20 volts. Membranes were blocked with 5% (w/v) low fat milk in Tris-buffered saline with Tween-20 (MilliporeSigma; CAEM9480) (TBS-T) (50 mM Tris base, 150 mM NaCl and 0.1% (v/v) Tween-20 (MilliporeSigma; CAEM9480), pH 7.6) for 1 hour. Membranes were incubated with the following primary antibodies at 4°C overnight: monoclonal mouse anti-XRCC1 (Abcam; ab1838; 1:500),

monoclonal mouse anti-PNKP (Dr. M. Weinfeld, University of Alberta; 1:1000), monoclonal rabbit anti-Cdk4 (Cell Signalling; 12790S), and anti-actin (Santa Cruz Biotechnology; sc-58673; 1:200). The membranes were then washed with TBS-T and incubated with the following secondary antibodies for 45 min at room temperature: alkaline phosphatase coupled anti-mouse (FisherScientific; PRS3721; 1:2500) or alkaline phosphatase coupled anti-rabbit (FisherScientific; PRS3731; 1:2500). The membranes were washed with TBS-T and developed using an alkaline phosphatase conjugate substrate kit (BioRad; 1706432). Development was stopped using Tris-EDTA (diaminoethane tetraacetic acid) buffer (10mM Tris base, 1mM EDTA, pH 8.0). Western blot analysis was performed at least three times.

4.8 Karyotyping

HT-29 cells were plated at 1.5 x 10^6/75 cm^2 flask respectively for 48 or 72 h prior to treatment. HT-29 cells were treated for 48 h followed by treatment of KaryoMAX colcemid (10 μg/ml) (Gibco; 15210-040) for 1 h at 37 ºC. Colcemid was used to increase the number of metaphase cells in a culture. Next, freshly prepared warm hypotonic solution (0.075 M KCl (MilliporeSigma; CAPX1405-1) in distilled H_2O was added to the cells for 30 min to make nuclei swell osmotically. Then, cells were fixed by adding Carnoy's fixative 3:1 methanol (FisherScientific; A4524) and acetic acid (MilliporeSigma; CAAX0073-9) solution and incubated for 10 min on ice followed by a mechanical shake-off to collect mitotic cells. Cells were placed into a pre-cooled 15 mL Falcon tube and spun down by 5 min centrifugation at 220 rcf. The supernatant was removed and cells were resuspended in 5 mL cold fixative and incubated on ice for 5 min followed by 5 min centrifugation at 220 rcf. This was repeated three times and after the last centrifugation cells were resuspended in 0.5 mL of fixative and the cell suspension was dropped on a cold, clean glass slide and blown hard to disperse the chromosomes. The slides were air dried at room temperature and stained with 300 nM DAPI (FisherScientific; LSD1306). Cells were observed on an Olympus BX41 microscope and images were captured using an Infinity 3 camera operated by Infinity Capture

imaging software (Lumenera Corporation). Images were prepared with Adobe Photoshop (CC 2017.0.1) software and chromosome configurations were determined. A minimum of 40 cells per treatment were observed and analyzed for genomic change. Experiments were repeated at least three times.

4.9 Mechanical shake-off

HT-29 cells were plated at 1 x 10^6 cells/75 cm^2 flask and incubated at 37°C for 48 or 72 h prior to treatment. After 48 h of treatment, medium was aspirated and cells were gently washed with PBS (137 mM NaCl, 3 mM KCl, 100 mM Na_2HPO_4, 18 mM KH_2PO_4). Fresh medium was added at 3 ml/75 cm^2 and the flask was tapped with medium force on all edges to extract rounded cells from flattened cells (Swift & Golsteyn, 2018).

4.10 Survival assay

HT-29 cells were plated at 1 x 10^6 cells/75 cm^2 flask and cultivated for 48 h prior to treatment. At 48 h after treatment, a mechanical shake off was performed to collect rounded cells. Collected rounded cells were counted using hemocytometer and cell viability was confirmed by vital dye exclusion. Cells were re-plated in a 25 cm^2 flask and placed in the incubator at 37°C until the desired time for survival analysis. At desired times, cells were collected by trypsinization and counted using a hemocytometer to determine the number of cells that survived. The percentage of re-cultivated cells that survived was estimated using the following formula:

$$N0 = 10^{\{\log NT-(\log 2/tg)\ T\}}$$

In the formula; NT = number of cells collected at the end of the survival assay, N0 = number of cells that were able to proliferate (i.e., survival cells), tg = generation time in hours, and T = time of culture in hours. Then, the percentage of surviving cells was calculated using the following formula:

$$P = (N0 / N) \times 100$$

In the formula; N = number of cells placed in the flask at the beginning of the survival assay and N0 = number of cells that were able to proliferate (i.e. survival cells) (Leibovitz & Mazur, 1977). Experiments were repeated at least three times.

4.11 Statistical analysis

Data were analyzed using Microsoft Excel 2010 and SPSS software. Data are presented as means ± SEM from three independent experiments and analyzed by one-way analysis of variance (ANOVA) with Tukey's post hoc test. A probability level of $p < 0.05$ was considered significant.

GENERAL DISCUSSION

In this thesis, we have investigated whether chromosomes undergo changes during the process of checkpoint adaptation. In particular, we found that in the relatively rare 1-2% of treated cells that survive checkpoint adaption, cells have increased numbers of interchromosomal and numerical rearrangements when compared to mock-treated cells. We then investigated if a PNKP inhibitor might alter the process of checkpoint adaptation or the outcomes of checkpoint adaptation. A better knowledge about the DNA damage and repair in checkpoint adaptation in needed to increase treatment efficiency. In this discussion, we will analyze the process by which CPT damages DNA, the mechanisms involved in the repair of this damage, and potential inhibitory targets to decrease checkpoint adaptation entrance or survival.

In our experimental model, the genotoxic agent used to induce checkpoint adaptation in HT-29 cells is the Topo1 inhibitor CPT. During the early G1 phase, G1/S phase and M phase of the cell cycle, Topo1 will bind to pre-replicative complexes to control the activation of replication origins (Abdurashidova et al., 2007). Topo1 nicks one DNA strand to release torsional tension that arises from DNA strand separation during replication (Wall & Wani, 1995; Pommier et al., 2010). After the nick is formed, Topo1 generates a Topo1-DNA cleavage complex by covalently binding to the 3'-P terminus (Xu & Her, 2015). This complex is stabilized by CPT, which prevents the re-ligation of the nick, leaving an SSB with a 3'-P end that is connected to Topo1 and a free 5'-OH group (Kerrigan & Pilch, 2001; Koster et al., 2007).

SSB repair is one major pathway that can be involved in the repair of DNA breaks induced by CPT. The SSB induced by CPT consists of a 3'-P-Topo1 end and a 5'-OH end, which cannot be used by DNA polymerases or ligases. These termini require processing before the nick can be repaired. Poly [ADP-ribose] polymerase 1 (PARP1) recognizes these ends and recruits the repair protein XRCC1, which leads to the recruitment of Tdp1 and PNKP. Tdp1 removes Topo1 from the 3'-P end and PNKP will convert this 3'-P end into the required 3'-OH end, and converts the 5'-OH

end to 5'-P. Termini in this configuration are substrates for DNA ligases. The re-ligation of the nick is primarily performed by DNA polymerase β and DNA ligase III, which are also recruited by XRCC1 (Pommier et al., 2006; Xu & Her, 2015).

In addition to processing of the Topo1-DNA cleavage complex by Tdp1, endonucleases can also process this complex. Endonucleases cleave the DNA a few nucleotides away from the Topo1-DNA cleavage complex to release the complex, converting the break ends into 3'-OH and 5'-OH, leaving a gap over a couple of nucleotides. This gap will lead to the activation of PARP1 and the recruitment of XRCC1, which in turn will recruit DNA polymerase β, which will catalyze the repair of the gap. The repair process results in a 5'-flap, and is aided by proliferating cell nuclear antigen (PCNA) and DNA polymerase β/ε. If PNKP does not convert the 5'-OH end, the 5'-flap can be removed by the endonuclease flap endonuclease 1 (FEN-1), and ligation of the nick will be performed by DNA ligase I (Pommier et al., 2006; Xu & Her, 2015).

During DNA replication, the SSBs are likely to be converted to one-ended DSBs (Ryan et al., 1991; Strumberg et al., 2000; Kerrigan & Pilch, 2001; Koster et al., 2007; Lin et al., 2009). A study of CPT-induced DNA breaks in HT-29 cells showed that these one-ended DSBs breaks are formed by replication fork run-off, producing a 5′ phosphorylated DSB only on the leading strand for DNA synthesis (Strumberg et al., 2000). It has been demonstrated that this break is resected to produce a 3' single-strand DNA overhang that triggers RAD51-dependent HR repair (Arnaudeau et al., 2001; Lundin et al., 2002).

There are two major DSB repair pathways used by cells, NHEJ and HR. A study of HR and NHEJ-deficient cell lines determined that HR-deficient cells are significantly more sensitive to CPT than NHEJ deficient cells, suggesting that HR is the primary pathway utilized for the repair of the replication-associated one-ended DSBs (Arnaudeau et al., 2001; Chapman et al., 2012). HR is active in late S/G2 phase, using the sister chromatid as a template for precise repair of the DNA (Hendrickson, 1997; Takata et al., 1998). It has been suggested that HR is rapidly activated upon

replication-associated DSBs to allow fast repair and recovery of the replication fork to proceed DNA replication (Arnaudeau et al., 2001).

The first step in HR is the recognition of the DSB by the meiotic recombination 11 (MRE11)/RAD50/nibrin (NBS1) complex that activates the ATM kinase, leading to a DDR response. This is followed by the break end resection from 5' to 3' by CtBP-interacting protein (CtIP)-mediated nuclease activity, forming single-strand DNA. This single-stranded DNA is coated with replication protein A (RPA) and activates the ATR response to facilitate HR. The RPA-coated single-stranded DNA is replaced with RAD51 nucleofilaments that performs homology sequence searching and mediated strand invasion, leading to a D-loop structure formation. DSBs are repaired by branch migration of the joint DNA molecule, DNA synthesis, DNA ligation, and the resolution of Holliday junctions to recover the replication fork (Kowalczykowski, 2000; Moynahan & Jasin, 2010; Peng & Lin, 2011; Symington & Gautier, 2011).

Occasionally, if two replication forks encounter each other at the SSB, it can form a two-ended DSB instead of a one-ended DBS and can be repaired by NHEJ which is primarily active in G1/early S phase (Hendrickson, 1997; Moynahan & Jasin, 2010). NHEJ is error-prone in which the break ends are directly ligated without using a homologous sequence as a template. The main proteins involved in NHEJ are Ku70, Ku80, XRCC4, DNA-dependent protein kinase catalytic subunit (DNA-PKcs) and DNA ligase IV (Lieber, 2010; Davis & Chen, 2013).

The treatment inefficiency observed in cancer patients has been suggested to be influenced by the DNA repair capacity of tumour cells in response to genotoxic agents. Therefore, inhibitors of DNA repair proteins are being studied for their ability to sensitize tumour cells to anti-cancer treatments (Bernstein et al., 2008; Allinson, 2010). One of these inhibitors targets PNKP and has been shown to sensitize cancer cells to IR or CPT treatment (Freschauf et al., 2009; Freschauf et al., 2010). In our study, we focused on the process of checkpoint adaptation, which is induced by toxic, yet pharmacological concentrations of CPT, which are lower than those that had been previously used in other studies. We were unable to detect an effect of PNKP inhibitors upon

checkpoint adaptation in cells treated with a pharmacological concentration of CPT. We were, however, able to observe a change in PNKP-XRCC1 interaction in treated cells, which suggests that the inhibitor A12B4C50 was affecting its target.

One explanation for this result might arise by acquiring more information about the DNA repair pathways that are involved in the repair of CPT induced breaks. As described above, CPT induced DSBs are mainly repaired by HR. Inhibition of PNKP will affect the SSB repair pathway and the NHEJ pathway (see chapter 3) and it may be necessary to evaluate further the relationship between HR, NHEJ and checkpoint adaptation in cells treated by CPT.

Other targets for the sensitization of cancer cells to CPT that undergo checkpoint adaptation might be the HR pathway. It has been previously shown that cells with HR gene defects are hypersensitive for chemotherapeutic drugs. HT-29 cells have been shown to be more sensitive to HR deficiency than NHEJ deficiency. However, inhibitors targeting HR protein in cancer cells directly are limited due to their often mutated genes (Pearl et al., 2015). A protein that plays a role in damaged DNA sensing is RPA. RPA has been suggested to be a protein that is involved in checkpoint adaptation and that protein defects can suppress checkpoint adaptation (Lee et al., 1998). Inhibition of RPA has shown to inhibit cell cycle progression, decreases cell viability and sensitizes cells to genotoxic agents (Shuck & Turchi, 2010). Another potential HR pathway target is RAD51. The small molecule RAD51 inhibitor RI-1 prevents the filament formation on the single-stranded DNA, leaving RPA coating unaffected. RI-1 was able to sensitize human cells in vitro up to 3 fold to chemotherapeutic drugs (Budke et al., 2012; Berte et al., 2016). Lastly, the DNA damage signalling inhibitor Mirin was shown to bind to MRE11 and inhibit its nuclease activity and the activation of the ATM/ATR-Chk1-Chk2 pathway. Mirin was also able to sensitize human cells to chemotherapeutic drugs (Berte et al., 2016). A defect of MRE11 protein in colon cancer cells has shown sensitization to CPT treatment (Wen et al., 2008). In addition to targeting HR, another strategy might be to target mitosis. Preventing cells from entering mitosis may prevent cells from undergoing checkpoint adaptation. It has been previously reported that inhibition of Cdk1 with CR8

prevented HT-29 cells from entering mitosis and induced cell death (Kubara et al., 2012). Additionally, the checkpoint adaptation pathway has been previously shown to be sensitive to Chk1 inhibitors causing a cell cycle arrest (Chen et al., 2012).

It is largely documented that HR is a repair pathway that is supposedly error-free. However, we have shown that the consequence of checkpoint adaptation, induced by CPT, is the acquisition of chromosomal rearrangements, as demonstrated by probes to chromosome 7. One explanation might be that these rearrangements have been formed by the NHEJ pathway that is involved in CPT-induced breaks to a lesser extent but could lead to erroneous rejoining of broken chromosomes. Another explanation might be the inability of the cohesion complex to tether one-ended DSBs that are formed in S phase upon CPT treatment. The cohesion complex assists to rejoin DSBs that are in proximity by tethering the ends of DSBs to maintain genome organization and prevents chromosome motility, hence chromosome rearrangements. The failure of binding to the one-ended DSB can result in the rejoining of DSBs that are distant from each other leading to interchromosomal rearrangements (Gelot et al., 2016).

Checkpoint adaptation in human cells is a relatively new discovered process. Previous studies have shown that cancer cells treated with pharmacological concentrations of genotoxic agents can enter checkpoint adaptation rather than die by apoptosis (Syljuasen, 2007; Swift & Golsteyn, 2016a; Jiang et al., 2017). A small number of cells undergoing checkpoint adaptation are able to exit and proliferate (Kubara et al., 2012). These survival cells acquired micronuclei, which was an indicator for chromosome instability (Crasta et al., 2012; Lewis & Golsteyn, 2016). The results in this thesis support our hypothesis that cells that survived checkpoint adaptation acquired chromosomal changes. This finding contributes to the growing understanding of the process of checkpoint adaptation, and might be significant in the understanding of treatment inefficiency seen in cancer patients. It is known that patients that are treated with genotoxic agents may develop secondary tumours that are genetically different from the primary tumour (Kastan & Bartek, 2004; Bartek & Lukas, 2007), and checkpoint adaptation might be one explanation as to how this occurs.

Our results are supported by the recently published increase of chromosome instability after chemotherapy and irradiation *in vivo* of cells from Hodgkin's lymphoma patients (Kaddour et al., 2017; Ramos et al., 2018).

Additionally, we demonstrated that it is possible to test DNA damage inhibitors, such as a series of PNKP inhibitors in this experimental model, and importantly detect a biochemical effect of the inhibitors. Future work is planned to analyze full chromosome changes (i.e. spectral karyotyping) in cells that survive checkpoint adaptation. By being able to isolate PNKP by immunoprecipitation, we can now explore the complete protein complex under different stages of DNA damage induction and checkpoint adaptation. To conclude, we have shown that cancer cells that survive checkpoint adaptation acquire chromosomal rearrangements, which can contribute to chromosome instability. Further studies need to focus on the DNA repair mechanisms that might be involved in the formation of chromosome rearrangements to sensitize cancer cells to genotoxic agents. Overall, more insight into checkpoint adaptation might contribute to the better understanding of the biology of cancer treatments.

REFERENCES

Abdurashidova, G., Radulescu, S., Sandoval, O., Zahariev, S., Danailov, M. B., Demidovich, A., Santamaria, L., Biamonti, G., Riva, S., and Falaschi, A. (2007). Functional interactions of DNA topoisomerases with a human replication origin. EMBO Journal, 26, 998-1009.

Adachi, N., So, S., and Koyama, H. (2004). Loss of nonhomologous end joining confers camptothecin resistance in DT40 cells. Implications for the repair of topoisomerase I-mediated DNA damage. Journal of Biological Chemistry, 279, 37343-33748.

Allinson, S. L. (2010). DNA end-processing enzyme polynucleotide kinase as a potential target in the treatment of cancer. Future Oncology, 6, 1031-1042.

Anderson, D. J., and Hetzer, M. W. (2008). Reshaping of the endoplasmic reticulum limits the rate for nuclear envelope formation. Journal of Cell Biology, 182, 911-924.

Apraiz, A., Boyano, M. D., and Asumendi, A. (2011). Cell-centric view of apoptosis and apoptotic cell death-inducing antitumoral strategies. Cancers (Basel), 3, 1042-1080.

Arnaudeau, C., Lundin, C., and Helleday, T. (2001). DNA double-strand breaks associated with replication forks are predominantly repaired by homologous recombination involving an exchange mechanism in mammalian cells. Journal of Molecular Biology, 307, 1235-1245.

Bakhoum, S. F., and Compton, D. A. (2012a). Chromosomal instability and cancer: a complex relationship with therapeutic potential. Journal of Clinical Investigation, 122, 1138-1143.

Bakhoum, S. F., and Compton, D. A. (2012b). Kinetochores and disease: keeping microtubule dynamics in check! Current Opinion in Cell Biology, 24, 64-70.

Bakhoum, S. F., Ngo, B., Laughney, A. M., Cavallo, J. A., Murphy, C. J., Ly, P., Shah, P., Sriram, R. K., Watkins, T. B. K., Taunk, N. K., Duran, M., Pauli, C., et al. (2018). Chromosomal instability drives metastasis through a cytosolic DNA response. Nature, 553, 467.

Bakhoum, S. F., Thompson, S. L., Manning, A. L., and Compton, D. A. (2009). Genome stability is ensured by temporal control of kinetochore-microtubule dynamics. Nature Cell Biology, 11, 27-35.

Bartek, J., and Lukas, J. (2007). DNA damage checkpoints: from initiation to recovery or adaptation. Current Opinion in Cell Biology, 19, 238-245.

Bernstein, N. K., Karimi-Busheri, F., Rasouli-Nia, A., Mani, R., Dianov, G., Glover, J. N., and Weinfeld, M. (2008). Polynucleotide kinase as a potential target for enhancing cytotoxicity by ionizing radiation and topoisomerase I inhibitors. Anti-Cancer Agents in Medicinal Chemistry, 8, 358-367.

Berte, N., Piee-Staffa, A., Piecha, N., Wang, M. W., Borgmann, K., Kaina, B., and Nikolova, T. (2016). Targeting homologous recombination by pharmacological inhibitors enhances the killing response of glioblastoma cells treated with alkylating drugs. Molecular Cancer Therapeutics, 15, 2665-2678.

Bhatia, A., and Kumar, Y. (2014). Relevance of microscopic indicators of chromosomal instability in routine reporting of malignancies. Diagnostic Cytopathology, 42, 181-188.

Birkbak, N. J., Eklund, A. C., Li, Q., McClelland, S. E., Endesfelder, D., Tan, P., Tan, I. B., Richardson, A. L., Szallasi, Z., and Swanton, C. (2011). Paradoxical relationship between chromosomal instability and survival outcome in cancer. Cancer Research, 71, 3447-3452.

Brown, J. M., and Attardi, L. D. (2005). The role of apoptosis in cancer development and treatment response. Nature Reviews Cancer, 5, 231-237.

Budke, B., Logan, H. L., Kalin, J. H., Zelivianskaia, A. S., McGuire, W. C., Miller, L. L., Stark, J. M., Kozikowski, A. P., Bishop, D. K., and Connell, P. P. (2012). RI-1: a chemical inhibitor of RAD51 that disrupts homologous recombination in human cells. Nucleic Acids Research, 40, 7347-7357.

Burke, B., and Ellenberg, J. (2002). Remodelling the walls of the nucleus. Nature Reviews Molecular Cell Biology, 3, 487-497.

Burrell, R. A., McGranahan, N., Bartek, J., and Swanton, C. (2013). The causes and consequences of genetic heterogeneity in cancer evolution. Nature, 501, 338-345.

Cahill, D. P., Kinzler, K. W., Vogelstein, B., and Lengauer, C. (1999). Genetic instability and darwinian selection in tumours. Trends Cell Biology, 9, M57-60.

Cahuzac, N., Studeny, A., Marshall, K., Versteege, I., Wetenhall, K., Pfeiffer, B., Leonce, S., Hickman, J. A., Pierre, A., and Golsteyn, R. M. (2010). An unusual DNA binding compound, S23906, induces mitotic catastrophe in cultured human cells. Cancer Letters, 289, 178-187.

Carrano, A. V., and Heddle, J. A. (1973). The fate of chromosome aberrations. Journal of Theoretical Biology, 38, 289-304.

Carroll, S. M., DeRose, M. L., Gaudray, P., Moore, C. M., Needham-Vandevanter, D. R., Von Hoff, D. D., and Wahl, G. M. (1988). Double minute chromosomes can be produced from precursors derived from a chromosomal deletion. Molecular Cell Biology, 8, 1525-1533.

Champoux, J. J. (2001). DNA topoisomerases: structure, function, and mechanism. Annual Review of Biochemistry, 70, 369-413.

Chang, B. D., Broude, E. V., Dokmanovic, M., Zhu, H., Ruth, A., Xuan, Y., Kandel, E. S., Lausch, E., Christov, K., and Roninson, I. B. (1999). A senescence-like phenotype distinguishes tumor cells that undergo terminal proliferation arrest after exposure to anticancer agents. Cancer Research, 59, 3761-3767.

Chapman, J. R., Taylor, M. R., and Boulton, S. J. (2012). Playing the end game: DNA double-strand break repair pathway choice. Molecular Cell, 47, 497-510.

Chen, A. Y., and Liu, L. F. (1994). DNA topoisomerases: essential enzymes and lethal targets. Annual Review of Pharmacology and Toxicology, 34, 191-218.

Chen, T., Stephens, P. A., Middleton, F. K., and Curtin, N. J. (2012). Targeting the S and G2 checkpoint to treat cancer. Drug Discovery Today, 17, 194-202.

Chu, E. H. Y. (1965). Effects of ultraviolet radiation on mammalian cells .I. induction of chromosome aberrations. Mutation Research, 2, 75.

Cimini, D., Fioravanti, D., Salmon, E. D., and Degrassi, F. (2002). Merotelic kinetochore orientation versus chromosome mono-orientation in the origin of lagging chromosomes in human primary cells. Journal of Cell Science, 115, 507-515.

Cimini, D., Howell, B., Maddox, P., Khodjakov, A., Degrassi, F., and Salmon, E. D. (2001). Merotelic kinetochore orientation is a major mechanism of aneuploidy in mitotic mammalian tissue cells. Journal of Cell Biology, 153, 517-527.

Cimini, D., Wan, X., Hirel, C. B., and Salmon, E. D. (2006). Aurora kinase promotes turnover of kinetochore microtubules to reduce chromosome segregation errors. Current Biology, 16, 1711-1718.

Clifford, B., Beljin, M., Stark, G. R., and Taylor, W. R. (2003). G2 arrest in response to topoisomerase II inhibitors: the role of p53. Cancer Research, 63, 4074-4081.

Crasta, K., Ganem, N. J., Dagher, R., Lantermann, A. B., Ivanova, E. V., Pan, Y., Nezi, L., Protopopov, A., Chowdhury, D., and Pellman, D. (2012). DNA breaks and chromosome pulverization from errors in mitosis. Nature, 482, 53-58.

Cremer, T., and Cremer, C. (2006). Rise, fall and resurrection of chromosome territories: a historical perspective. Part I. The rise of chromosome territories. European Journal of Histochemistry, 50, 161-176.

Curtin, N. J. (2012). DNA repair dysregulation from cancer driver to therapeutic target. Nature Reviews Cancer, 12, 801-817.

Dalal, S. N., Schweitzer, C. M., Gan, J., and DeCaprio, J. A. (1999). Cytoplasmic localization of human cdc25C during interphase requires an intact 14-3-3 binding site. Molecular Cell Biology, 19, 4465-4479.

Davis, A. J., and Chen, D. J. (2013). DNA double strand break repair via non-homologous end-joining. Translational Cancer Research, 2, 130-143.

Demarcq, C., Bunch, R. T., Creswell, D., and Eastman, A. (1994). The role of cell cycle progression in cisplatin-induced apoptosis in Chinese hamster ovary cells. Cell Growth Differentiation, 5, 983-993.

Dewey, W. C., Ling, C. C., and Meyn, R. E. (1995). Radiation-induced apoptosis: Relevance to radiotherapy. International Journal of Radiation Oncology*Biology*Physics, 33, 781-796.

Ding, L., Ley, T. J., Larson, D. E., Miller, C. A., Koboldt, D. C., Welch, J. S., Ritchey, J. K., Young, M. A., Lamprecht, T., McLellan, M. D., McMichael, J. F., Wallis, J. W., et al. (2012). Clonal evolution in relapsed acute myeloid leukaemia revealed by whole-genome sequencing. Nature, 481, 506-510.

Fenech, M. (1993). The cytokinesis-block micronucleus technique and its application to genotoxicity studies in human-populations. Environmental Health Perspectives, 101, 101-107.

Fenech, M. (2006). Cytokinesis-block micronucleus assay evolves into a "cytome" assay of chromosomal instability, mitotic dysfunction and cell death. Mutation Research, 600, 58-66.

Fenech, M. (2007). Cytokinesis-block micronucleus cytome assay. Nature Protocols, 2, 1084-1104.

Fenech, M., Kirsch-Volders, M., Natarajan, A. T., Surralles, J., Crott, J. W., Parry, J., Norppa, H., Eastmond, D. A., Tucker, J. D., and Thomas, P. (2011). Molecular mechanisms of micronucleus, nucleoplasmic bridge and nuclear bud formation in mammalian and human cells. Mutagenesis, 26, 125-132.

Freschauf, G. K., Karimi-Busheri, F., Ulaczyk-Lesanko, A., Mereniuk, T. R., Ahrens, A., Koshy, J. M., Rasouli-Nia, A., Pasarj, P., Holmes, C. F., Rininsland, F., Hall, D. G., and Weinfeld, M. (2009). Identification of a small molecule inhibitor of the human DNA repair enzyme polynucleotide kinase/phosphatase. Cancer Research, 69, 7739-7746.

Freschauf, G. K., Mani, R. S., Mereniuk, T. R., Fanta, M., Virgen, C. A., Dianov, G. L., Grassot, J. M., Hall, D. G., and Weinfeld, M. (2010). Mechanism of action of an imidopiperidine inhibitor of human polynucleotide kinase/phosphatase. Journal of Biological Chemistry, 285, 2351-2360.

Gant, T. M., and Wilson, K. L. (1997). Nuclear assembly. Annual Review of Cell and Developmental Biology, 13, 669-695.

Garsed, D. W., Marshall, O. J., Corbin, V. D., Hsu, A., Di Stefano, L., Schroder, J., Li, J., Feng, Z. P., Kim, B. W., Kowarsky, M., Lansdell, B., Brookwell, R., et al. (2014). The architecture and evolution of cancer neochromosomes. Cancer Cell, 26, 653-667.

Gascoigne, K. E., and Taylor, S. S. (2008). Cancer cells display profound intra- and interline variation following prolonged exposure to antimitotic drugs. Cancer Cell, 14, 111-122.

Gelot, C., Guirouilh-Barbat, J., and Lopez, B. S. (2016). The cohesin complex prevents the end-joining of distant DNA double-strand ends in S phase: Consequences on genome stability maintenance. Nucleus, 7, 339-345.

Gelot, C., Magdalou, I., and Lopez, B. S. (2015). Replication stress in mammalian cells and its consequences for mitosis. Genes (Basel), 6, 267-298.

Geraud, G., Laquerriere, F., Masson, C., Arnoult, J., Labidi, B., and Hernandezverdun, D. (1989). 3-dimensional organization of micronuclei induced by colchicine in Ptk1 cells. Experimental Cell Research, 181, 27-39.

Gieni, R. S., Chan, G. K., and Hendzel, M. J. (2008). Epigenetics regulate centromere formation and kinetochore function. Journal of Cell Biochemistry, 104, 2027-2039.

Giovanella, B. C., Stehlin, J. S., Wall, M. E., Wani, M. C., Nicholas, A. W., Liu, L. F., Silber, R., and Potmesil, M. (1989). DNA topoisomerase I--targeted chemotherapy of human colon cancer in xenografts. Science, 246, 1046-1048.

Goldwasser, F., Bae, I., Valenti, M., Torres, K., and Pommier, Y. (1995). Topoisomerase I-related parameters and camptothecin activity in the colon carcinoma cell lines from the National Cancer Institute anticancer screen. Cancer Research, 55, 2116-2121.

Gregan, J., Polakova, S., Zhang, L., Tolic-Norrelykke, I. M., and Cimini, D. (2011). Merotelic kinetochore attachment: causes and effects. Trends in Cell Biology, 21, 374-381.

Habraken, Y., and Verly, W. G. (1988). Further purification and characterization of the DNA 3'-phosphatase from rat-liver chromatin which is also a polynucleotide 5'-hydroxyl kinase. European Journal of Biochemistry, 171, 59-66.

Hall, E. J., and Giaccia, A. J. (2006). *Radiobiology for the radiologist*: Lippincott Williams & Wilkins.

Hanahan, D., and Weinberg, R. A. (2011). Hallmarks of cancer: the next generation. Cell, 144, 646-674.

Hartwell, L., Weinert, T., Kadyk, L., and Garvik, B. (1994). Cell cycle checkpoints, genomic integrity, and cancer. Cold Spring Harbor Symposia on Quantitative Biology, 59, 259-263.

Hatch, E. M., Fischer, A. H., Deerinck, T. J., and Hetzer, M. W. (2013). Catastrophic nuclear envelope collapse in cancer cell micronuclei. Cell, 154, 47-60.

Heit, R., Rattner, J. B., Chan, G. K., and Hendzel, M. J. (2009). G2 histone methylation is required for the proper segregation of chromosomes. Journal of Cell Science, 122, 2957-2968.

Helleday, T., Petermann, E., Lundin, C., Hodgson, B., and Sharma, R. A. (2008). DNA repair pathways as targets for cancer therapy. Nature Reviews Cancer, 8, 193-204.

Hendrickson, E. A. (1997). Cell-cycle regulation of mammalian DNA double-strand-break repair. The American Journal of Human Genetics, 61, 795-800.

Hermine, T., Jones, N. J., and Parry, J. M. (1997). Comparative induction of micronuclei in repair-deficient and -proficient Chinese hamster cell lines following clastogen or aneugen exposures. Mutation Research, 392, 151-163.

Hirsch, D., Kemmerling, R., Davis, S., Camps, J., Meltzer, P. S., Ried, T., and Gaiser, T. (2013). Chromothripsis and focal copy number alterations determine poor outcome in malignant melanoma. Cancer Research, 73, 1454-1460.

Hoffelder, D. R., Luo, L., Burke, N. A., Watkins, S. C., Gollin, S. M., and Saunders, W. S. (2004). Resolution of anaphase bridges in cancer cells. Chromosoma, 112, 389-397.

Holland, A. J., and Cleveland, D. W. (2012). Chromoanagenesis and cancer: mechanisms and consequences of localized, complex chromosomal rearrangements. Nature Medicine, 18, 1630-1638.

Huang, T.-H., Chen, H.-C., Chou, S.-M., Yang, Y.-C., Fan, J.-R., and Li, T.-K. (2010). Cellular processing determinants for the activation of damage signals in response to topoisomerase I-linked DNA breakage. Cell Research, 20, 1060.

Hubner, B., Strickfaden, H., Muller, S., Cremer, M., and Cremer, T. (2009). Chromosome shattering: a mitotic catastrophe due to chromosome condensation failure. European Biophysics Journal, 38, 729-747.

Hunter, C., Smith, R., Cahill, D. P., Stephens, P., Stevens, C., Teague, J., Greenman, C., Edkins, S., Bignell, G., Davies, H., O'Meara, S., Parker, A., et al. (2006). A hypermutation phenotype and somatic MSH6 mutations in recurrent human malignant gliomas after alkylator chemotherapy. Cancer Research, 66, 3987-3991.

Jackson, S. P., and Bartek, J. (2009). The DNA-damage response in human biology and disease. Nature, 461, 1071-1078.

Janssen, A., van der Burg, M., Szuhai, K., Kops, G. J., and Medema, R. H. (2011). Chromosome segregation errors as a cause of DNA damage and structural chromosome aberrations. Science, 333, 1895-1898.

Jazayeri, A., Falck, J., Lukas, C., Bartek, J., Smith, G. C., Lukas, J., and Jackson, S. P. (2006). ATM- and cell cycle-dependent regulation of ATR in response to DNA double-strand breaks. Nature Cell Biology, 8, 37-45.

Jekimovs, C., Bolderson, E., Suraweera, A., Adams, M., O'Byrne, K. J., and Richard, D. J. (2014). Chemotherapeutic compounds targeting the DNA double-strand break repair pathways: the good, the bad, and the promising. Frontiers in Oncology, 4, 86.

Jiang, X. J., Wang, J., Xing, L. X., Shen, H. T., Lian, W. G., Yi, L., Zhang, D. H., Yang, H. Y., Liu, J. H., and Zhang, X. H. (2017). Sterigmatocystin-induced checkpoint adaptation depends on Chk1 in immortalized human gastric epithelial cells in vitro. Archives of Toxicology, 91, 259-270.

Kaddour, A., Colicchio, B., Buron, D., El Maalouf, E., Laplagne, E., Borie, C., Ricoul, M., Lenain, A., Hempel, W. M., Morat, L., Al Jawhari, M., Cuceu, C., et al. (2017). Transmission of induced chromosomal aberrations through successive mitotic divisions in human lymphocytes after in vitro and in vivo radiation. Scientific Reports, 7, 3291.

Kalsbeek, D., and Golsteyn, R. M. (2017). G2/M-phase checkpoint adaptation and micronuclei formation as mechanisms that contribute to genomic instability in human cells. International Journal of Molecular Sciences, 18.

Kandoth, C., McLellan, M. D., Vandin, F., Ye, K., Niu, B., Lu, C., Xie, M., Zhang, Q., McMichael, J. F., Wyczalkowski, M. A., Leiserson, M. D., Miller, C. A., et al. (2013). Mutational landscape and significance across 12 major cancer types. Nature, 502, 333-339.

Kastan, M. B., and Bartek, J. (2004). Cell-cycle checkpoints and cancer. Nature, 432, 316-323.

Kawai, K., Viars, C., Arden, K., Tarin, D., Urquidi, V., and Goodison, S. (2002). Comprehensive karyotyping of the HT-29 colon adenocarcinoma cell line. Genes Chromosomes Cancer, 34, 1-8.

Kelland, L. (2007). The resurgence of platinum-based cancer chemotherapy. Nature Reviews Cancer, 7, 573-584.

Kerrigan, J. E., and Pilch, D. S. (2001). A structural model for the ternary cleavable complex formed between human topoisomerase I, DNA, and camptothecin. Biochemistry, 40, 9792-9798.

Kinsella, M., Patel, A., and Bafna, V. (2014). The elusive evidence for chromothripsis. Nucleic Acids Research, 42, 8231-8242.

Kirby, T. W., Gassman, N. R., Smith, C. E., Pedersen, L. C., Gabel, S. A., Sobhany, M., Wilson, S. H., and London, R. E. (2015). Nuclear localization of the DNA repair scaffold XRCC1: uncovering the functional role of a bipartite NLS. Scientific Reports, 5, 13405.

Kisurina-Evgenieva, O. P., Bryantseva, S. A., Shtil', A. A., and Onishchenko, G. E. (2006). Antitubulin agents can initiate different apoptotic pathways. Biophysics, 51, 771-775.

Kisurina-Evgenieva, O. P., Sutiagina, O. I., and Onishchenko, G. E. (2016). Biogenesis of micronuclei. Biochemistry (Moscow), 81, 453-464.

Koster, D. A., Palle, K., Bot, E. S., Bjornsti, M. A., and Dekker, N. H. (2007). Antitumour drugs impede DNA uncoiling by topoisomerase I. Nature, 448, 213-217.

Kowalczykowski, S. C. (2000). Initiation of genetic recombination and recombination-dependent replication. Trends Biochemical Sciences, 25, 156-165.

Krishnaja, A. P., and Sharma, N. K. (2004). Transmission of gamma-ray-induced unstable chromosomal aberrations through successive mitotic divisions in human lymphocytes in vitro. Mutagenesis, 19, 299-305.

Kubara, P. M., Kerneis-Golsteyn, S., Studeny, A., Lanser, B. B., Meijer, L., and Golsteyn, R. M. (2012). Human cells enter mitosis with damaged DNA after treatment with pharmacological concentrations of genotoxic agents. Biochemical Journal, 446, 373-381.

Lee, S. E., Moore, J. K., Holmes, A., Umezu, K., Kolodner, R. D., and Haber, J. E. (1998). Saccharomyces Ku70, mre11/rad50 and RPA proteins regulate adaptation to G2/M arrest after DNA damage. Cell, 94, 399-409.

Leibovitz, A., and Mazur, K. C. (1977). A generation-time technique. TCA manual/Tissue Culture Association, 3, 655-657.

Lemaitre, J. M., Geraud, G., and Mechali, M. (1998). Dynamics of the genome during early Xenopus laevis development: karyomeres as independent units of replication. Journal of Cell Biology, 142, 1159-1166.

Lewis, C. W., and Golsteyn, R. M. (2016). Cancer cells that survive checkpoint adaptation contain micronuclei that harbor damaged DNA. Cell Cycle, 15, 3131-3145.

Lieber, M. R. (2010). The mechanism of double-strand DNA break repair by the nonhomologous DNA end-joining pathway. Annual Review of Biochemistry, 79, 181-211.

Lin, C. P., Ban, Y., Lyu, Y. L., and Liu, L. F. (2009). Proteasome-dependent processing of topoisomerase I-DNA adducts into DNA double strand breaks at arrested replication forks. Journal of Biological Chemistry, 284, 28084-28092.

Liu, P., Carvalho, C. M., Hastings, P. J., and Lupski, J. R. (2012). Mechanisms for recurrent and complex human genomic rearrangements. Current Opinion in Genetics & Development, 22, 211-220.

Liu, P., Erez, A., Nagamani, S. C., Dhar, S. U., Kolodziejska, K. E., Dharmadhikari, A. V., Cooper, M. L., Wiszniewska, J., Zhang, F., Withers, M. A., Bacino, C. A., Campos-Acevedo, L. D., et al. (2011). Chromosome catastrophes involve replication mechanisms generating complex genomic rearrangements. Cell, 146, 889-903.

Lu, L., Ladinsky, M. S., and Kirchhausen, T. (2011). Formation of the postmitotic nuclear envelope from extended ER cisternae precedes nuclear pore assembly. Journal of Cell Biology, 194, 425-440.

Lundin, C., Erixon, K., Arnaudeau, C., Schultz, N., Jenssen, D., Meuth, M., and Helleday, T. (2002). Different roles for nonhomologous end joining and homologous recombination following replication arrest in mammalian cells. Molecular and Cellular Biology, 22, 5869-5878.

Luzhna, L., Kathiria, P., and Kovalchuk, O. (2013). Micronuclei in genotoxicity assessment: from genetics to epigenetics and beyond. Frontiers in Genetics, 4, 131.

Magrangeas, F., Avet-Loiseau, H., Munshi, N. C., and Minvielle, S. (2011). Chromothripsis identifies a rare and aggressive entity among newly diagnosed multiple myeloma patients. Blood, 118, 675-678.

Mak, J. P., Man, W. Y., Chow, J. P., Ma, H. T., and Poon, R. Y. (2015). Pharmacological inactivation of CHK1 and WEE1 induces mitotic catastrophe in nasopharyngeal carcinoma cells. Oncotarget, 6, 21074-21084.

Malik, M., and Nitiss, J. L. (2004). DNA repair functions that control sensitivity to topoisomerase-targeting drugs. Eukaryotic Cell, 3, 82-90.

Martinez, N. J., Asawa, R. R., Cyr, M. G., Zakharov, A., Urban, D. J., Roth, J. S., Wallgren, E., Klumpp-Thomas, C., Coussens, N. P., Rai, G., Yang, S. M., Hall, M. D., et al. (2018). A widely-applicable high-throughput cellular thermal shift assay (CETSA) using split Nano Luciferase. Scientific Reports, 8, 9472.

McClelland, S. E. (2017). Role of chromosomal instability in cancer progression. Endocrine-Related Cancer, 24, T23-T31.

Medvedeva, N. G., Panyutin, I. V., Panyutin, I. G., and Neumann, R. D. (2007). Phosphorylation of histone H2AX in radiation-induced micronuclei. Radiation Research, 168, 493-498.

Meyerson, M., and Pellman, D. (2011). Cancer genomes evolve by pulverizing single chromosomes. Cell, 144, 9-10.

Molenaar, J. J., Koster, J., Zwijnenburg, D. A., van Sluis, P., Valentijn, L. J., van der Ploeg, I., Hamdi, M., van Nes, J., Westerman, B. A., van Arkel, J., Ebus, M. E., Haneveld, F., et al. (2012). Sequencing of neuroblastoma identifies chromothripsis and defects in neuritogenesis genes. Nature, 483, 589-593.

Moynahan, M. E., and Jasin, M. (2010). Mitotic homologous recombination maintains genomic stability and suppresses tumorigenesis. Nature Reviews Molecular Cell Biology, 11, 196-207.

Network, T. C. G. A. R. (2008). Comprehensive genomic characterization defines human glioblastoma genes and core pathways. Nature, 455, 1061-1068.

Network, T. C. G. A. R. (2012). Comprehensive molecular characterization of human colon and rectal cancer. Nature, 487, 330-337.

Obe, G., Beek, B., and Vaidya, V. G. (1975). The human leukocyte test system. III. Premature chromosome condensation from chemically and x-ray induced micronuclei. Mutation Research, 27, 89-101.

Okamoto, A., Utani, K., and Shimizu, N. (2012). DNA replication occurs in all lamina positive micronuclei, but never in lamina negative micronuclei. Mutagenesis, 27, 323-327.

Orthwein, A., Fradet-Turcotte, A., Noordermeer, S. M., Canny, M. D., Brun, C. M., Strecker, J., Escribano-Diaz, C., and Durocher, D. (2014). Mitosis inhibits DNA double-strand break repair to guard against telomere fusions. Science, 344, 189-193.

Palmitelli, M., de Campos-Nebel, M., and Gonzalez-Cid, M. (2015). Progression of chromosomal damage induced by etoposide in G2 phase in a DNA-PKcs-deficient context. Chromosome Research, 23, 719-732.

Paull, T. T., Rogakou, E. P., Yamazaki, V., Kirchgessner, C. U., Gellert, M., and Bonner, W. M. (2000). A critical role for histone H2AX in recruitment of repair factors to nuclear foci after DNA damage. Current Biology, 10, 886-895.

Pearl, L. H., Schierz, A. C., Ward, S. E., Al-Lazikani, B., and Pearl, F. M. (2015). Therapeutic opportunities within the DNA damage response. Nature Reviews Cancer, 15, 166-180.

Peng, G., and Lin, S. Y. (2011). Exploiting the homologous recombination DNA repair network for targeted cancer therapy. World Journal of Clinical Oncology, 2, 73-79.

Petsalaki, E., Dandoulaki, M., Morrice, N., and Zachos, G. (2014). Chk1 protects against chromatin bridges by constitutively phosphorylating BLM serine 502 to inhibit BLM degradation. Journal of Cell Science, 127, 3902-3908.

Pheiffer, B. H., and Zimmerman, S. B. (1982). 3'-Phosphatase activity of the DNA kinase from rat liver. Biochemical and Biophysical Research Communications, 109, 1297-1302.

Pilie, P. G., Tang, C., Mills, G. B., and Yap, T. A. (2018). State-of-the-art strategies for targeting the DNA damage response in cancer. Natature Reviews Clinical Oncology.

Pizzolato, J. F., and Saltz, L. B. (2003). The camptothecins. Lancet, 361, 2235-2242.

Pommier, Y., Barcelo, J. M., Rao, V. A., Sordet, O., Jobson, A. G., Thibaut, L., Miao, Z. H., Seiler, J. A., Zhang, H., Marchand, C., Agama, K., Nitiss, J. L., et al. (2006). Repair of topoisomerase I-mediated DNA damage. Progress in Nucleic Acid Research and Molecular Biology, 81, 179-229.

Pommier, Y., Leo, E., Zhang, H., and Marchand, C. (2010). DNA topoisomerases and their poisoning by anticancer and antibacterial drugs. Chemistry & Biology, 17, 421-433.

Pommier, Y., Redon, C., Rao, V. A., Seiler, J. A., Sordet, O., Takemura, H., Antony, S., Meng, L., Liao, Z., Kohlhagen, G., Zhang, H., and Kohn, K. W. (2003). Repair of and checkpoint response to topoisomerase I-mediated DNA damage. Mutation Research, 532, 173-203.

Ramos, S., Navarrete-Meneses, P., Molina, B., Cervantes-Barragán, D. E., Lozano, V., Gallardo, E., Marchetti, F., and Frias, S. (2018). Genomic chaos in peripheral blood lymphocytes of Hodgkin's lymphoma patients one year after ABVD chemotherapy/radiotherapy Genomic Chaos in Peripheral Blood Lymphocytes. Environmental and molecular mutagenesis, 59, 755-768.

Rasouli-Nia, A., Karimi-Busheri, F., and Weinfeld, M. (2004). Stable down-regulation of human polynucleotide kinase enhances spontaneous mutation frequency and sensitizes cells to genotoxic agents. Proceedings of the National Academy of Sciences of the United Stated of America, 101, 6905-6910.

Rausch, T., Jones, D. T., Zapatka, M., Stutz, A. M., Zichner, T., Weischenfeldt, J., Jager, N., Remke, M., Shih, D., Northcott, P. A., Pfaff, E., Tica, J., et al. (2012). Genome sequencing of pediatric medulloblastoma links catastrophic DNA rearrangements with TP53 mutations. Cell, 148, 59-71.

Raymond, E., Campone, M., Stupp, R., Menten, J., Chollet, P., Lesimple, T., Fety-Deporte, R., Lacombe, D., Paoletti, X., Fumoleau, P., Group, E. E. C. S., Brain Tumor Studies, G., et al. (2002). Multicentre phase II and pharmacokinetic study of RFS2000 (9-nitro-camptothecin) administered orally 5 days a week in patients with glioblastoma multiforme. European Journal of Cancer, 38, 1348-1350.

Rivory, L. P., Haaz, M. C., Canal, P., Lokiec, F., Armand, J. P., and Robert, J. (1997). Pharmacokinetic interrelationships of irinotecan (CPT-11) and its three major plasma metabolites in patients enrolled in phase I/II trials. Clinical Cancer Research, 3, 1261-1266.

Rode, A., Maass, K. K., Willmund, K. V., Lichter, P., and Ernst, A. (2015). Chromothripsis in cancer cells: An update. International Journal of Cancer, 138, 2322-2333.

Roschke, A. V., Stover, K., Tonon, G., Schaffer, A. A., and Kirsch, I. R. (2002). Stable karyotypes in epithelial cancer cell lines despite high rates of ongoing structural and numerical chromosomal instability. Neoplasia, 4, 19-31.

Rothblum-Oviatt, C. J., Ryan, C. E., and Piwnica-Worms, H. (2001). 14-3-3 binding regulates catalytic activity of human Wee1 kinase. Cell Growth & Differentiation, 12, 581-589.

Ryan, A. J., Squires, S., Strutt, H. L., Evans, A., and Johnson, R. T. (1994). Different fates of camptothecin-induced replication fork-associated double-strand DNA breaks in mammalian-cells. Carcinogenesis, 15, 823-828.

Ryan, A. J., Squires, S., Strutt, H. L., and Johnson, R. T. (1991). Camptothecin cytotoxicity in mammalian cells is associated with the induction of persistent double strand breaks in replicating DNA. Nucleic Acids Research, 19, 3295-3300.

Sackton, K. L., Dimova, N., Zeng, X., Tian, W., Zhang, M., Sackton, T. B., Meaders, J., Pfaff, K. L., Sigoillot, F., Yu, H., Luo, X., and King, R. W. (2014). Synergistic blockade of mitotic exit by two chemical inhibitors of the APC/C. Nature, 514, 646-649.

Sandell, L. L., and Zakian, V. A. (1993). Loss of a yeast telomere: Arrest, recovery, and chromosome loss. Cell, 75, 729-739.

Santaguida, S., and Amon, A. (2015). Short- and long-term effects of chromosome mis-segregation and aneuploidy. Nature Reviews Molecular Cell Biology, 16, 473-485.

Shibata, T., Shibamoto, Y., Sasai, K., Oya, N., Murata, R., Takagi, T., Hiraoka, M., Takahashi, M., and Abe, M. (1996). Tirapazamine: hypoxic cytotoxicity and interaction with radiation as assessed by the micronucleus assay. British Journal of Cancer, 27, S61-64.

Shimizu, N. (2011). Molecular mechanisms of the origin of micronuclei from extrachromosomal elements. Mutagenesis, 26, 119-123.

Shimizu, N., Misaka, N., and Utani, K. (2007). Nonselective DNA damage induced by a replication inhibitor results in the selective elimination of extrachromosomal double minutes from human cancer cells. Genes Chromosomes Cancer, 46, 865-874.

Shimizu, N., Shimura, T., and Tanaka, T. (2000). Selective elimination of acentric double minutes from cancer cells through the extrusion of micronuclei. Mutation Research, 448, 81-90.

Shuck, S. C., and Turchi, J. J. (2010). Targeted inhibition of replication protein A reveals cytotoxic activity, synergy with chemotherapeutic DNA-damaging agents, and insight into cellular function. Cancer Research, 70, 3189-3198.

Snyder, R. D., and Diehl, M. S. (2005). Hypoxia-induced micronucleus formation in mice. Drug and Chemical Toxicology, 28, 373-378.

Solari, F., Domenget, C., Gire, V., Woods, C., Lazarides, E., Rousset, B., and Jurdic, P. (1995). Multinucleated cells can continuously generate mononucleated cells in the absence of mitosis: a study of cells of the avian osteoclast lineage. Journal of Cell Science, 108 (Pt 10), 3233-3241.

Solyom, S., Pylkas, K., and Winqvist, R. (2010). Screening for large genomic rearrangements of the BRIP1 and CHK1 genes in Finnish breast cancer families. Familial Cancer, 9, 537-540.

Soto, M., Raaijmakers, J. A., Bakker, B., Spierings, D. C. J., Lansdorp, P. M., Foijer, F., and Medema, R. H. (2017). p53 Prohibits Propagation of Chromosome Segregation Errors that Produce Structural Aneuploidies. Cell Reports, 19, 2423-2431.

Spann, T. P., Goldman, A. E., Wang, C., Huang, S., and Goldman, R. D. (2002). Alteration of nuclear lamin organization inhibits RNA polymerase II-dependent transcription. Journal of Cell Biology, 156, 603-608.

Spann, T. P., Moir, R. D., Goldman, A. E., Stick, R., and Goldman, R. D. (1997). Disruption of nuclear lamin organization alters the distribution of replication factors and inhibits DNA synthesis. Journal of Cell Biology, 136, 1201-1212.

Stephens, P. J., Greenman, C. D., Fu, B., Yang, F., Bignell, G. R., Mudie, L. J., Pleasance, E. D., Lau, K. W., Beare, D., Stebbings, L. A., McLaren, S., Lin, M. L., et al. (2011). Massive genomic rearrangement acquired in a single catastrophic event during cancer development. Cell, 144, 27-40.

Stevens, J. B., Liu, G., Bremer, S. W., Ye, K. J., Xu, W., Xu, J., Sun, Y., Wu, G. S., Savasan, S., Krawetz, S. A., Ye, C. J., and Heng, H. H. (2007). Mitotic cell death by chromosome fragmentation. Cancer Research, 67, 7686-7694.

Storchova, Z., and Kloosterman, W. P. (2016). The genomic characteristics and cellular origin of chromothripsis. Current Opinion in Cell Biology, 40, 106-113.

Strumberg, D., Pilon, A. A., Smith, M., Hickey, R., Malkas, L., and Pommier, Y. (2000). Conversion of topoisomerase 1 cleavage complexes on the leading strand of ribosomal DNA into 5 '-phosphorylated DNA double-strand breaks by replication runoff. Molecular and Cellular Biology, 20, 3977-3987.

Swift, L. H. (2015). *Investigation Of Checkpoint Adaptation In Human Cancer Cells Treated With The Genotoxic Agent Cisplatin.* (Doctor of Philosophy), University of Lethbridge, AB, Canada.

Swift, L. H., and Golsteyn, R. M. (2014). Genotoxic anti-cancer agents and their relationship to DNA damage, mitosis, and checkpoint adaptation in proliferating cancer cells. International Journal of Molecular Sciences, 15, 3403-3431.

Swift, L. H., and Golsteyn, R. M. (2016a). Cytotoxic amounts of cisplatin induce either checkpoint adaptation or apoptosis in a concentration-dependent manner in cancer cells. Biology of the Cell, 108, 127-148.

Swift, L. H., and Golsteyn, R. M. (2016b). The relationship between checkpoint adaptation and mitotic catastrophe in genomic changes in cancer cells (pp. 373-389).

Swift, L. H., and Golsteyn, R. M. (2018). Experimental determination of checkpoint adaptation by mitotic shake-off and microscopy. Methods in Molecular Biology, 1769, 159-168.

Syljuasen, R. G. (2007). Checkpoint adaptation in human cells. Oncogene, 26, 5833-5839.

Syljuasen, R. G., Jensen, S., Bartek, J., and Lukas, J. (2006). Adaptation to the ionizing radiation-induced G2 checkpoint occurs in human cells and depends on checkpoint kinase 1 and Polo-like kinase 1 kinases. Cancer Research, 66, 10253-10257.

Symington, L. S., and Gautier, J. (2011). Double-strand break end resection and repair pathway choice. Annual Review of Genetics, 45, 247-271.

Tahbaz, N., Subedi, S., and Weinfeld, M. (2012). Role of polynucleotide kinase/phosphatase in mitochondrial DNA repair. Nucleic Acids Research, 40, 3484-3495.

Takata, M., Sasaki, M. S., Sonoda, E., Morrison, C., Hashimoto, M., Utsumi, H., Yamaguchi-Iwai, Y., Shinohara, A., and Takeda, S. (1998). Homologous recombination and non-homologous end-joining pathways of DNA double-strand break repair have overlapping roles in the maintenance of chromosomal integrity in vertebrate cells. EMBO Journal, 17, 5497-5508.

Tanaka, K., and Hirota, T. (2016). Chromosomal instability: A common feature and a therapeutic target of cancer. Biochimica et Biophysica Acta, 1866, 64-75.

Tang, C. W., Maya-Mendoza, A., Martin, C., Zeng, K., Chen, S., Feret, D., Wilson, S. A., and Jackson, D. A. (2008). The integrity of a lamin-B1-dependent nucleoskeleton is a fundamental determinant of RNA synthesis in human cells. Journal of Cell Science, 121, 1014-1024.

Terradas, M., Martin, M., and Genesca, A. (2016). Impaired nuclear functions in micronuclei results in genome instability and chromothripsis. Archives Toxicology, 90, 2657-2667.

Terradas, M., Martin, M., Hernandez, L., Tusell, L., and Genesca, A. (2012). Nuclear envelope defects impede a proper response to micronuclear DNA lesions. Mutation Research, 729, 35-40.

Terradas, M., Martin, M., Tusell, L., and Genesca, A. (2009). DNA lesions sequestered in micronuclei induce a local defective-damage response. DNA Repair (Amst), 8, 1225-1234.

Terradas, M., Martin, M., Tusell, L., and Genesca, A. (2010). Genetic activities in micronuclei: is the DNA entrapped in micronuclei lost for the cell? Mutation Research, 705, 60-67.

Thompson, L. L., Jeusset, L. M., Lepage, C. C., and McManus, K. J. (2017). Evolving therapeutic strategies to exploit chromosome instability in cancer. Cancers (Basel), 9, 151.

Thompson, S. L., and Compton, D. A. (2010). Proliferation of aneuploid human cells is limited by a p53-dependent mechanism. Journal of Cell Biology, 188, 369-381.

Tkacz-Stachowska, K., Lund-Andersen, C., Velissarou, A., Myklebust, J. H., Stokke, T., and Syljuasen, R. G. (2011). The amount of DNA damage needed to activate the radiation-induced G2 checkpoint varies between single cells. Radiotherapy Oncology, 101, 24-27.

Toczyski, D. P., Galgoczy, D. J., and Hartwell, L. H. (1997). CDC5 and CKII control adaptation to the yeast DNA damage checkpoint. Cell, 90, 1097-1106.

Utani, K., Okamoto, A., and Shimizu, N. (2011). Generation of micronuclei during interphase by coupling between cytoplasmic membrane blebbing and nuclear budding. PLoS One, 6, e27233.

Vargas-Rondon, N., Villegas, V. E., and Rondon-Lagos, M. (2017). The role of chromosomal instability in cancer and therapeutic responses. Cancers (Basel), 10, 4.

Visconti, R., Della Monica, R., and Grieco, D. (2016). Cell cycle checkpoint in cancer: a therapeutically targetable double-edged sword. Journal of Experimental & Clinical Cancer Research, 35, 153.

Visconti, R., Della Monica, R., Palazzo, L., D'Alessio, F., Raia, M., Improta, S., Villa, M. R., Del Vecchio, L., and Grieco, D. (2015). The Fcp1-Wee1-Cdk1 axis affects spindle assembly checkpoint robustness and sensitivity to antimicrotubule cancer drugs. Cell Death & Differentiation, 22, 1551-1560.

Wall, M. E., and Wani, M. C. (1995). Camptothecin and taxol: discovery to clinic--thirteenth Bruce F. Cain Memorial Award Lecture. Cancer Research, 55, 753-760.

Wang, H., Peng, B., Pandita, R. K., Engler, D. A., Matsunami, R. K., Xu, X., Hegde, P. M., Butler, B. E., Pandita, T. K., Mitra, S., Xu, B., and Hegde, M. L. (2017). Aurora kinase B dependent phosphorylation of 53BP1 is required for resolving merotelic kinetochore-microtubule attachment errors during mitosis. Oncotarget, 8, 48671-48687.

Warmerdam, D. O., Brinkman, E. K., Marteijn, J. A., Medema, R. H., Kanaar, R., and Smits, V. A. (2013). UV-induced G2 checkpoint depends on p38 MAPK and minimal activation of ATR-Chk1 pathway. Journal of Cell Science, 126, 1923-1930.

Weihua, Z., Lin, Q., Ramoth, A. J., Fan, D., and Fidler, I. J. (2011). Formation of solid tumors by a single multinucleated cancer cell. Cancer, 117, 4092-4099.

Weinfeld, M., Mani, R. S., Abdou, I., Aceytuno, R. D., and Glover, J. N. (2011). Tidying up loose ends: the role of polynucleotide kinase/phosphatase in DNA strand break repair. Trends in Biochemical Sciences, 36, 262-271.

Wen, Q., Scorah, J., Phear, G., Rodgers, G., Rodgers, S., and Meuth, M. (2008). A mutant allele of MRE11 found in mismatch repair-deficient tumor cells suppresses the cellular response to DNA replication fork stress in a dominant negative manner. Mololecular Biology of the Cell, 19, 1693-1705.

Whitehouse, C. J., Taylor, R. M., Thistlethwaite, A., Zhang, H., Karimi-Busheri, F., Lasko, D. D., Weinfeld, M., and Caldecott, K. W. (2001). XRCC1 stimulates human polynucleotide kinase activity at damaged DNA termini and accelerates DNA single-strand break repair. Cell, 104, 107-117.

Xu, B., Sun, Z., Liu, Z., Guo, H., Liu, Q., Jiang, H., Zou, Y., Gong, Y., Tischfield, J. A., and Shao, C. (2011). Replication stress induces micronuclei comprising of aggregated DNA double-strand breaks. PLoS One, 6, e18618.

Xu, Y., and Her, C. (2015). Inhibition of topoisomerase (DNA) I (TOP1): DNA damage repair and anticancer therapy. Biomolecules, 5, 1652-1670.

Zeng, X., Sigoillot, F., Gaur, S., Choi, S., Pfaff, K. L., Oh, D. C., Hathaway, N., Dimova, N., Cuny, G. D., and King, R. W. (2010). Pharmacologic inhibition of the anaphase-promoting complex induces a spindle checkpoint-dependent mitotic arrest in the absence of spindle damage. Cancer Cell, 18, 382-395.

Zhang, C. Z., Leibowitz, M. L., and Pellman, D. (2013). Chromothripsis and beyond: rapid genome evolution from complex chromosomal rearrangements. Genes & Development, 27, 2513-2530.

Zhang, C. Z., Spektor, A., Cornils, H., Francis, J. M., Jackson, E. K., Liu, S., Meyerson, M., and Pellman, D. (2015). Chromothripsis from DNA damage in micronuclei. Nature, 522, 179-184.

Zhang, L., Wu, C., and Hoffman, R. M. (2015). Prostate cancer heterogeneous high-metastatic multi-organ-colonizing chemo-resistant variants selected by serial metastatic passage in nude mice are highly enriched for multinucleate giant cells. PLoS One, 10, e0140721.

Zhang, Y. W., Otterness, D. M., Chiang, G. G., Xie, W., Liu, Y. C., Mercurio, F., and Abraham, R. T. (2005). Genotoxic stress targets human Chk1 for degradation by the ubiquitin-proteasome pathway. Molecular Cell, 19, 607-618.

Zhu, Y., Hu, J., Hu, Y., and Liu, W. (2009). Targeting DNA repair pathways: a novel approach to reduce cancer therapeutic resistance. Cancer Treatment Reviews, 35, 590-596.